nature neuroscience

Article

https://doi.org/10.1038/s41593-025-02062-6

Muscle-derived miR-126 regulates TDP-43 axonal local synthesis and NMJ integrity in ALS models

Received: 14 December 2023

Accepted: 18 August 2025

Published online: 3 October 2025

Check for updates

Ariel Ionescu[1,12], Lior Ankol[1,12], Anand Ganapathy Subramaniam[1], Topaz Altman[1], Iddo Magen[2,3], Yahel Cohen[2,3], Yehuda Danino[2,3], Tal Gradus-Pery[1], Yoav Niv[1], Ori Bar Avi[1], Danielle Geller[1], Amjd Ibraheem[1], Ruilei Cheng[1], Noam Steinberg[1], Leenor Alfahel[4,5], Pauline Duc[6], Zeynep Ergul-Ulger[7], Doruk Arslan[7], Ersin Tan[7], Florence Rage[6], Nilo Riva[8], Angello Quattrini[9], Can Ebru Bekircan-Kurt[7], Adrian Israelson[4,5], Amir Dori[1,10], Eran Hornstein[2,3] & Eran Perlson[1,11]

Amyotrophic lateral sclerosis (ALS) is characterized by neuromuscular junction (NMJ) disruption and neurodegeneration. Recent findings highlight a pivotal role for TAR DNA-binding protein 43 (TDP-43) in forming axonal pathological condensates and facilitating NMJ disruption through inhibition of local protein synthesis. However, the mechanisms that drive local TDP-43 accumulation remain unknown. Here we identify that the TDP-43 axonal accumulation in peripheral nerves of SOD1 patients and mice stems from its aberrant local synthesis. This is a non-cell-autonomous process driven by muscle-derived miR-126a-5p extracellular vesicles (EVs). Inhibiting muscle secretion of miR-126a-5p prompts presynaptic TDP-43 synthesis and accumulation, which disrupts axonal translation and causes NMJ degeneration. Introducing miR-126 to SOD1^{G93A} mice, primary co-cultures and human induced pluripotent stem cell (iPSC)-derived co-cultures with ALS mutations exhibits neuroprotective effects and delays motor decline. These findings identify a transcellular communication axis between muscles and motor neurons that regulates axonal local synthesis and NMJ maintenance, offering insights into ALS onset and progression.

ALS is a lethal adult-onset motor neuron (MN) disease, characterized by disruption of NMJs, axonal degeneration and neuronal death[1–4]. Most ALS cases are linked to TDP-43 pathology, characterized by its mislocalization from the nucleus to the cytoplasm and the formation of phosphorylated aggregates[5–7].

TDP-43 is a multifunctional DNA/RNA-binding protein with roles in transcriptional and splicing regulation, RNA processing and RNA transport/subcellular localization[8–12]. Recently, we showed that TDP-43 co-localizes with the core stress granule component G3BP1 in axonal condensates of patients with ALS and mice. These TDP-43-G3BP1 condensates sequester RNA and inhibit local protein synthesis, resulting in mitochondrial malfunction and NMJ disruption with subsequent axonal degeneration[13]. Thus, TDP-43 has profound effects in axons and NMJs, and its aggregation causes pathology not limited to the spinal MN cell bodies but also found in the distal portions of motor axons. Furthermore, recent studies revealed aggregation of TDP-43 in peripheral motor axons of patients with ALS during initial diagnosis[14,15]. Thus, axonal TDP-43 condensates exert pathological regulation over essential local synthesis events.

A full list of affiliations appears at the end of the paper. e-mail: eranpe@tauex.tau.ac.il

https://doi.org/10.1038/s41593-025-02062-6

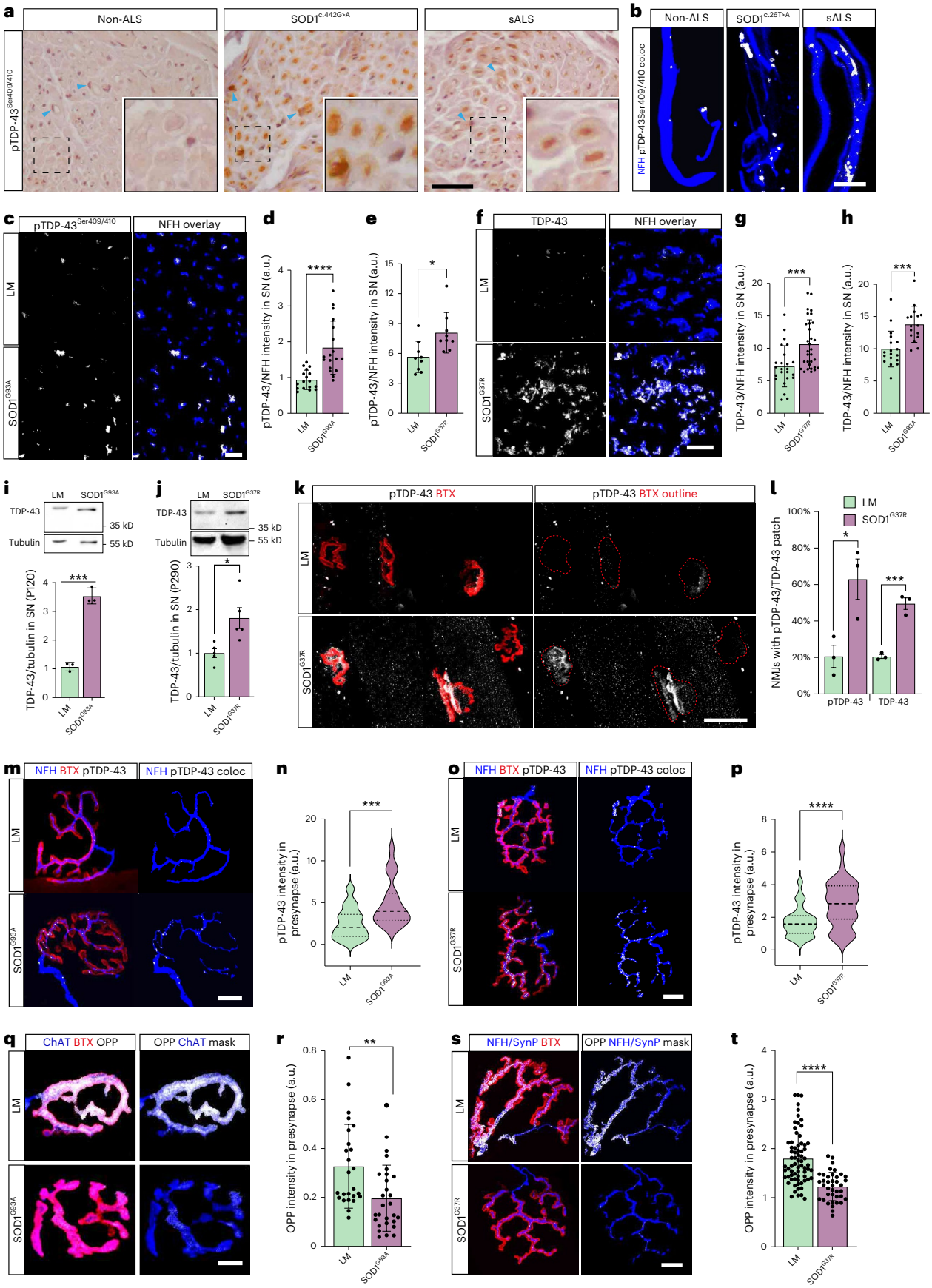

Fig. 1 | TDP-43 peripheral pathology in *SOD1* patients and *SOD1* mouse models. a, Immunohistochemical staining for pTDP-43 in obturator nerve biopsies of non-ALS patients (motor neuropathy), patients with *SOD1* (*c.442 G > A*) and patients with sALS. Arrowheads indicate Schwann cells. Scale bar, 10 µm. **b**, Immunofluorescent staining for pTDP-43 in intramuscular nerves in biopsies of non-ALS patients, patients with *SOD1* (*c.26 T > A*) and patients with sALS. White indicates NFH–pTDP-43 co-localization. Scale bar, 5 µm. **c**–**e**, Immunofluorescent images and quantification of pTDP-43 in sciatic nerve cross-sections of SOD1^{G93A} (**d**) and SOD1^{G37R} (**e**) mice and their littermates. White indicates NFH-masked TDP-43. Scale bar, 10 µm. $n = 17$ (**d**) and $n = 9$ (**e**) nerve sections. $^{*}P = 0.0368$, $^{****}P = 0.000044$. **f**–**h**, Immunofluorescent images and quantification of TDP-43 in sciatic nerve cross-sections of SOD1^{G37R} (**g**) and SOD1^{G93A} (**h**) mice and their littermates. White indicates NFH-masked TDP-43. Scale bar, 10 µm. $n = 24, 31$ (**g**) and $n = 18, 16$ (**h**) nerve sections. $^{***}P = 0.0006$ (**g**), $P = 0.0004$ (**h**). **i**,**j**, Representative images and quantification of western blots for TDP-43 (43 kD) and tubulin (55 kD) in sciatic nerve axoplasms of SOD1^{G93A} (**i**) and SOD1^{G37R} (**j**) mice versus their littermates. $n = 3, 4$ mice, respectively. $^{*}P = 0.0149$ (**j**), $^{***}P = 0.0002$ (**i**). **k**,**l**, Representative images and quantitative analysis for the percent of NMJs with apparent TDP-43/pTDP-43 patch in EDL muscles from P290 SOD1^{G37R} and littermate controls. Red dashed line marks BTX perimeter. Scale bar, 30 µm. $n = 3$ mice per group. $^{***}P = 0.0009$, $^{*}P = 0.0288$. **m**–**p**, Immunofluorescent images and quantification of NFH–pTDP-43 co-localization in NMJs of presymptomatic (P60) SOD1^{G93A} (**m**,**n**) and (P290) SOD1^{G37R} (**o**,**p**) mice versus their littermates. White indicates NFH–pTDP-43 co-localization. Scale bar, 15 µm. $n = 29, 20$ (**n**); $n = 53, 59$ (**p**) NMJs. $^{***}P = 0.0005$ (**n**), $^{****}P = 0.000019$ (**p**). **q**–**t**, Representative images and quantification of the OPP labeling in NMJs of presymptomatic (P60) SOD1^{G93A} (**q**,**r**) and (P290) SOD1^{G37R} (**s**,**t**) mice and their littermates. White indicates OPP–ChAT or OPP–NFH–synaptophysin three-dimensional co-localization. Scale bar, 10 µm. $n = 30$ (**r**) and $n = 72, 40$ (**t**) NMJs. $^{**}P = 0.0032$, $^{****}P = 1.21 \times 10^{-6}$. For **d**,**e**,**g**,**h**,**r**,**t**, data are shown as the mean ± s.d., repeated in three mice per genotype. For **i**,**j**,**k**,**l**, data are shown as the mean ± s.e.m., repeated in three mice per genotype. For **n**,**p**, data are shown in violin density plots with markings of first, median and third quartiles, repeated in three mice per genotype. For **d**,**e**,**g**–**l**,**n**,**p**,**r**,**t**, two-tailed unpaired Student's *t*-test. coloc, co-localization; LM, littermate; SN, sciatic nerve.

Localized protein synthesis is a mechanism enabling spatially constrained and temporally sensitive cellular responses to changes in intracellular or extracellular environment[16–18]. Neurons, with their extensively long axons, rely on local protein synthesis for proper function and survival[19–21]. Alterations in this process can lead to various neuropathological disorders, including ALS[10,11,22–26]. Each MN harbors numerous remote NMJs, and how translation is coordinated within each synapse is still unknown. Moreover, although TDP-43 is a potent driver of ALS toxicity and a key local synthesis regulator, the mode of its accumulation along axons and NMJs is a critical unaddressed question.

Here, we studied the localized accumulation of TDP-43 in axons and NMJs. Our findings highlight the presence of distal TDP-43 pathology in patients with SOD1 ALS and mouse models. We found that TDP-43 accumulates at NMJs due to aberrant local synthesis triggered by a reduction in miR-126a-5p within muscle EVs. This chain of events ultimately initiates neurodegeneration. Notably, miR-126 is neuroprotective in neuromuscular co-cultures, delays TDP-43 accumulation at NMJs and postpones the onset of motor symptoms in SOD1^{G93A} mice. This unveils a new role for muscle EV-loaded micro RNAs (miRNAs) in regulating NMJ protein synthesis, thereby affecting NMJ maintenance and disruption in ALS.

Results

TDP-43 peripheral pathology in SOD1 patients and SOD1 mouse models

TDP-43 pathology is not limited to the spinal MN cell bodies but is also found in motor axons of patients with ALS[13–15]. SOD1 patients are traditionally considered negative for TDP-43 pathology based on observations from postmortem spinal and cortical MNs. However, unexpectedly, when analyzing their peripheral nerves, we identified phosphorylated TDP-43 (pTDP-43) aggregates along the axons in an obturator nerve biopsy from a SOD1 c.442 G > A mutant patient and in intramuscular nerves from a SOD1 c.26 T > A mutant patient (Fig. 1a,b and Extended Data Fig. 1). These pTDP-43 aggregates resemble those found in sporadic ALS (sALS) biopsies and minimally detectable in non-ALS pathologies. We next examined TDP-43 in SOD1^{G93A} and SOD1^{G37R} mouse models. Immunofluorescent and biochemical analyses of sciatic nerves from both models indicated the accumulation of TDP-43 and pTDP-43 in peripheral nerves at symptomatic stages of the disease (Fig. 1c–j and Extended Data Figs. 1b–f and 2). Notably, we did not observe TDP-43 mislocalization or aggregation in cell bodies of spinal MNs (Extended Data Fig. 3). Additionally, using three-dimensional co-localization analysis, we discovered that pTDP-43 accumulates in NMJs of SOD1^{G93A} and SOD1^{G37R} mice before symptom onset and throughout disease progression (Fig. 1k–p and Extended Data Fig. 4a–h). Interestingly, the pathology was more apparent in fast fatigable extensor digitorum longus (EDL) muscles compared to the slow fatigable soleus muscles (Fig. 1k,l and Extended Data Fig. 4i–l). Accumulation of TDP-43 in NMJs is negatively correlated with local protein synthesis[13]. To verify whether this also occurs in SOD1 mutants, we used O-propargyl puromycin (OPP) to label and quantify newly synthesized proteins in NMJs. Indeed, analysis of the OPP signal specifically within presynaptic axons revealed a reduction in presynaptic protein synthesis in both SOD1^{G93A} and SOD1^{G37R} NMJs as well as in NMJs in SOD1^{G93A} primary co-cultures (Fig. 1q–t and Supplementary Fig. 1). Thus, our findings reveal a confined accumulation of TDP-43 in peripheral nerves and NMJs of patients with SOD1 ALS and animal models, which may affect local protein synthesis. Furthermore, TDP-43 retains its typical nuclear localization in the SOD1 models, suggesting that this process can be regulated by local translation within distal axons and NMJs.

Muscles restrain local TDP-43 mRNA translation

Reanalyzing axonal RNA sequencing (RNA-seq) data[27], we found that TDP-43 mRNA is abundant in axons (Extended Data Fig. 5a). To

Fig. 2 | TDP-43 mRNA localization and local translation in MN axons. **a**, Quantitative RT–PCR analysis of the relative mRNA levels of TDP-43 and PolB in RNA preparations from soma or axonal compartments of radial MFCs. $n = 3$ neuronal cultures; each repeat represents a pool of several radial chambers. RQ, relative quantification. NS = 0.9814, $^{**}P = 0.0015$. **b**, Representative image of an agarose gel with cDNA amplicons of TDP-43, PolB and β-actin amplified from sciatic nerve axoplasm RNA. $n = 5$ mice. **c**, Representative images of smFISH for mRNA of TDP-43 and β-actin in primary MN axons compared to no probe control. Scale bar, 5 µm. **d**, Representative images of smFISH for mRNAs of TDP-43 and β-actin in EDL muscle NMJs compared to no probe control. White indicates smFISH–NFH three-dimensional co-localization result. Scale bar, 10 µm. **e**,**f**, Representative images and quantification of TDP-43 puro-PLA in axons in the presence or absence of anisomycin (40 µM) and in in vitro NMJs (lowest panel). Scale bars, 20 µm and 5 µm. $n = 97, 91, 62$ axons and NMJs, respectively. NS = 0.0525, $^{****}P = 3 \times 10^{-15}$ (Aniso), $P = 1.31 \times 10^{-6}$ (NMJ). **g**,**h**, Representative images and orthogonal slices of TDP-43 puro-PLA in EDL NMJs treated with puromycin (**g**) or with anisomycin + puromycin (**h**) muscles. **i**,**j**, Representative images and orthogonal slices of β-actin puro-PLA labeling in EDL NMJs treated with puromycin (**i**) or with anisomycin + puromycin (**j**) muscles. SynP, synaptophysin labeling. Scale bar, 10 µm. For **a**, data are shown as the mean ± s.e.m., two-way ANOVA with multiple comparisons. For **c**, representative experiment repeated in three neuronal cultures. For **d**, representative experiment repeated in three ex vivo muscle preparations. For **f**, data are shown in violin density plots with markings of first, median and third quartiles, one-way ANOVA with Holm–Sidak correction for multiple comparisons, repeated in three neuronal cultures. Aniso, anisomycin; coloc, co-localization; NS, not significant.

https://doi.org/10.1038/s41593-025-02062-6

determine whether TDP-43 mRNA is localized and locally translated in axons, we isolated pure axonal RNA from primary MN cultures using radial microfluidic chambers (MFCs)[13] and performed quantitative polymerse chain reaction (qPCR). This revealed a roughly similar abundance of TDP-43 mRNA in axons and somata (Fig. 2a). Additionally, we purified RNA from sciatic nerve axoplasms after PCR amplification for TDP-43 (*Tardbp*), polymerase-β (*Polb*; soma marker, negative control for axonal RNA) and β-actin (*Actb*) mRNAs (as a positive control for axonal RNA). We detected clear amplicons of both TDP-43 and β-actin mRNAs in the absence of Polb (Fig. 2b). Moreover, single-molecule fluorescence in situ hybridization (smFISH) in primary MNs revealed axonal-localized puncta of TDP-43 and β-actin mRNA (Fig. 2c and

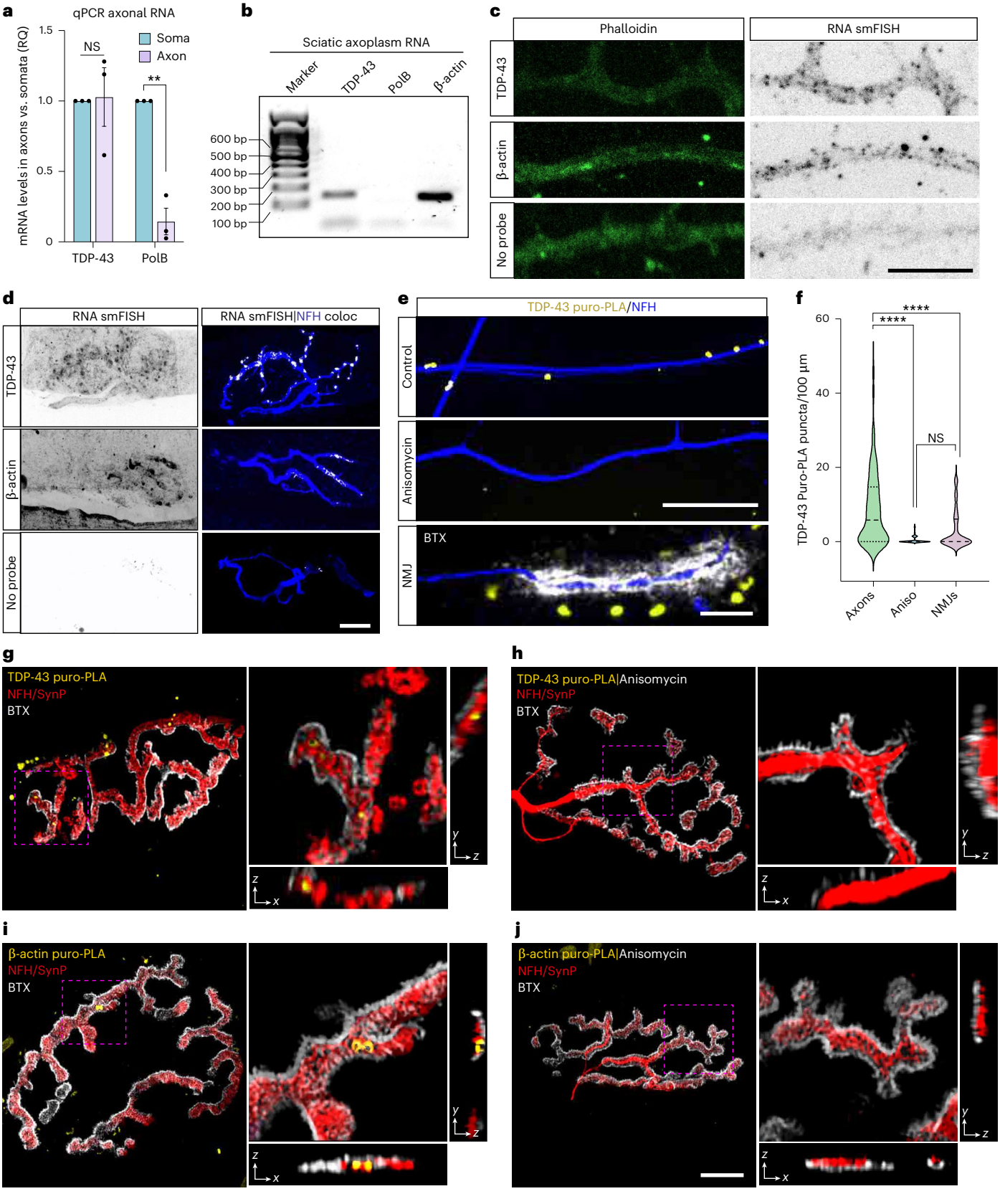

Extended Data Fig. 5b). smFISH for TDP-43 and β-actin on EDL muscles showed that both mRNAs are localized in presynaptic axons at NMJs (Fig. 2d). Altogether, this evidence indicates that TDP-43 mRNA is localized in distal axons and NMJs both in vitro and in vivo.

To test whether TDP-43 mRNA is locally translated in axons and NMJs, we used a puromycin proximity ligation assay (puro-PLA)[28]. Quantitative analysis of TDP-43 puro-PLA in primary MNs grown in compartmental MFCs indicated that TDP-43 is synthesized in axons (Fig. 2e,f). This was further validated by ablation of axonal TDP-43 followed by TDP-43 small interfering RNA (siRNA) treatment (Extended Data Fig. 5c,d). Next, we repeated the TDP-43 puro-PLA in a compartmental neuromuscular co-culture[13,29,30]. Unexpectedly, the number of TDP-43 puro-PLA puncta in presynaptic axons was markedly reduced, implying a role for muscles in controlling local protein synthesis (Fig. 2f and Extended Data Fig. 5e). We also visualized TDP-43 and β-actin local translation ex vivo, detecting presynaptic TDP-43 synthesis in a small fraction of NMJs (Fig. 2g–j and Supplementary Fig. 2a). Lastly, examination of NMJs within EDL muscle of SOD1^{G37R} mice suggests increase in local translation of TDP-43 (Supplementary Fig. 2b). Overall, these results indicate that TDP-43 mRNA is distributed into axons where it can be locally translated, a process that is limited in the NMJ but may increase in mice harboring SOD1 mutations.

Muscles communicate with presynaptic axons via miRNA-loaded EVs

Our results suggest that the presynaptic local synthesis of TDP-43 can be silenced by transcellular processes, such as by miRNA-loaded EVs[31]. Therefore, we hypothesized that the EV machinery is also present in the postsynaptic apparatus in NMJs. Using in vivo immunofluorescence, we found that several hallmark EV markers, such as CD63, CHMP2A and CD81, are enriched in postsynaptic regions in muscles (Fig. 3a–c and Extended Data Fig. 6a–d). To determine whether these represent functionally secreted EVs, we used compartmental neuromuscular co-cultures in which muscles were transfected with CD63-pHluorin (Fig. 3d)[32]. Live imaging of CD63-pHluorin in co-cultures shows a strong signal rising in synaptic regions (bungarotoxin (BTX) positive) compared to extrasynaptic regions in muscles, reinforcing our observation of EV enrichment in NMJs (Fig. 3e,f, Extended Data Fig. 6e and Supplementary Video 1). Similar experiments with CD63–GFP visualize the transmission of EVs from skeletal muscles and their uptake into axons (Supplementary Fig. 3a–f and Supplementary Videos 2 and 3). Using SYTO RNASelect to label total RNA in primary muscle cultures, we further observed the uptake and the intra-axonal shuttling of muscle-derived RNA (Supplementary Fig. 3g,h). To further characterize this process, we isolated muscle-derived EVs from the conditioned media of primary myocytes by ultracentrifugation[33]. Transmission electron microscopy (TEM) and nanoparticle tracking analysis (NTA) validated the predominant presence of bi-layer EVs with an average diameter of 100 nm, congruent with the size of exosomes (Fig. 3g,h). RNA-seq analysis of axonal RNA from axons treated with muscle-derived EVs identified transcriptional changes, implying that these EVs carry miRNAs, as suggested by the immediate reduction in the abundance of multiple transcripts (Supplementary Fig. 3i and Supplementary Table 1). Additionally, western blot characterization of EV preparations validated the presence of the hallmark exosome marker CD63 and the inclusion of the RNA-induced silencing complex (RISC) component Argonaut 2 (Ago2), as also previously reported[34], suggesting the transmission of miRNAs and RISC machinery through muscle EVs (Fig. 3i and Supplementary Fig. 4a,b). Notably, we did not detect traces of TDP-43 in these preparations, suggesting that it is not primarily sorted into muscle EVs. Using an NMJ co-culture, we transfected primary muscle cells with Ago2–GFP and observed Ago2–GFP puncta in adjacent axons (Supplementary Fig. 5a,b and Supplementary Videos 4 and 5). Immunostaining confirmed Ago2 transfer from muscles to axons (Fig. 3j,k and Supplementary Fig. 5c). Additionally, miRNA sequencing of axons treated with muscle-derived EVs revealed an increase in muscle-specific miRNAs (myomiRs) and a decrease in axonal protein synthesis (Supplementary Fig. 4c–h and Supplementary Table 1). Together, these results suggest that RISC components are transferred from muscle to neuron via exosome-like EVs, regulating the RNA population at the NMJ.

EV-derived miR-126a-5p regulates TDP-43 turnover at NMJs

To elucidate the function of muscle-derived EVs in presynaptic axons, we performed small RNA-seq for muscle EVs and whole-cell lysates. This revealed a subpopulation of miRNAs that is compartmentalized into EVs (Fig. 4a and Supplementary Table 2). Of the most compartmentalized miRNAs in muscle-derived EVs, we identified miR-126a-5p, which we previously reported to be downregulated in SOD1^{G93A} muscles and MNs[35]. This result was further validated by specific TaqMan RT–qPCR for muscle-derived miR-126a-5p (Fig. 4b). The compartmentalization of miR-126a-5p and other miRNAs implies a paracrine function rather than an autocrine function, such as was previously indicated for miR-206 (ref. 36) (which was not compartmentalized in muscle-derived EVs). Based on this assumption, we performed miRNA FISH for miR-126a-5p in EDL muscles and confirmed that its expression was almost exclusively confined to the NMJ region, strengthening our hypothesis that these miRNAs target mRNA transcripts in non-muscle neighboring cells such as presynaptic motor axons (Fig. 4c). Next, we used TargetScan miRNA target predictions to test whether any of the ALS-associated genes (Amyotrophic Lateral Sclerosis online Database (ALSoD)[37]) are predicted targets of miR-126a-5p. This revealed more than 50 out of the 154 genes, of which six are definitive ALS genes, including TDP-43 having the highest prediction score of all (*TARDBP*; Supplementary Table 3). Our verification revealed that the majority of both the mouse and human *TARDBP* mRNA transcript variants include at least one binding site for miR-126a-5p (miR-126-5p in humans).

The dominant axonal mouse variant of *Tardbp* mRNA is isoform 3 (Supplementary Table 4; NM_001003899.2), which contains two binding sites for miR-126a-5p in its 3′ untranslated region (UTR).

Fig. 3 | Muscles communicate with presynaptic axons via EVs. **a**–**c**, Representative images and quantitative analysis (**b**,**c**) of NMJ immunolabeling for CD63 (upper panel **b**) and CHMP2A (lower panel **c**). Gray indicates three-dimensional co-localization result of CD63/CHMP2A and BTX. Scale bar, 10 µm. $n = 19$ (**b**) and $n = 39$ (**c**) muscles. ***$P = 0.00012$ (**b**), ****$P = 1.17 \times 10^{-10}$ (**c**). **d**, Illustration of experimental setup in **e** and **f**. Primary skeletal muscles were transfected with CD63-pHluorin vector and co-cultured with primary MNs in compartmental MFCs. **e**,**f**, Representative images and quantification of CD63-pHluorin signal and localization in neuromuscular co-cultures. Scale bar, 20 µm. $n = 24$ muscles from three independent repeats. Two-tailed paired Student's *t*-test, **$P = 0.0015$. **g**, Representative TEM images of muscle-derived EVs. Scale bars, 300 nm (left panel) and 100 nm (right panel). **h**, Representative NTA plot for muscle conditioned media. **i**, Representative images of western blots for CD63 (55 kD), CD81 (26 kD), CD9 (22 kD), Ago2 (87 kD) and TDP-43 (43 kD) in protein lysates of primary muscles and primary muscle-derived EVs. **j**, Illustration of experimental setup for **j**. Primary skeletal muscles were transfected with Ago2–GFP vector and co-cultured with primary MNs in compartmental MFCs. **k**, Upper panel: representative images of immunolabeling for Ago2 and GFP in neuromuscular co-cultures. Lower panel: inset and representative image of Imaris puncta analysis for Ago2 and GFP antibody labeling within axons. Yellow arrowheads indicate co-localized GFP and Ago2 signals in axons. Scale bar, 10 µm. For **b**,**c**,**f**, data are shown as pairs of signal intensity in synaptic versus extra-synaptic regions within the same muscle. For **b**,**c**, experiment was repeated in three mice. For **f**, experiment was repeated in three co-cultures. For **b**,**c**,**f**, two-tailed paired Student's *t*-test. For **g**,**h**,**I**, representative for three biological repeats of muscle culture and EV preparation. For **k**, repeated once. Representative of 15 images. coloc, co-localization; Ex.synaptic, extra-synaptic.

https://doi.org/10.1038/s41593-025-02062-6

We validated the ability of miR-126a-5p to silence *Tardbp* as well as several other predicted and MN-related transcripts after lentiviral delivery of miR-126 to primary MNs (Fig. 4d,e and Extended Data Fig. 7a,b). Notably, we validated that miR-126-5p regulation over TDP-43 mRNAs is conserved in humans (Extended Data Fig. 7c–f). Next, we confirmed the direct interaction between miR-126a-5p and TDP-43 mRNA using dual-luciferase reporter assay, which showed that the effect of miR-126-5p is abolished upon mutation of TDP-43 binding site (Fig. 4f,g). Furthermore, miR-126 overexpression in primary MNs led to a mild decrease in TDP-43 protein levels in whole-cell lysates, potentially due to the existence of additional TDP-43 mRNA isoforms in cell bodies with non-affinity or lower affinity to miR-126a-5p (Fig. 4h). Thus, our observations reveal a population of muscle-derived miRNAs with unique compartmentalization to NMJs, suggesting that at least part of these may participate in regulating presynaptic mRNA translation. Specifically, we identified the EV-localized and NMJ-localized miR-126a-5p as a potential suppressor of presynaptic TDP-43 translation.

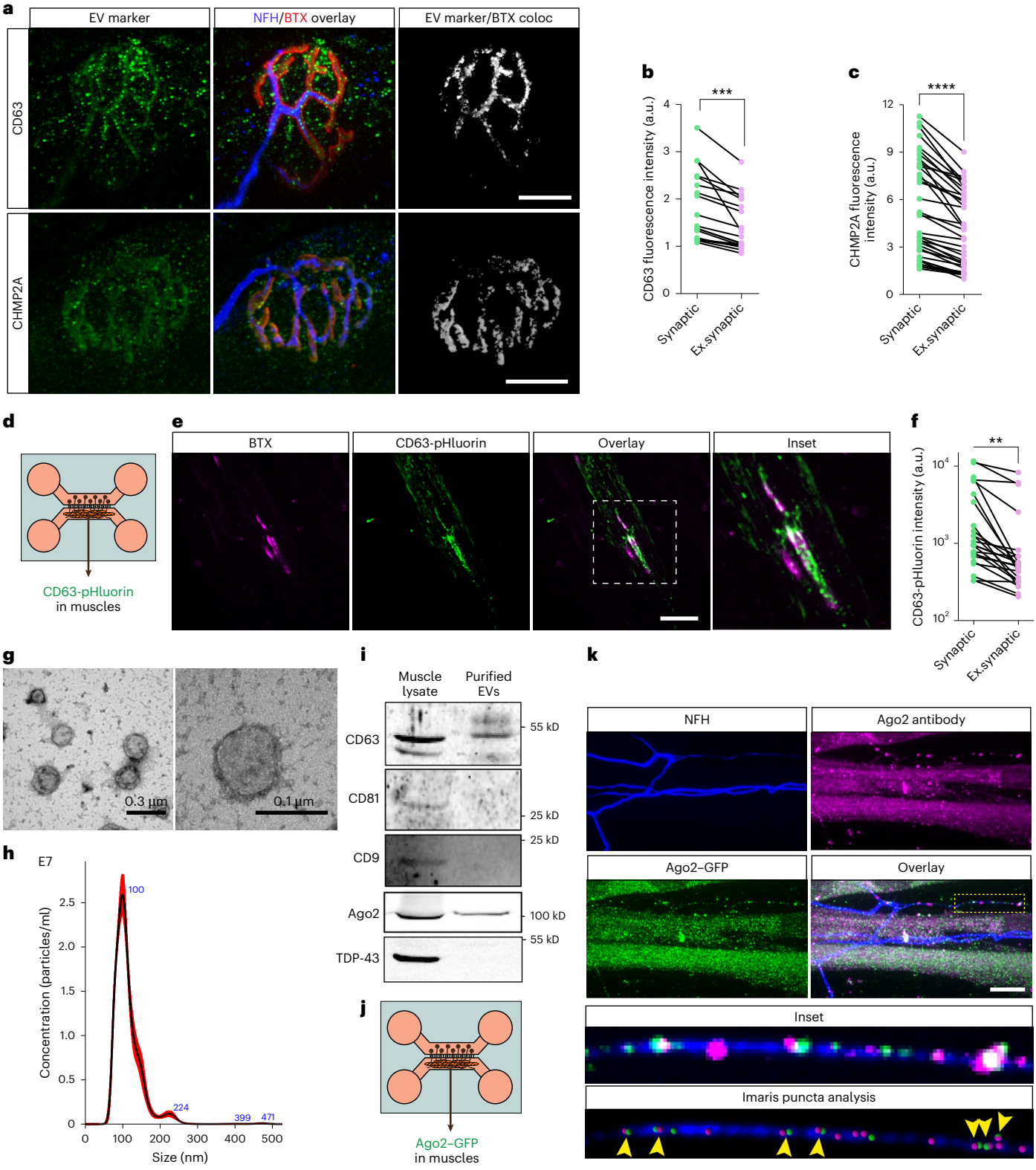

https://doi.org/10.1038/s41593-025-02062-6

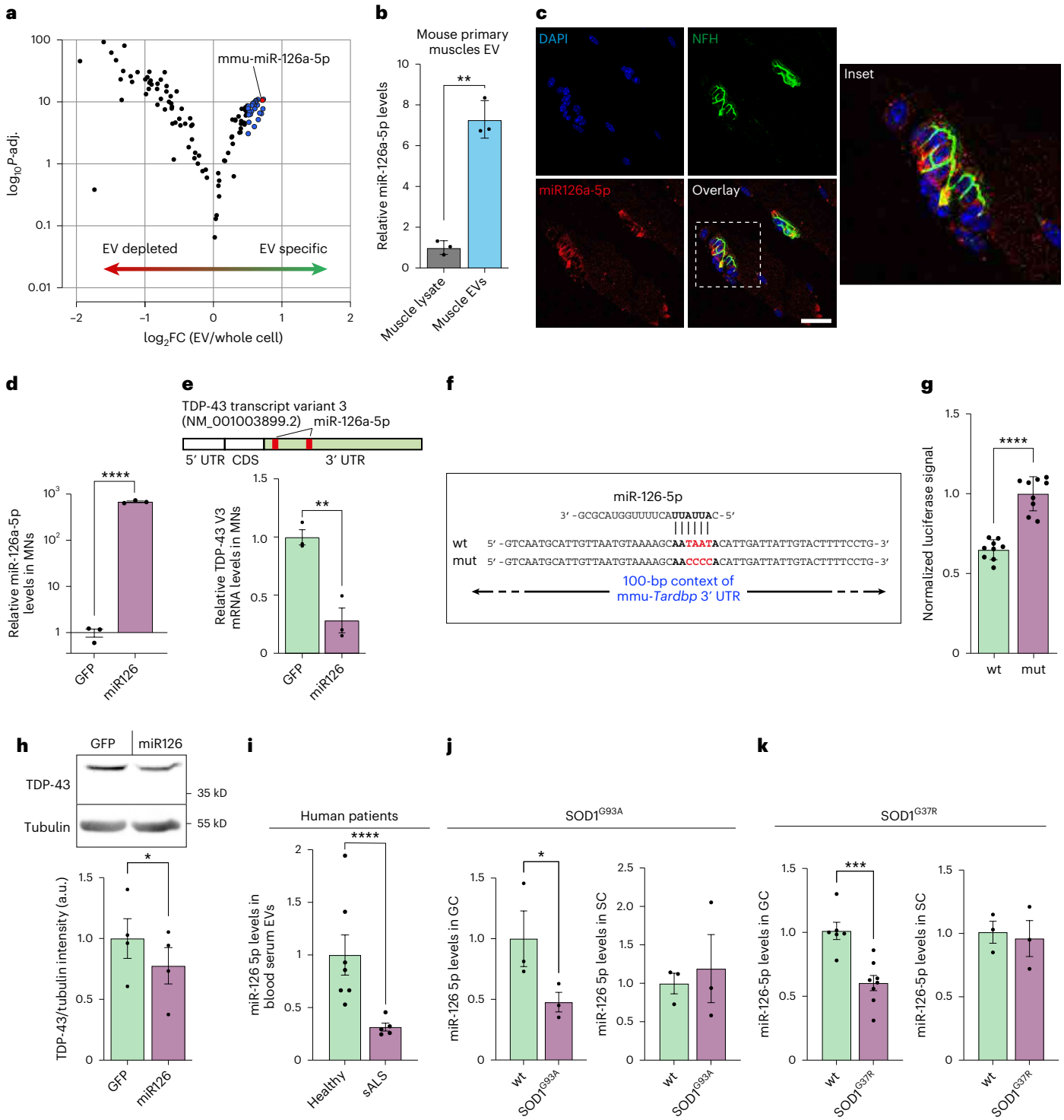

Deregulation of miR-126 in patients with ALS and SOD1 models

Our data imply that miR-126a-5p is a potent muscle-derived repressor of TDP-43. Considering its unique NMJ compartmentalization, its enrichment in EVs and the observed effect of muscles over TDP-43 synthesis in NMJs, we sought to determine whether alterations in miR-126-5p levels could potentially increase the local synthesis of TDP-43 in NMJs of ALS models. Indeed, our previous studies revealed deregulation of miR-126a-5p in both SOD1^{G93A} and TDP-43^{A315T} models of ALS[27,35].

We assessed the levels of miR-126-5p in ALS patient-derived serum EVs as an indication of its state in muscles, as also previously reported for other myomiRs[38]. We found an approximately threefold reduction in the relative abundance of miR-126-5p in patients with sALS compared to healthy donors (Fig. 4i). Due to the local accumulation of TDP-43 in peripheral nerves of SOD1 mice models (Fig. 1 and Extended Data Fig. 1), we examined the abundance of miR-126a-5p in the spinal cords and gastrocnemius muscles of SOD1^{G93A} and SOD1^{G37R}. In both mutant SOD1 models, the levels of miR-126a-5p were specifically reduced in the muscles of SOD1 mutants yet remained unaffected in their spinal cords (Fig. 4j,k and Extended Data Fig. 7g). Because we identified that miR-126a-5p is compartmentalized to NMJs, we further inspected if its low expression in mutant SOD1 muscles also reflects its presence in NMJs. Indeed, miR-126a-5p FISH in EDL NMJs of presymptomatic (postnatal day 60 (P60)) SOD1^{G93A} mice and their littermates revealed a profound reduction, specifically in NMJs (Extended Data Fig. 7h,i). Overall, these data

Fig. 4 | Local deregulation of EV-loaded miR-126a-5p in NMJs may directly regulate TDP-43 expression. a, Volcano plot of small RNA-seq from muscle-derived EVs and whole-cell lysates of muscle cultures. Data are shown as $\log_2$FC of EV miRNAs over whole-cell lysates. Blue dots indicate miRNA with $\log_2$FC > 0.5 and $-\log_{10}$*P*adj > 2. *n* = 3 cultures/isolated EVs. Wald test with correction for multiple comparisons. **b**, Quantitative TaqMan RT–PCR for miR-126a-5p in whole-cell muscle lysates versus muscle-derived EVs. *n* = 3 cultures/isolated EVs. $^{**}P = 0.0073$. **c**, Representative images of miR-126a-5p FISH in NMJs of EDL muscles. Scale bar, 10 µm. **d**, TaqMan RT–qPCR analysis of miR-126a-5p levels in GFP-infected and miR-126-infected primary MNs. U6 was used as loading control. *n* = 3 neuronal cultures. $^{****}P = 0.000014$. **e**, Top, scheme of TDP-43 transcript variant 3 mRNA with marking of the approximate location of two miR-126a-5p binding sites. Bottom, RT–qPCR for mmu-*Tardbp* transcript variant 3 in primary MNs infected with either empty GFP backbone or miR126–GFP vector. *n* = 3 neuronal cultures. $^{**}P = 0.0046$. **f**,**g**, Scheme and quantitative analysis (**g**) of dual-luciferase assay for miR-126a-5p and mmu-*Tardbp* mRNA interaction. One hundred base pairs (bp) of the 3′ UTR of mmu-*Tardbp* mRNA, including one miR-126a-5p (wt) or a mutant miR-126a-5p (mut), were inserted into dual-luciferase reporter plasmid. *n* = 9 replicates from three repeats. $^{****}P = 2.46 \times 10^{-7}$. **h**, Representative images and quantification of western blots for TDP-43 (43 kD) in primary MNs infected with GFP or with miR126–GFP vector. Tubulin (55 kD) was used as loading control. *n* = 4 neuronal cultures. $^{*}P = 0.0258$. **i**, TaqMan RT–qPCR analysis for miR-126-5p in serum-derived EVs of patients with sALS (*n* = 7) and healthy controls (*n* = 5). $^{****}P = 0.000019$. **j**,**k**, TaqMan RT–qPCR for miR-126-5p in P60 $SOD1^{G93A}$ GC muscles and P60 $SOD1^{G93A}$ SC (**j**) and P357 $SOD1^{G37R}$ GC muscles and P357 $SOD1^{G37R}$ SC (**k**). U6 was used as loading control. *n* = 3 (SC), *n* = 3 (**j**; GC) and *n* = 6–8 (**k**; GC) mice in each group. One-tailed (**j**; GC) or two-tailed (**j**,**k**) unpaired *t*-test, $^{*}P$ (**j**) < 0.0491, NS (**j**) = 0.6973, $^{***}P$ (**k**) < 0.0004, NS (**k**) = 0.9591. For **b**,**d**,**e**,**h**–**k**, data are shown as the mean ± s.e.m. For **g**, data are shown as the mean ± s.d. For **b**, two-tailed paired Student's *t*-test. For **d**,**e**,**g**,**h**,**i**,**j** (SC),**k**, two-tailed unpaired Student's *t*-test. For **j** (GC), one-tailed unpaired Student's *t*-test. For **c**, images represent eight repeats in mouse muscles. FC, fold change; CDS, coding sequence; GC, gastrocnemius; mut, mutant; NS, not significant; *P*adj, adjusted *P* value; SC, spinal cord; wt, wild-type.

suggest a mechanism that local TDP-43 accumulation is suppressed by muscle-derived mir-126-5p, and this process is disrupted in SOD1 ALS.

Muscle EVs protect NMJs by limiting TDP-43 synthesis

To analyze the effect of muscle-derived EVs containing miR-126a-5p on NMJ integrity and functionality, we first adopted a previously described conditional knockdown (KD) method for Rab27a, a GTPase controlling the release of exosomes from cells[39]. We validated that Rab27a is expressed in skeletal muscles and is present in NMJs (Fig. 5a), and then we used compartmental microfluidic co-cultures to specifically knock down Rab27a in muscles using a doxycycline induction system (Fig. 5b). Western blot and NTA confirmed the induction and function of shRab27a in muscles (Fig. 5c–e). Co-culture analysis revealed an increase in newly synthesized TDP-43 at presynaptic axons upon Rab27a KD in muscles (Fig. 5f,g and Supplementary Fig. 6a,b). Given the central role of TDP-43 in local protein synthesis, we performed a similar experiment using OPP to label total protein synthesis in presynaptic axons and found an overall decrease in axonal protein synthesis (Fig. 5h,i and Supplementary Fig. 6c), resembling our observations in the TDP-43ΔNLS model[13]. Lastly, we assessed the impact of Rab27a KD on NMJ function and integrity. We detected impairment in NMJ function as measured by the percent of contracting innervated muscles (Fig. 5j). Additionally, co-cultures labeled for presynaptic and postsynaptic markers (NFH/BTX) revealed significant NMJ disruption and axon degeneration (Fig. 5k,l). These results were also replicated using the neutral sphingomyelinase inhibitor GW4869, known for its robustness in blocking exosome release[40] (Fig. 5m–p and Supplementary Fig. 6d–f). Notably, GW4869 was demonstrated before to also block the clearance of pathological TDP-43 from cells via exosomes[41]. This, together with our attempt to overexpress TDP-43–eGFP in muscles in co-culture (Supplementary Fig. 7), and its absence in muscle EV fractions, confirms that the main source of axonal TDP-43 in the NMJ is local translation rather than its transmission from muscles. Hence, the inhibition of EV machinery in postsynaptic muscles reduces general presynaptic protein synthesis via increased local expression of axonal TDP-43. Furthermore, prolonged disruption of the EV machinery promoted NMJ dysfunction and degeneration, indicating a vital mode for muscle-derived EV secretion in NMJ maintenance.

miR-126a-5p protects NMJs by repressing TDP-43 synthesis

To ensure that alteration in muscle-derived miR-126a-5p but not general EV secretion is vital for NMJ function, we repeated this set of experiments using an antisense oligonucleotide against miR-126a-5p (miR126i), which sequesters miR-126a-5p in stable heteroduplexes and effectively prevents its binding to endogenous targets[42]. First, the potency of miR126i was validated by transfecting it into primary muscles and performing RT–qPCR for TDP-43 mRNA after 5 days (Fig. 6a). Next, we introduced miR126i specifically to the neuromuscular compartments of co-culture (Fig. 6b; at 5 days in co-culture). Five days later, we found a marked increase in the density of TDP-43 in distal axons within the neuromuscular compartment (Fig. 6c,d). As in the shRab27a-treated and GW4869-treated co-cultures, miR126i led to a significant increase in newly synthesized TDP-43 in presynaptic axons (Fig. 6e,f and Supplementary Fig. 8a,b). This was associated with an increase in presynaptic pTDP-43 (Supplementary Fig. 8c,d), a decrease in overall presynaptic protein synthesis (Fig. 6g,h) and NMJ dysfunction and degeneration (Fig. 6i–k). Altogether, these observations indicate

Fig. 5 | Muscle EVs preserve NMJ integrity by regulating TDP-43 synthesis. **a**, Representative images of Rab27a in NMJs. Top, NMJ markers; bottom, co-localization of Rab27a with BTX (yellow). Scale bar, 10 µm. **b**, Experimental setup in **c** and **d**. Tet-On shRNA-Rab27 vectors were transfected into primary muscles that were co-cultured in MFCs with primary MNs. At co-culture day 5, doxycycline was added to the muscle compartment. TRE, tetracycline responsive element. **c**, Representative western blot and quantificaton of Rab27a (29 kD) in primary muscles transfected with Tet-On shRNA-Rab27 +/− doxycycline. Tubulin was used as a loading control. *n* = 3 muscle cultures. $^{**}P < 0.0016$. **d**, Representative NTA histograms comparing size distribution of EVs from Tet-On shRNA-Rab27a transfected primary muscles +/− doxycycline. **e**, NTA particle concentrations analysis in the EVs above. $^{****}P = 2.43 \times 10^{-7}$. *n* = 4 EV preparations from four muscle cultures. **f**,**g**, Representative images and quantification of TDP-43 puro-PLA in presynaptic axons in co-cultures with Tet-On shRNA-Rab27a-expressing muscles +/− doxycycline. TDP-43 puro-PLA–NFH co-localization is shown in gray (right). Scale bar, 10 µm. *n* = 151, 140 NMJs. $^{****}P = 4.2 \times 10^{-14}$. **h**,**i**, Representative images and quantification of OPP labeling in Tet-On shRNA-Rab27a co-cultures +/− doxycycline. OPP–NFH co-localization is shown in gray (right). Scale bar, 10 µm. *n* = 61, 25 NMJs $^{****}P = 9.75 \times 10^{-6}$. **j**, Percent of contracting innervated muscles in Tet-On shRNA-Rab27a co-cultures +/− doxycycline. *n* = 9, 9, 5 co-cultures. $^{***}P = 0.0004$, NS = 0.7059. **k**,**l**, Representative images and quantification of NMJ disruption in Tet-On shRNA-Rab27a co-cultures +/− doxycycline. Scale bar, 10 µm. *n* = 4 co-cultures. $^{**}P = 0.0010$. **m**, Representative NTA histogram comparing size distribution of EVs from primary muscles cultured in the presence of 10 µM GW4869 or DMSO in the culture media. **n**, NTA particle concentration analysis in the EVs above. *n* = 3 EV preparations from three muscle cultures $^{****}P = 1.28 \times 10^{-6}$. **o**, Analysis of TDP-43 puro-PLA in presynaptic axons in DMSO-treated versus GW4860-treated (10 µM) co-cultures. *n* = 128, 131 NMJs $^{****}P = 3.5 \times 10^{-8}$. **p**, Analysis of OPP labeling in DMSO-treated versus GW4860-treated (10 µM) co-cultures. *n* = 94, 95 NMJs $^{****}P = 4.3 \times 10^{-10}$. For **d**,**e**,**i**,**m**,**n**,**p**, data are shown as the mean ± s.d., repeated in three independent repeats. For **c**,**j**,**l**, data are shown as the mean ± s.e.m., repeated in three independent repeats. For **g**,**o** data are shown in violin density plots with markings of first, median and third quartiles, repeated in three independent repeats. For **b**,**c**,**e**,**g**,**i**,**l**,**n**–**p**, two-tailed unpaired Student's *t*-test. For **j**, one-way ANOVA with Holm–Sidak correction for multiple comparisons. coloc, co-localization; Dox, doxycycline; NS, not significant.

https://doi.org/10.1038/s41593-025-02062-6

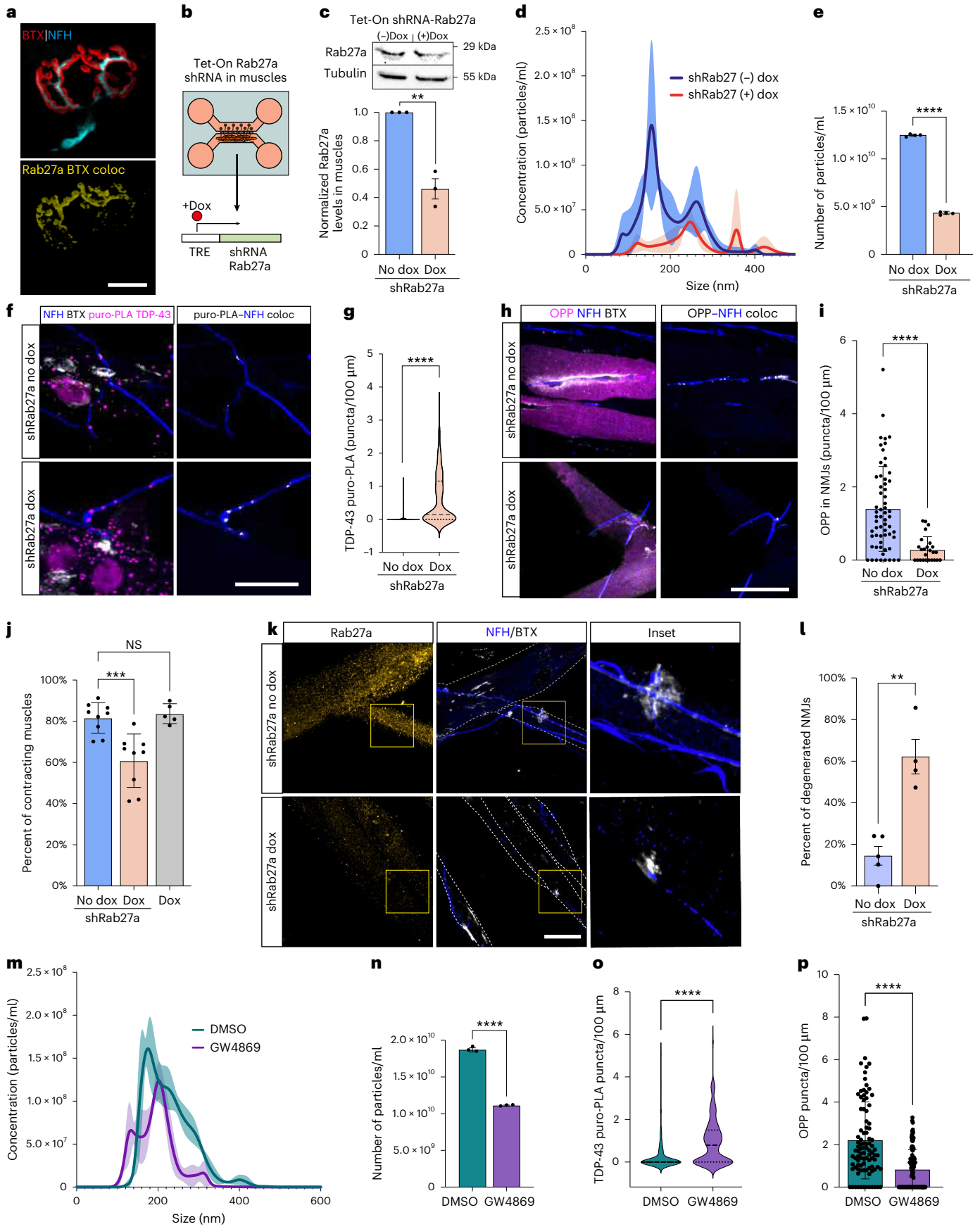

https://doi.org/10.1038/s41593-025-02062-6

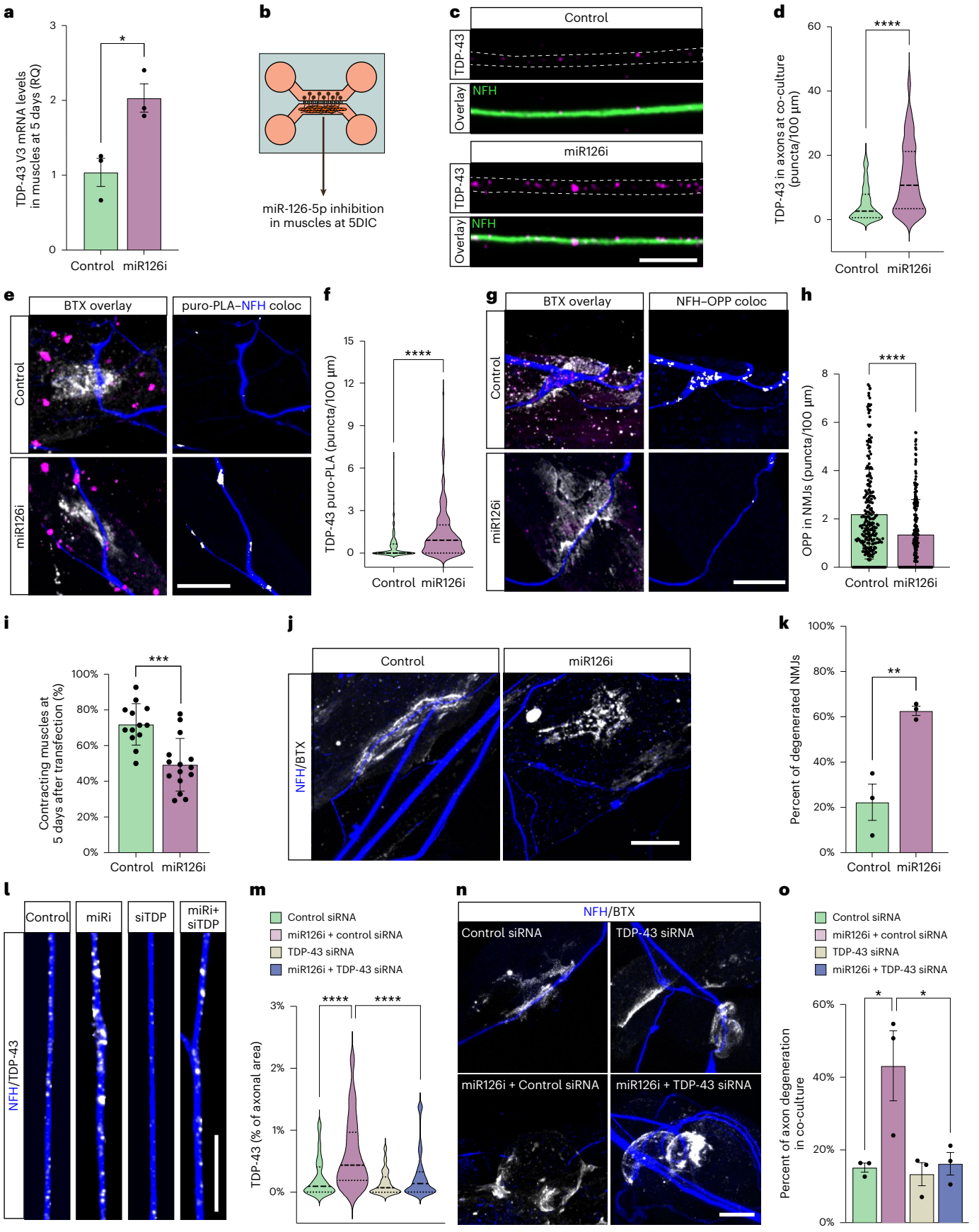

Fig. 6 | Postsynaptic miR-126a-5p preserves NMJ integrity via regulation of TDP-43 expression in axons. a, RT-qPCR for TDP-43 mRNA in primary muscles 5 days after miR126i treatment. GAPDH was used as loading control. RQ, relative quantification. $n = 3$ cultures $^{*}P = 0.0203$. **b**, Illustration of experimental setup in **c**–**k**. Neuromuscular compartment in co-cultures was exclusively transfected at day 5 with miR126i. **c**,**d**, Representative images and analysis of TDP-43 density (puncta/100 µm) in axons within the neuromuscular compartment in control versus miR126i-treated co-cultures 5 days after transfection. Scale bar, 5 µm. $n = 222, 216$ axons. $^{****}P < 1 \times 10^{-15}$. **e**,**f**, Representative images and quantification of TDP-43 puro-PLA signal in presynaptic axons in control and miR126i-treated co-cultures. White indicates TDP-43 puro-PLA–NFH co-localization (right). Scale bar, 10 µm. $n = 62, 80$ NMJs. $^{****}P = 3.39 \times 10^{-13}$. **g**,**h**, Representative images and quantification of OPP labeling in control and miR126i-treated co-cultures. White indicates OPP–NFH co-localization (right). Scale bar, 10 µm. $n = 259, 212$ NMJs $^{****}P = 1.12 \times 10^{-7}$. **i**, Percent of contracting innervated muscles in control and miR126i-treated co-cultures. $n = 13, 15$ co-cultures. $^{***}P = 0.00014$. **j**,**k**, Representative image and quantification of NMJ disruption in control and miR126i-treated co-cultures. Scale bar, 10 µm. $n = 13, 15$ microfluidic co-cultures. $^{**}P = 0.0084$. **l**,**m**, Representative images and quantification of axonal TDP-43 density in control-siRNA-treated or TDP-43-siRNA-treated co-cultures in presence/absence of miR126i. Scale bar, 10 µm. $n = 96, 89, 70, 73$ axons. Control siRNA versus miR126i+control siRNA: $^{****}P = 4.15 \times 10^{-10}$; miR126i+control siRNA versus miR126i+TDP-43 siRNA: $^{****}P = 1.05 \times 10^{-7}$. **n**, Representative images of NMJs in control-siRNA-treated or TDP-43-siRNA-treated co-cultures in presence/absence of miR126i. Scale bar, 10 µm. **o**, Percent of axon degeneration in co-cultures treated as described above. $n = 3$ co-cultures. Control siRNA versus miR126i+control siRNA: $^{*}P = 0.0296$; miR126i+control siRNA versus miR126i+TDP-43 siRNA: $^{*}P = 0.0296$. For **h**,**l**, data are shown as the mean ± s.d., repeated in three independent repeats. For **a**,**k**,**o**, data are shown as the mean ± s.e.m., repeated in three independent repeats. For **d**,**f**,**m**, data are shown in violin density plots with markings of first, median and third quartiles, repeated in three independent repeats. For **a**,**d**,**f**,**h**,**i**,**k**, two-tailed unpaired Student's *t*-test. For **m**,**o**, one-way ANOVA with Holm–Sidak correction for multiple comparisons. In **e**–**o**, miR126i or siRNA was administered exclusively to the neuromuscular compartment. coloc, co-localization.

that muscle-derived EV-loaded miR-126a-5p maintains NMJ integrity and function. Because miR-126 may silence the translation of other presynaptic mRNAs, such as NRP1 (ref. 35), we aimed to investigate whether TDP-43 synthesis is essential for the NMJ disruption caused by miR-126-5p inhibition. To test this, we repeated the miR-126-5p inhibition experiment while simultaneously applying it with TDP-43 siRNAs, control siRNA or TDP-43 siRNAs alone. The inclusion of TDP-43 siRNAs in the axons completely prevented both the accumulation of axonal TDP-43 and the subsequent degeneration induced by miR-126 inhibition (Fig. 6l–o and Supplementary Fig. 8e), suggesting that, indeed, miR-126 acts upon TDP-43. Thus, the loss of miR-126-5p facilitates local translation and accumulation of TDP-43 in presynaptic axons, which is sufficient to drive axon degeneration.

miR-126 protects motor function in SOD1^{G93A} mice via TDP-43

Overexpression of miR-126 in SOD1^{G93A} muscles can delay NMJ disruption and improve motor function in vivo[35]. miR-126a-5p levels decrease in axons of SOD1 and TDP-43 mutants[27]. Therefore, we used a lentivirus to overexpress miR-126 in primary MNs (Extended Data Fig. 8a–c) and in co-cultures of MNs expressing SOD1 (Fig. 7a and Extended Data Fig. 8d). Co-culture analysis of the percent of contracting muscles revealed NMJ dysfunction in this ALS model, which was prevented by the overexpression of miR-126 (Fig. 7b). To test the effect of mir-126a-5p in vivo, we introduced PHP.eB adeno-associated virus (AAV) particles expressing miR-126–GFP to the central nervous system via retro-orbital injections and to one gastrocnemius muscle at a single timepoint to presymptomatic (P60) SOD1^{G93A} and littermate mice. As a control, we used GFP PHP.eB AAV particles (Fig. 7c and Extended Data Fig. 9a–c). CatWalk gait analysis performed at two timepoints of the disease—symptomatic and late symptomatic (P90 and P130, respectively)—revealed complete preservation of motor functions in the miR-126-injected SOD1^{G93A} mice as indicated by their stand duration, run duration and the percent of base of support on four limbs (Fig. 7d and Extended Data Fig. 9d,e). Furthermore, visual assessment of the hindlimb splay reflex showed no defects in this ability in the miR-126-injected SOD1^{G93A} mice versus the GFP-injected ones (Extended Data Fig. 9f,g). Notably, quantitative three-dimensional co-localization analysis in the NMJs of these mice at their endstage showed a marked reduction in pTDP-43 in presynaptic axons within the still intact NMJs (Fig. 7e,f). Notwithstanding these results, tracking the weight and survival of these mice for longer periods did not unveil a positive outcome over these parameters (Extended Data Fig. 9h,i). Analyzing the expression of miR-126a-5p in the injected gastrocnemius at the endstage of these mice revealed that the overexpression was not sufficient to overcome miR-126-5p deficiency (Fig. 7g). Altogether, these observations provide in vivo proof of concept that miR-126 targets TDP-43 accumulation in SOD1^{G93A} axons and NMJs. However, achieving survival effect likely requires more consistent and robust infection.

miR-126 prevents TDP-43 toxicity in human ALS models

Human iPSC-derived models might offer potential advantages over rodent models for ALS research, providing a more accurate

Fig. 7 | miR-126 overexpression preserves motor functions in ALS models via regulation of presynaptic TDP-43 expression. a, Illustration of experimental setup in **b**. GFP-infected or miR-126–GFP-infected primary MNs were co-cultured with primary skeletal muscles. **b**, Percent of contracting muscles at tenth day of co-culture. $n = 23, 23, 21, 13$ co-cultures, NS = 0.3070, $^{**}P = 0.0026$, $^{****}P = 1.54 \times 10^{-6}$, NS = 0.307. **c**, Illustration of experimental setup for **d**–**g**. SOD1^{G93A} and littermate mice (P60) were injected with PHP.eB miR126–GFP or GFP-only AAV retro-orbitally and to the right gastrocnemius muscle. Bottom, representative image of an NMJ in the left gastrocnemius muscle of littermate miR126–GFP-injected mouse. Scale bar, 10 µm. **d**, Run duration analysis for GFP-infected and miR126–GFP-infected WT and SOD1^{G93A} mice at P90 and P130. $n = 8$ mice in each group. WT+GFP versus SOD1^{G93A}+GFP $^{*}P = 0.0193$, SOD1^{G93A}+GFP versus SOD1^{G93A}+miR126 $^{*}P = 0.0287$; P130: WT+GFP versus SOD1^{G93A}+GFP $^{*}P = 0.0172$, SOD1^{G93A}+GFP versus SOD1^{G93A}+miR126 $^{*}P = 0.0359$. **e**,**f**, Representative images and quantification of pTDP-43 in presynaptic axons in NMJs of GFP-infected and miR-126–GFP-infected SOD1^{G93A} mice at disease endstage. White indicates pTDP-43–NFH three-dimensional co-localization (rightmost). Scale bar, 10 µm. $n = 24, 31$ NMJs. $^{****}P = 2 \times 10^{-6}$. **g**, miR-126a-5p RT–qPCR in right gastrocnemius muscles of GFP-treated and miR-126-treated SOD1^{G93A} compared to littermate–GFP-treated muscles. $^{**}P = 0.0028$, NS = 0.3570. **h**,**i**, Representative images and analysis of pTDP-43 density in distal axons of pLV-hSyn–GFP-infected or pLV-hSyn-miR126–GFP-infected SOD1^{A5V} iPSC–MN co-cultures with SOD1^{A5V} iPSC-muscles expressing similar plasmids under CMV promoter. Scale bar, 5 µm. $n = 18, 24$ images. $^{**}P = 0.0082$. **j**,**k**, Representative images and analysis of axonal degeneration index in the neuromuscular compartment of SOD1^{A5V} co-cultures expressing the above vectors. Scale bar, 20 µm. $n = 19, 25$ $^{****}P = 6 \times 10^{-12}$. **l**,**m**, Representative images and analysis of pTDP-43 density in distal axons TDP-43^{M337V} iPSC-derived MN-muscle co-cultures expressing the same vectors. Scale bar, 5 µm. $n = 26, 36$ images. $^{****}P = 7.88 \times 10^{-9}$. **n**,**o**, Representative images and analysis of axonal degeneration index within the distal compartment of above TDP-43^{M337V} co-cultures. Scale bar, 20 µm. $n = 24, 36$ $^{****}P = 1.16 \times 10^{-7}$. For **f**,**j**,**o**, data are shown as the mean ± s.d., repeated in three mice per genotype or three independent repeats. For **b**,**d**,**g**, data are shown as the mean ± s.e.m., repeated in three mice per genotype. For **i**,**m**, data are shown in violin density plots with markings of first, median and third quartiles, repeated in three independent repeats. For **d** (P90), multiple unpaired one-tailed Student's *t*-tests. For **f**,**g**,**i**,**k**,**m**,**o**, two-tailed unpaired Student's *t*-test. For **b**,**d** (P130), one-way ANOVA with Holm–Sidak correction. LV, lentivirus; NS, not significant; s, seconds; WT, wild-type.

https://doi.org/10.1038/s41593-025-02062-6

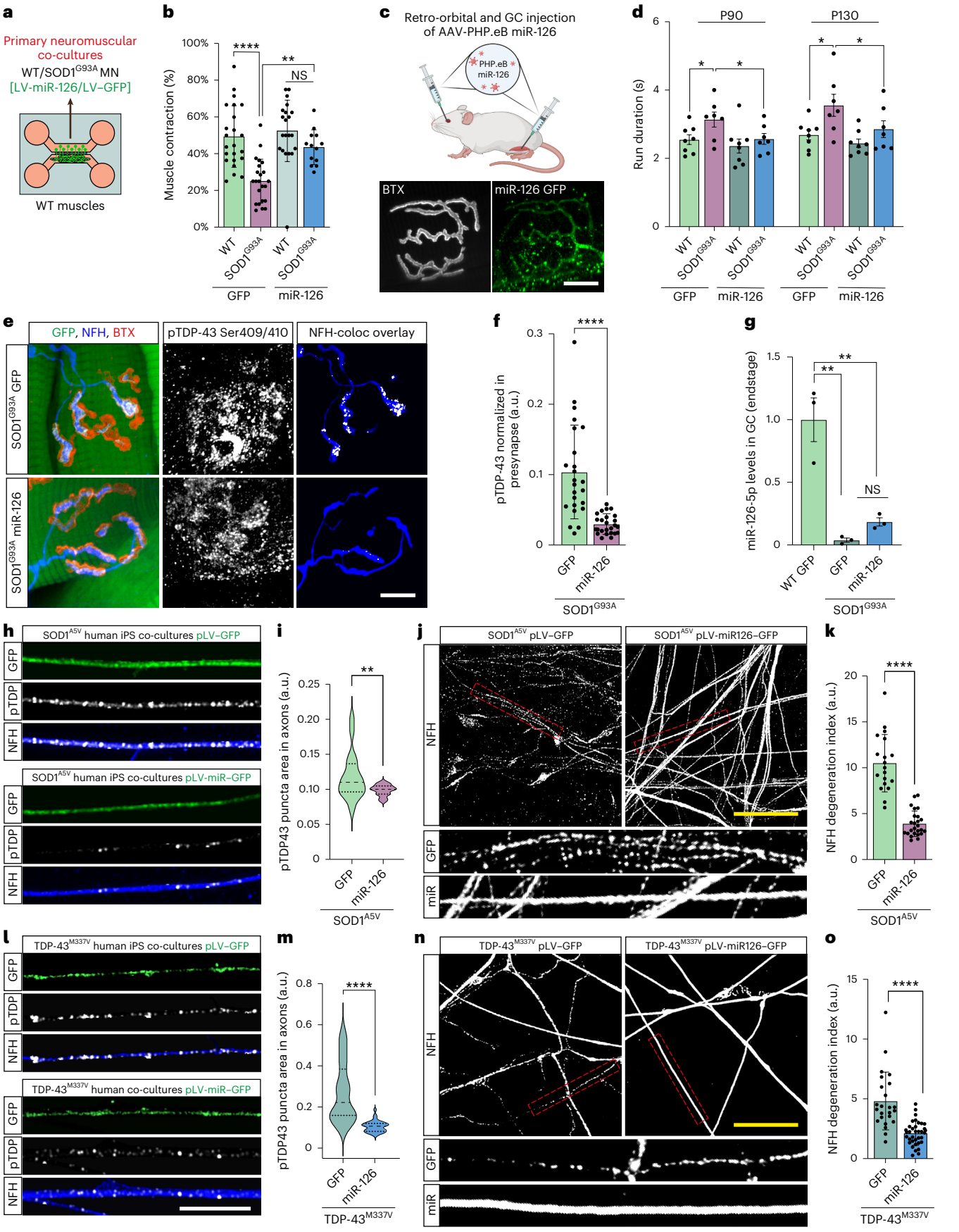

https://doi.org/10.1038/s41593-025-02062-6

representation of human disease mechanisms and phenotypes that are absent in mice. To better replicate the human neuromuscular environment, we used a human motor unit model of iPSC-derived neuromuscular co-cultures growing in a compartmental chamber. The effect of miR-126 on axonal TDP-43 accumulation and degeneration was tested on iPSC co-cultures carrying SOD1^{A5V} and TDP-43^{M337V} mutations that exhibit these pathologies (Extended Data Fig. 10a–c). iPSC-derived MNs and muscle cells were infected with lentiviral vectors expressing either GFP or miR-126–GFP (Extended Data Fig. 10d,e). Expression of miR-126 significantly reduced pTDP-43 accumulation along axons and protected against degeneration in the ALS mutant co-cultures (Fig. 7h–o). Together, these findings identify miR-126 as a suppressor of axonal TDP-43 accumulation also in human models and highlight its potential role for mitigating TDP-43 pathology and associated neurodegeneration in ALS.

In summary, our study identifies miR-126-5p as a key limiter of axonal TDP-43 accumulation and its toxic effects in ALS. We demonstrate that miR-126-5p controls local protein synthesis at NMJs, which is crucial for its maintenance. Disruption of this mechanism leads to NMJ degeneration in ALS. These findings highlight the role of muscle-derived EV-loaded miRNAs in NMJ function and suggest that modulating miR-126-5p expression could offer a potential therapeutic strategy to prevent NMJ degeneration in ALS.

Discussion

Despite the crucial role of TDP-43 in ALS pathology, the way it accumulates along axons and NMJs was unknown. Here we establish the basis for the presence of TDP-43 pathology in peripheral nerves and NMJs in ALS SOD1 mutants. We uncover a novel communication pathway between muscles and axons that governs the accumulation of presynaptic TDP-43 and regulates NMJ integrity. Intriguingly, we found that this accumulation is induced by the local synthesis of TDP-43 at NMJs, a process that is regularly restrained by miR-126a-5p EVs derived from muscles (Fig. 8). These observations align with our previous identification of a novel ALS mechanism, wherein TDP-43 accumulates within axons, sequesters RNA and inhibits local protein synthesis. This process triggers mitochondrial dysfunction, disrupts NMJs and leads to degeneration[13].

This newly discovered communication pathway profoundly influences NMJ stability at individual synapses, providing crucial insights into how an NMJ independently adjusts its protein profile in response to changing conditions. This supports the notion that TDP-43 condensates along axons can govern spatiotemporal signaling and metabolic processes[43–46]. Such regulation relies on precise control over local protein synthesis, enabling neurons to respond spatially restricted and time sensitive to environmental changes while maintaining axon and synapse homeostasis[47,48]. Anomalies within axonal TDP-43 condensates make neurons more susceptible to local stress, affecting their ability to regenerate, ultimately culminating in neurodegeneration. Hence, we propose this as a dynamic process regulated at the single-synapse level through the localized synthesis of TDP-43.

Our observations point to a local accumulation of TDP-43 in NMJs and peripheral nerves of SOD1 mice without apparent cytoplasmic mislocalization in spinal MNs. Indeed, we identified local deregulation of miR-126a-5p in SOD1 models in muscles and specifically in its NMJ localization, whereas its expression remains unchanged in the spinal cord.

Still, we detected reduced miR-126-5p levels in blood serum EVs of a small cohort of patients with sALS. Skeletal muscle-derived miRNAs were previously recorded in circulating exosomes[38,49], suggesting that the observed reduction in serum miR-126-5p in patients reflects the expression of this miRNA in skeletal muscles. Notably, miR-126a-5p expression might mirror the condition of TDP-43 accumulation in tissues, thus suggesting the involvement of miR-126a-5p in the pathogenesis of additional non-SOD1 ALS cases. Future studies in larger patient groups will have to validate this finding and may serve as a basis for using miR-126a-5p as a biomarker.

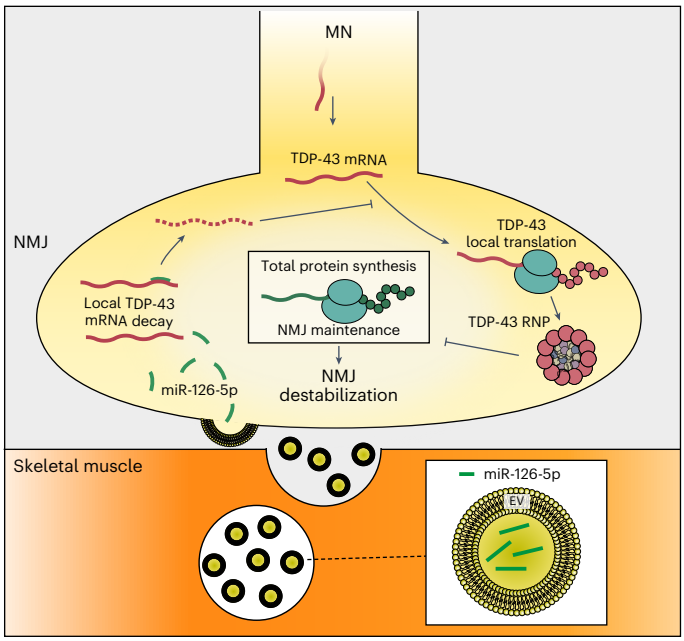

Fig. 8 | Graphical abstract. Local protein synthesis in presynaptic motor axons is a key process essential for the function, maintenance and survival of NMJs. To function properly, local protein synthesis depends on mRNA availability, which is controlled by anterograde axonal transport and local ribonucleoproteins. We identified that muscle-derived miR-126a-5p is enriched in NMJs and regulates the translation of TDP-43 mRNA in presynaptic axons through EVs. Deregulation of muscle-derived miR-126a-5p releases the inhibition of TDP-43 mRNA, leading to its local translation and accumulation in the presynaptic axon, thereby facilitating NMJ disruption via TDP-43-mediated local translation arrest.

Local synthesis of TDP-43 in motor axons and NMJs

In this study, we report, to our knowledge for the first time, that TDP-43 mRNA is distributed into axons where it can be locally translated. TDP-43 is a major regulator of the axonal transcriptome, primarily by binding and shuttling mRNAs, including its own mRNA[10–12,50–52]. We previously identified Elavl2 (also known as HuB) transcripts in MN axons, of which expression is altered upon SOD1^{G93A} and TDP-43^{A315T} overexpression[27]. Interestingly, Elavl2 mRNA is also a predicted target of miR-126a-5p. Recently, the RNA-binding protein (RBP) Khsrp was reported to locally translate in axons upon nerve injury and, thus, to regulate local RNA pools[53]. Additionally, the same report indicated that the levels of several other RBPs increase upon injury, suggesting that local translation is a common origin of several axonal RBPs. Moreover, transcriptome analysis of microdissected ventral roots highlighted the ribonucleoprotein complex mRNAs group as one of the axonal-enriched cellular components mRNA[54]. Hence, the discovery of TDP-43 local translation may mark only a drop within a larger pool of axonal RBPs and RNA regulators awaiting characterization.

Synaptic miRNA-loaded EVs as a new mode of local synthesis control

Previous studies, including ours, highlighted the crucial role of local protein synthesis in preserving synaptic function, integrity, plasticity and mitochondrial health[13,55–57]. This process relies on mRNA continuously moving into axons and synapses[20,58–60]. However, understanding of how specific transcripts are precisely translated or silenced at individual synapses with high spatiotemporal precision remains limited. Previous studies established glia–axon communication through miRNA-loaded and ribosome-loaded exosomes that promotes neuronal growth and response to injury[61–63].

The synaptic transmission of miR-126a-5p, which limits the presynaptic synthesis of TDP-43, represents a new mode of local

communication between postsynaptic muscles and presynaptic axons in the form of RNA-loaded EVs. However, several more miRNAs are potentially also compartmentalized in postsynaptic muscle EVs. MicroRNAs are master regulators of translation, having the potency to target and silence tens to hundreds of transcripts[64]. With respect to the axonal transcriptome and the existence of axonal-specific 3′ UTR variants[65–67], our findings suggest that muscle-derived miRNAs can coordinate complex synaptic processes. Such a mode of local regulation would explain how MNs can respond precisely and timely to changes within each of its numerous presynaptic terminals while avoiding global transcriptome modifications. Indeed, miR-126-5p can silence several ALS-related genes associated with key metabolic and signaling pathways essential for spatiotemporal neuronal homeostasis (Extended Data Fig. 7b and Supplementary Table 3), whereas alterations in these genes can propagate neurodegeneration. Moreover, previous studies revealed that miR-126-5p regulates semaphorins, neuropilins[35,68] and caspase-3 (ref. 69), which, in combination with our current observations, suggests that, like neurotrophins, miR-126-5p routine transmission is neuroprotective, whereas disruption in its transmission, whether controlled or pathological, may orchestrate synapse destabilization or elimination by alleviating transcript inhibition of several transcripts and controlling various synaptic processes (that is, TDP-43 mitochondria and energy homeostasis, neuropilin 1 cytoskeleton, etc.). Notwithstanding, blocking TDP-43 synthesis in axons using siRNA halts the neurodegeneration in co-cultures treated with miR-126-5p inhibitor, suggesting that accumulation of axonal TDP-43 alone is sufficient to drive NMJ disruption and axon degeneration. Future research will focus more in depth on the multilevel regulation of synaptic miR-126a-5p as well as establish the function of other miRNAs in NMJs.

Limitations and future directions

Several limitations must be acknowledged. First, the cohort size of patients with ALS, and specifically of mutant SOD1 biopsies, was limited in demonstrating both the decrease in miR-126a-5p exosomes and the accumulation of axonal TDP-43 pathology. Larger patient cohorts are needed to validate these findings and better understand the variability in miR-126 expression and its impact on NMJ integrity. Additionally, although we identified the pathological accumulation of TDP-43 at the presynapse, TDP-43 is accumulated at the NMJs and also in other neighboring cells, such as Schwann cells. This process remains unexplored. Future studies should investigate the biology and role of TDP-43 in these non-neuronal cells and their potential involvement in NMJ pathology. Another limitation lies in the mode of miR-126a-5p delivery used in our study. Although we demonstrated neuroprotective effects using overexpression strategies, developing clinically viable delivery methods for miR-126a-5p in vivo remains a challenge. Optimizing targeted delivery systems, such as modified exosomes or nanoparticle-based carriers, could enhance the translational potential of this therapeutic approach.

Altogether, we demonstrate the contribution of localized transcellular delivery from muscle to neuron of miR-126-5p to the accumulation of axonal and presynaptic TDP-43 in ALS. This discovery strengthens previous studies underlining the physiological and pathogenic role of early TDP-43 accumulation in peripheral nerves to the progression of ALS and opens new avenues for both understanding ALS disease etiology and therapy development. Our results implicate EV-loaded miRNAs as central players in the maintenance of NMJ integrity, laying the foundation for further exploration of exosome-mediated intercellular communication in human physiology.

Online content

Any methods, additional references, Nature Portfolio reporting summaries, source data, extended data, supplementary information, acknowledgements, peer review information; details of author contributions and competing interests; and statements of data and code availability are available at https://doi.org/10.1038/s41593-025-02062-6.

References

1. Peters, O. M., Ghasemi, M. & Brown, R. H. Emerging mechanisms of molecular pathology in ALS. *J. Clin. Invest.* **125**, 1767–1779 (2015).
2. Fischer, L. R. et al. Amyotrophic lateral sclerosis is a distal axonopathy: evidence in mice and man. *Exp. Neurol.* **185**, 232–240 (2004).
3. Frey, D. et al. Early and selective loss of neuromuscular synapse subtypes with low sprouting competence in motoneuron diseases. *J. Neurosci.* **20**, 2534–2542 (2000).
4. Moloney, E. B., de Winter, F. & Verhaagen, J. ALS as a distal axonopathy: molecular mechanisms affecting neuromuscular junction stability in the presymptomatic stages of the disease. *Front. Neurosci.* **8**, 252 (2014).
5. Taylor, J. P., Brown, R. H. & Cleveland, D. W. Decoding ALS: from genes to mechanism. *Nature* **539**, 197–206 (2016).
6. Neumann, M. et al. Ubiquitinated TDP-43 in frontotemporal lobar degeneration and amyotrophic lateral sclerosis. *Science* **314**, 130–133 (2006).
7. Neumann, M. et al. Phosphorylation of S409/410 of TDP-43 is a consistent feature in all sporadic and familial forms of TDP-43 proteinopathies. *Acta Neuropathol.* **117**, 137–149 (2009).
8. Buratti, E. & Baralle, F. E. The molecular links between TDP-43 dysfunction and neurodegeneration. *Adv. Genet.* **66**, 1–34 (2009).
9. Lagier-Tourenne, C. & Cleveland, D. W. Rethinking ALS: the FUS about TDP-43. *Cell* **136**, 1001–1004 (2009).
10. Alami, N. H. et al. Axonal transport of TDP-43 mRNA granules is impaired by ALS-causing mutations. *Neuron* **81**, 536–543 (2014).
11. Fallini, C., Bassell, G. J. & Rossoll, W. The ALS disease protein TDP-43 is actively transported in motor neuron axons and regulates axon outgrowth. *Hum. Mol. Genet.* **21**, 3703–3718 (2012).
12. Coyne, A. N. et al. FUTSCH/MAP1B mRNA is a translational target of TDP-43 and is neuroprotective in a Drosophila model of amyotrophic lateral sclerosis. *J. Neurosci.* **34**, 15962–15974 (2014).
13. Altman, T. et al. Axonal TDP-43 condensates drive neuromuscular junction disruption through inhibition of local synthesis of nuclear encoded mitochondrial proteins. *Nat. Commun.* **12**, 6914 (2021).
14. Kurashige, T. et al. TDP-43 accumulation within intramuscular nerve bundles of patients with amyotrophic lateral sclerosis. *JAMA Neurol.* **79**, 693–701 (2022).
15. Riva, N. et al. Phosphorylated TDP-43 aggregates in peripheral motor nerves of patients with amyotrophic lateral sclerosis. *Brain* **145**, 276–284 (2022).
16. Perry, R. B. & Fainzilber, M. Local translation in neuronal processes–in vivo tests of a 'heretical hypothesis'. *Dev. Neurobiol.* **74**, 210–217 (2014).
17. Larance, M. & Lamond, A. I. Multidimensional proteomics for cell biology. *Nat. Rev. Mol. Cell Biol.* **16**, 269–280 (2015).
18. Jung, H., Yoon, B. C. & Holt, C. E. Axonal mRNA localization and local protein synthesis in nervous system assembly, maintenance and repair. *Nat. Rev. Neurosci.* **13**, 308–324 (2012).
19. Fellows, A. D., Rhymes, E. R., Gibbs, K. L., Greensmith, L. & Schiavo, G. IGF 1R regulates retrograde axonal transport of signalling endosomes in motor neurons. *EMBO Rep.* **21**, e49129 (2020).
20. Shigeoka, T. et al. Dynamic axonal translation in developing and mature visual circuits. *Cell* **166**, 181–192 (2016).
21. Holt, C. E., Martin, K. C. & Schuman, E. M. Local translation in neurons: visualization and function. *Nat. Struct. Mol. Biol.* **26**, 557–566 (2019).
22. Gershoni-Emek, N., Chein, M., Gluska, S. & Perlson, E. Amyotrophic lateral sclerosis as a spatiotemporal mislocalization disease: location, location, location. *Int. Rev. Cell Mol. Biol.* **315**, 23–71 (2015).

23. Barmada, S. J. Linking RNA dysfunction and neurodegeneration in amyotrophic lateral sclerosis. *Neurotherapeutics* **12**, 340–351 (2015).
24. Fratta, P., Birsa, N., Tosolini, A. P. & Schiavo, G. Travelling together: a unifying pathomechanism for ALS. *Trends Neurosci*. 43, 1–2 (2020).
25. López-Erauskin, J. et al. ALS/FTD-linked mutation in FUS suppresses intra-axonal protein synthesis and drives disease without nuclear loss-of-function of FUS. *Neuron* **100**, 816–830 (2018).
26. Lai, A., Valdez-Sinon, A. N. & Bassell, G. J. Regulation of RNA granules by FMRP and implications for neurological diseases. *Traffic* **21**, 454–462 (2020).
27. Rotem, N. et al. ALS along the axons – expression of coding and noncoding RNA differs in axons of ALS models. *Sci. Rep.* **7**, 44500 (2017).
28. Tom Dieck, S. et al. Direct visualization of identified and newly synthesized proteins in situ. *Nat. Methods* **12**, 411–414 (2015).
29. Ionescu, A., Zahavi, E. E., Gradus, T., Ben-Yaakov, K. & Perlson, E. Compartmental microfluidic system for studying muscle-neuron communication and neuromuscular junction maintenance. *Eur. J. Cell Biol.* **95**, 69–88 (2016).
30. Ionescu, A. & Perlson, E. Microfluidic neuromuscular co-culture system for tracking cell-to-cell transfer and axonal transport of labeled proteins. *Methods Mol. Biol.* **2431**, 145–161 (2022).
31. Valadi, H. et al. Exosome-mediated transfer of mRNAs and microRNAs is a novel mechanism of genetic exchange between cells. *Nat. Cell Biol.* **9**, 654–659 (2007).
32. Verweij, F. J. et al. Quantifying exosome secretion from single cells reveals a modulatory role for GPCR signaling. *J. Cell Biol.* **17**, 1129–1142 (2018).
33. Forterre, A. et al. Myotube-derived exosomal miRNAs downregulate Sirtuin1 in myoblasts during muscle cell differentiation. *Cell Cycle* **13**, 78–89 (2014).
34. McKenzie, A. J. et al. KRAS-MEK signaling controls Ago2 sorting into exosomes. *Cell Rep.* **15**, 978–987 (2016).
35. Maimon, R. et al. Mir126-5p downregulation facilitates axon degeneration and NMJ disruption via a non–cell-autonomous mechanism in ALS. *J. Neurosci.* **38**, 5478–5494 (2018).
36. Hak, K. K., Yong, S. L., Sivaprasad, U., Malhotra, A. & Dutta, A. Muscle-specific microRNA miR-206 promotes muscle differentiation. *J. Cell Biol.* **174**, 677–687 (2006).
37. Abel, O., Powell, J. F., Andersen, P. M. & Al-Chalabi, A. ALSoD: a user-friendly online bioinformatics tool for amyotrophic lateral sclerosis genetics. *Hum. Mutat.* **33**, 1345–1351 (2012).
38. Mytidou, C. et al. Muscle-derived exosomes encapsulate myomiRs and are involved in local skeletal muscle tissue communication. *FASEB J.* **35**, e21279 (2021).
39. Ostrowski, M. et al. Rab27a and Rab27b control different steps of the exosome secretion pathway. *Nat. Cell Biol.* **12**, 19–30 (2010).
40. Trajkovic, K. et al. Ceramide triggers budding of exosome vesicles into multivesicular endosomes. *Science* **319**, 1244–1247 (2008).
41. Iguchi, Y. et al. Exosome secretion is a key pathway for clearance of pathological TDP-43. *Brain* **139(Pt12)**, 3187–3201 (2016).
42. Davis, S., Lollo, B., Freier, S. & Esau, C. Improved targeting of miRNA with antisense oligonucleotides. *Nucleic Acids Res.* **34**, 2294–2304 (2006).
43. Sidibé, H. et al. TDP-43 stabilizes G3BP1 mRNA: relevance to amyotrophic lateral sclerosis/frontotemporal dementia. *Brain* **144**, 3461–3476 (2021).
44. Koehler, L. C. et al. TDP-43 oligomerization and phase separation properties are necessary for autoregulation. *Front. Neurosci.* **16**, 818655 (2022).
45. Piol, D., Robberechts, T. & Da Cruz, S. Lost in local translation: TDP-43 and FUS in axonal/neuromuscular junction maintenance and dysregulation in amyotrophic lateral sclerosis. *Neuron* **111**, 1355–1380 (2023).
46. Ionescu, A., Altman, T. & Perlson, E. Looking for answers far away from the soma—the (un)known axonal functions of TDP-43, and their contribution to early NMJ disruption in ALS. *Mol. Neurodegener.* **18**, 35 (2023).
47. Fernandopulle, M. S., Lippincott-Schwartz, J. & Ward, M. E. RNA transport and local translation in neurodevelopmental and neurodegenerative disease. *Nat. Neurosci.* **24**, 622–632 (2021).
48. Dalla Costa, I. et al. The functional organization of axonal mRNA transport and translation. *Nat. Rev. Neurosci.* **22**, 77–91 (2021).
49. Aoi, W. & Tanimura, Y. Roles of skeletal muscle-derived exosomes in organ metabolic and immunological communication. *Front. Endocrinol. (Lausanne)* **12**, 697204 (2021).
50. Briese, M. et al. Loss of Tdp-43 disrupts the axonal transcriptome of motoneurons accompanied by impaired axonal translation and mitochondria function. *Acta Neuropathol. Commun.* **8**, 116 (2020).
51. Nagano, S. et al. TDP-43 transports ribosomal protein mRNA to regulate axonal local translation in neuronal axons. *Acta Neuropathol.* **140**, 695–713 (2020).
52. Gopal, P. P., Nirschl, J. J., Klinman, E. & Holzbaurb, E. L. F. Amyotrophic lateral sclerosis-linked mutations increase the viscosity of liquid-like TDP-43 RNP granules in neurons. *Proc. Natl Acad. Sci. USA* **114**, E2466–E2475 (2017).
53. Patel, P. et al. Intra-axonal translation of Khsrp mRNA slows axon regeneration by destabilizing localized mRNAs. *Nucleic Acids Res.* **50**, 5772–5792 (2022).
54. Farias, J., Holt, C. E., Sotelo, J. R. & Sotelo-Silveira, J. R. Axon microdissection and transcriptome profiling reveals the in vivo RNA content of fully differentiated myelinated motor axons. *RNA* **26**, 595–612 (2020).
55. Sun, C. et al. The prevalence and specificity of local protein synthesis during neuronal synaptic plasticity. *Sci. Adv.* **7**, eabj0790 (2021).
56. Wong, H. H.-W., Watt, A. J. & Sjöström, P. J. Synapse-specific burst coding sustained by local axonal translation. *Neuron* **112**, 264–276 (2023).
57. Kuzniewska, B. et al. Mitochondrial protein biogenesis in the synapse is supported by local translation. *EMBO Rep.* **21**, e48882 (2020).
58. Glock, C. et al. The translatome of neuronal cell bodies, dendrites, and axons. *Proc. Natl Acad. Sci. USA* **118**, e2113929118 (2021).
59. Maciel, R. et al. The human motor neuron axonal transcriptome is enriched for transcripts related to mitochondrial function and microtubule-based axonal transport. *Exp. Neurol.* **307**, 155–163 (2018).
60. Sahoo, P. K., Smith, D. S., Perrone-Bizzozero, N. & Twiss, J. L. Axonal mRNA transport and translation at a glance. *J. Cell Sci.* **131**, jcs196808 (2018).
61. Lopez-Leal, R. & Court, F. A. Schwann cell exosomes mediate neuron–glia communication and enhance axonal regeneration. *Cell. Mol. Neurobiol.* **36**, 429–436 (2016).
62. Court, F. A., Hendriks, W. T. J. J., MacGillavry, H. D., Alvarez, J. & Van Minnen, J. Schwann cell to axon transfer of ribosomes: toward a novel understanding of the role of glia in the nervous system. *J. Neurosci.* **28**, 11024–11029 (2008).
63. López-Leal, R. et al. Schwann cell reprogramming into repair cells increases miRNA-21 expression in exosomes promoting axonal growth. *J. Cell Sci.* **133**, jcs239004 (2020).
64. Bartel, D. P. Metazoan microRNAs. *Cell* **173**, 20–51 (2018).

65. Farberov, L. et al. Multiple copies of microRNA binding sites in long 3′UTR variants regulate axonal translation. *Cells* **12**, 233 (2023).
66. Mattioli, C. C. et al. Alternative 3′ UTRs direct localization of functionally diverse protein isoforms in neuronal compartments. *Nucleic Acids Res.* **47**, 2560–2573 (2019).
67. Tushev, G. et al. Alternative 3′ UTRs modify the localization, regulatory potential, stability, and plasticity of mRNAs in neuronal compartments. *Neuron* **98**, 495–511 (2018).
68. Villain, G. et al. miR-126-5p promotes retinal endothelial cell survival through setD5 regulation in neurons. *Development* **145**, dev156232 (2018).
69. Santovito, D. et al. Noncanonical inhibition of caspase-3 by a nuclear microRNA confers endothelial protection by autophagy in atherosclerosis. *Sci. Transl. Med.* **12**, eaaz2294 (2020).

[1]Faculty of Medical & Health Sciences, Tel Aviv University, Tel Aviv, Israel. [2]Department of Molecular Genetics, Weizmann Institute of Science, Rehovot, Israel. [3]Department of Molecular Neuroscience, Weizmann Institute of Science, Rehovot, Israel. [4]Department of Physiology and Cell Biology, Ben-Gurion University of the Negev, Beersheba, Israel. [5]The School of Brain Sciences and Cognition, Ben-Gurion University of the Negev, Beersheba, Israel. [6]Institut de Génétique Moléculaire de Montpellier, IGMM UMR535, Montpellier, France. [7]Department of Neurology, Neuromuscular Diseases Research Laboratory, Hacettepe University, Altındağ, Turkey. [8]3rd Neurology Unit and Motor Neuron Disease Centre, Department of Clinical Neurosciences, Fondazione IRCCS Istituto Neurologico Carlo Besta, Milan, Italy. [9]Institute of Experimental Neurology (INSPE), IRCCS San Raffaele Scientific Institute, Milan, Italy. [10]Department of Neurology, Sheba Medical Center, Tel-Hashomer, Ramat-Gan, Israel. [11]Sagol School of Neuroscience, Tel Aviv University, Tel Aviv, Israel. [12]These authors contributed equally: Ariel Ionescu, Lior Ankol. ✉e-mail: eranpe@tauex.tau.ac.il

Methods

This research complies with all relevant ethical regulations as detailed in the relevant sections below.

Human muscle biopsy for intramuscular nerve staining and human obturator nerve

Intramuscular nerve staining was performed on muscle biopsies from a patient with *SOD1* ALS, a patient with sALS and a male non-ALS patient (Supplementary Table 5). Obturator nerve biopsies were obtained from a patient with *SOD1* ALS, a patient with sALS and a non-ALS patient (Supplementary Table 5). The local ethics committee of the San Raffaele Hospital on human experimentation approved the study protocol (RF-2019-12369320); obturator nerves were collected and stored in our tissue bank, after informed consent, both for patients with ALS and for controls. All clinical and muscle biopsy materials used in this study were obtained with written informed consent during 2016–2020 for diagnostic purposes followed by research application, approved by the institutional review board. Biceps skeletal muscle samples were excised via open biopsies, and pathological analysis was performed at the Hacettepe University School of Medicine, Neuromuscular Diseases Research Laboratory, in Ankara, Turkey (Hacettepe University ethics committee approval no. GO20/177, 11/02/2020) and at the neuromuscular pathology laboratory at Sheba Medical Center in Ramat-Gan, Israel. All procedures involving human participants were approved by the Sheba Medical Center institutional review board, with approval numbers 0004871-18, 0001680-7 and 0001681-7, in accordance with the Declaration of Helsinki. Patients with ALS and non-ALS patients were all Caucasian males, aged 26–66 years (48.33 ± 13.12). Patients with ALS were diagnosed with clinically definite or probable ALS according to El Escorial criteria[70]. Non-ALS control muscles included a variation of findings, which were consistent with a diagnosis of normal muscle, severe, chronic ongoing denervation and reinnervation due to spinal stenosis.

Frozen muscle biopsies were cryosectioned to 10-µm-thick slices, mounted onto slides and air dried for 30 minutes at room temperature. Sections were washed in PBS, fixed in 4% paraformaldehyde (PFA) for 20 minutes, permeabilized with 0.1% Triton and blocked with 5% goat serum (The Jackson Laboratory) and 1 mg ml^{-1} BSA (Amresco). Sections were then incubated with appropriate antibodies overnight at 4 °C in blocking solution: rabbit anti-phosphorylated TDP-43 (1:1,000; Proteintech) and chicken anti-NFH (1:1,000; Abcam). Sections were washed again and incubated for 2 hours with secondary antibodies (1:1,000; The Jackson Laboratory and Thermo Fisher Scientific), washed and mounted with ProLong Gold (Life Technologies).

For obturator nerve biopsies, the anterior motor branch of the obturator nerve was sampled and processed in all patients according to our standardized protocols[15,71]

Experimental animals

SOD1$^{G93A-ChAT::tdTomato}$ and LM$^{ChAT::tdTomato}$ embryos were obtained by mating ChAT::ROSA^{tdTomato} females with SOD1^{G93A} males. Embryos were genotyped to distinguish wild-type from SOD1^{G93A} embryos. The colony was maintained by breeding males and females within the colony. HB9–GFP (The Jackson Laboratory, stock no. 005029) mice were originally obtained from The Jackson Laboratory. The colony was maintained by breeding with ICR mice (Institute of Animal Science, Harlan). B6SJL.SOD1^{G93A} (The Jackson Laboratory, stock no, 002726) colonies were maintained by breeding with C57BL/6J mice. Genotyping was performed using PCR (Kapa Biosystems), and DNA samples were generated from ear or tail tissue biopsies. B6SJK.SOD1^{G93A} and littermate males were used to characterize TDP-43 pathology. For the in vivo miR-126 and GFP PHP-eB AAV injections in B6SJK.SOD1^{G93A} and littermates, four female and three male mice of B6SJK.SOD1^{G93A} and five female and three male littermate mice were used. All animal experiments were approved and supervised by the Animal Ethics Committee of Tel Aviv University. Colonies of LoxSOD1^{G37R} mice (The Jackson Laboratory, stock no. 016149) harboring a floxed transgene comprising human *SOD1* gene bearing G37R mutation[72,73] were maintained by breeding heterozygous loxSOD1^{G37R} males with females with pure C57BL/6J background to eliminate confounding genetic influences. LoxSOD1^{G37R} and littermates of both sexes were used to characterize TDP-43 pathology. B6.SOD1^{G93A} (The Jackson Laboratory, stock no. 004435) colonies were maintained by breeding with female C57BL/6J mice. Mice were genotyped by PCR of DNA extracted from a tail biopsy. B6.SOD1^{G93A} and littermate males were used to characterize TDP-43 pathology. All animal procedures were approved by the Institutional Animal Care and Use Committee of Ben-Gurion University of the Negev, in compliance with Israel's Animal Welfare Act (1994) and the National Institutes of Health (NIH) Guide for the Care and Use of Laboratory Animals (National Research Council, 2011). The animal facility is approved by the US Office of Laboratory Animal Welfare (assurance no. A5060-01) and is fully accredited by the Association for Assessment and Accreditation of Laboratory Animal Care International.

Differentiation of iPSCs into functional MNs, myotubes and neuromuscular co-culture

SOD1^{A5V} and TDP-43^{M337V} iPSC lines used in this study were obtained from Michael Ward (NIH) and the iPSC Neurodegenerative Disease Initiative. The use of these lines was approved by the institutional ethics committee of Tel Aviv University (approval no. 0001160). All lines were derived with informed donor consent under NIH protocols and in accordance with the Declaration of Helsinki. iPSC colony maintenance and differentiation into MNs was performed as previously described[13,74]. In brief, MN transcription factor cassette including the transcription factors islet 1 (ISL1) and LIM homeobox 3 (LHX3) along with NGN2 were integrated into a safe harbor locus in iPSCs under a doxycycline-inducible promoter[74].

Skeletal myotube differentiation was performed as follows. Direct myogenic conversion of human iPSCs was performed by transfection of iPSCs using a doxycycline-inducible MYOD1-shOct4 cassette as described, and this cassette was a gift from Michael Ward (Addgene plasmid no. 182309; http://n2t.net/addgene:182309; RRID: Addgene_182309). iPSC clones were cultured in six-well plates coated with Matrigel (Corning, 356234), grown in mTesr1 medium (STEMCELL Technologies, 85850) and passaged with mTesr1 medium containing 10 µM Rho-kinase inhibitor (RI) (Sigma-Aldrich, Y0503) for 1 day after passaging. Culture media were refreshed daily until colonies reached 80% confluence. For differentiation, 300,000 iPSCs were plated in a 35-mm dish coated with Matrigel (1:100) in mTesr1-RI medium. On the following day, media were replaced with induction medium supplement containing DMEM/F12 (Gibco, 31330038), 1× sodium pyruvate (Gibco, 11360070), 1% NEAA (Biological Industries, 01-340-1B) with 10 µM RI, 0.1 mM β-mercaptoethanol, 2 µg ml^{-1} doxycycline (Sigma-Aldrich, D9891) and 10 µg ml^{-1} recombinant human insulin (R&D Systems, 11376497001). This induction medium is replaced every day for two consecutive days, and then half-media volume is replaced for every alternate day until day 6. After the first 2 days of differentiation, RI is removed from the induction medium. On day 7, fresh induction medium containing 3 µM CHIR99021 is added for 48 hours along with induction medium. Followed by CHIR treatment, induction medium is replaced by maturation media containing the following: Neurobasal A medium (Gibco, 10888022), 1× B27 Plus supplement (Gibco, A3582801), 1% NEAA (Biological Industries, 01-340-1B), 1% Optimal-Culture-One supplement (Gibco, A3320201), 0.1 µg ml^{-1} Agrin (R&D Systems, 6624-AG-050), 0.05 µg ml^{-1} Sonic Hedgehog (PeproTech, 100-45), 2 µg ml^{-1} doxycycline, 0.01 µg ml^{-1} IGF1 (PeproTech, 100-11), 0.05 µg ml^{-1} Laminin and 200 µM ascorbic acid (Thomas Scientific, C988E92). This maturation medium is replaced every day for two consecutive days, and then half-media volume is replaced with fresh media every 2–3 days for 1 month.

Human MN–myotube co-culture in MFCs

Day 2 differentiated myotubes were cultured in the distal part of MFCs coated with ECM (1:100) and maintained with induction medium as mentioned above.

For MN cultures, iPSC clones were cultured in six-well plates coated with Matrigel (Corning, 356234), grown in mTesr1 medium (STEMCELL Technologies, 85850) and passaged with mTesr1 medium containing 10 µM RI (Sigma-Aldrich, Y0503) for 1 day after passaging. Culture media were refreshed daily until colonies reached 80% confluence. Doxycyline-induced differentiation into lower MNs was performed as previously described with minor modifications. In total, 300,000 iPSCs were plated in a 35-mm dish in mTesr1-RI medium. On the following day, media were replaced with induction medium supplement containing DMEM/F12 (Gibco, 31330038), 1% N-2 Supplement (Gibco, 17502048), 1% NEAA (Biological Industries, 01-340-1B) and 1% GlutaMAX (Gibco, 35050038) with 10 µM RI, 2 µg ml^{-1} doxycycline (Sigma-Aldrich, D9891) and 0.2 µM Compound E (Merck, 565790).

After day 9, day 2 differentiated MN cells (48 hours after doxycycline induction) were resuspended with Accutase (Sigma-Aldrich, SCR005) and re-plated in the proximal compartment of MFCs at a concentration of 50,000 MNs per MFC. Prior to plating, MFCs were coated overnight with 0.1 mg ml^{-1} PDL (Sigma-Aldrich, P6407) in PBS and 15 µg ml^{-1} Laminin (Sigma-Aldrich, L2020) for 4 hours on the following day. To prevent outgrowth of mitotically active cells, 40 µM BrdU (Sigma-Aldrich, B9285) was added to the medium during the first 24 hours after plating. At the fourth day, cells were treated with MM medium containing the following: Neurobasal medium (Gibco, 21103049), 1% B27 (Gibco, 17504044), 1% N-2, 1% NEAA, 1% Optimal-Culture-One supplement (Gibco, A3320201), 1 µg ml^{-1} Laminin, 20 ng ml^{-1} BDNF, 20 ng ml^{-1} GDNF and 10 ng ml^{-1} NT3 (Alomone Labs, N-260). Medium was refreshed every 3 days.

MN crossing into the myotube compartment was observed usually within 3–4 days after culturing. Throughout the co-culture condition, separate media components for MNs and myotubes were followed as aforementioned. For imaging, chambers were fixed using 4% PFA for 15 minutes and then processed for immunofluorescence protocol.

Automated image analyses using CellProfiler

Along with ImageJ, CellProfiler 4 was used to build an unbiased semi-automated image analysis to perform quantitation of percentage of degenerated neurons (neurofilament heavy chain (NFH) staining) and amount of axonal pTDP-43 in MN–myotube co-culture of isogenic and ALS lines. Deconvolution of *z*-stacked images is performed using ImageJ where each slice from each fluorescent channel is exported as a TIFF file. To begin quantification, the images to be quantified must first be loaded into the input panel. For both NFH degeneration and axonal pTDP-43 analysis, maximum intensity projections of NFH and pTDP-43 channel images were loaded into the pipeline module. Once an image has been loaded into the pipeline, the image will be converted into separate grayscale images representing each of the color channels using the 'ColorToGray' module. To enhance neurite particles within images, we use the 'EnhanceOrSuppressFeatures' module to apply filtering and opt to enhance the identification of neurites. To identify 'intact NFH', we use the 'IdentifyPrimaryObjects' module using the grayscale maximum intensity of NFH channel image as the input image. Within the 'IdentifyPrimaryObjects' module, we selected 'Global Otsu Thresholding' using two-class thresholding, set typical diameter of objects between 10 and 120 pixel units and used both 'intensity' and 'shape' features to differentiate clumped objects. To identify 'degenerated NFH' objects from the same NFH channel, we used the same method of 'IdentifyPrimaryObjects' module of same thresholding and set the typical diameter of objects between 3 and 8 pixel units. For axonal pTDP-43 quantification, a separate image analysis pipeline was generated with additional modules. In addition to the initial steps of 'ColorToGray' module and 'IdentifyPrimaryObjects' module to identify NFH and pTDP-43 from their image channels, additional modules such as 'RelateObjects' and 'MaskObjects' were used to identify axonal pTDP-43 co-localization. To identify the individual pTDP-43 particles within each NFH image, we used 'NFH' objects as the parent objects and 'pTDP-43' objects as the child objects within the module. Ultimately, this allows for the counting of 'pTDP43 objects' per 'NFH objects'. Lastly, all the data collected were exported into separate spreadsheets using the 'ExportToSpreadsheet' module that is provided with counts of particles per image in .csv format. From this, the ratio of particle count of degenerated NFH to intact NFH is used to calculate the percent of degenerated axons in each co-culture, and the ratio of number of pTDP43 objects present in each NFH object is used to calculate the amount of axonal pTDP-43.

Immunofluorescent staining of cryosections

Sciatic nerve and spinal cord sections were prepared from fixating respective tissues in 4% PFA for 16 hours at 4 °C and then incubated with 20% sucrose for 16 hours at 4 °C and cryo-embedding in Tissue-Tek OCT compound (SciGen). Tissues were then cryosectioned to 10-µm-thick slices and washed with PBS, followed by permeabilization and blocking in solution containing 10% goat serum, 1 mg ml^{-1} BSA and 0.1% Triton in PBS for 1 hour. Later, the sections were incubated overnight at 4 °C with primary antibodies: rabbit anti-TDP-43 (1:2,000; Proteintech, 10782-2-AP), rabbit anti-pTDP-43 (1:2,000, Proteintech, 22309-1-AP), chicken anti-NFH (1:500; Abcam, ab72996) and mouse anti-S100 B (1:300; Sigma-Aldrich, S2532). This was followed by 2-hour incubation at room temperature with secondary antibodies: goat anti-chicken 405 (1:500; Abcam, ab175675), goat anti-chicken 594 (1:500; Thermo Fisher Scientific, A-11042), goat anti-mouse 488 (1:500; Abcam, ab150113) and goat anti-rabbit (1:500; Abcam, ab150083). Samples were washed with PBS and mounted with ProLong Gold (Life Technologies).

Immunofluorescent labeling of cell cultures

Cell cultures (either mass cultures or in MFCs) were performed as previously described. In brief, cultures were fixed for 15 minutes with 4% PFA at room temperature, followed by consecutive PBS washes. For co-cultures, labeling of postsynaptic AChRs was performed prior to permeabilization by incubation with either BTX-ATTO-633 or TMR-BTX (0.5–1 mg ml^{-1} in PBS) for 15 minutes at room temperature. After PBS wash, cultures were permeabilized for 30 minutes at room temperature with 0.1% Triton X-100 in PBS or with permeabilization/blocking solution (0.1% Triton X-100, 5% goat serum and 1 mg ml^{-1} BSA in PBS) for 30 minutes. After PBS rinse, cultures were incubated for 1 hour with blocking solution (5% goat serum and 1 mg ml^{-1} BSA in PBS), following overnight incubation at 4 °C with primary antibodies in blocking solution. After PBS rinse, cultures were incubated for 2 hours at room temperature with secondary antibodies in blocking solution, followed by several PBS washes.

Samples were mounted with ProLong Gold antifade reagent (±DAPI; Molecular Probes). In some experiments, samples were labeled with Phalloidin-FITC (1:250) after permeabilization (and other relevant labeling procedures) to mark axons instead of immunofluorescent labeling. Primary antibodies used included: rabbit anti-TDP-43 (1:2,000; Proteintech, 10782-2-AP), rabbit anti-pTDP-43 (1:2,000; Proteintech, 22309-1-AP), chicken anti-NFH (1:500; Abcam, ab72996), rabbit anti-NFH (1:1,000; Sigma-Aldrich, N4142), rabbit anti-Rab27a (1:200; Proteintech, 17817-1-AP), chicken anti-GFP (1:500; Abcam, ab13970), rabbit anti-Ago2 (1:500; Abcam, ab32381) and mouse anti-Titin (1:500; DSHB, 9D10). Secondary antibodies used included: goat anti-chicken 405 (1:1,000; Abcam, ab175675), goat anti-rabbit 405 (1:500; Abcam, ab175654), goat anti-chicken 488 (1:1,000; Abcam, ab150173), goat anti-rabbit 594 (1:1,000; The Jackson Laboratory, 111-585-144), goat anti-rabbit 488 (1:1,000; Invitrogen, A11034), goat anti-mouse 488 (1:500; Abcam, ab150113), goat anti-mouse 594 (1:1,000; Invitrogen, A11032) and goat anti-rabbit 647 (1:500; Abcam, ab150083).

Whole-mount NMJ staining

Gastrocnemius, tibialis anterior, EDL and soleus muscles were dissected from adult mice, cleared from connective tissue and kept in 4% PFA until use. Muscles were washed in PBS, dissected into small muscle bundles (approximately 200 fibers per bundle) and stained for postsynaptic AChR with αBTX-ATTO-633 (Alomone Labs) or αBTX-TMR-594 (Sigma-Aldrich) at 1 μg ml^{-1} for 20 minutes at room temperature while rocking. Next, muscles were permeabilized with ice-cold MeOH at −20 °C for 5 minutes, blocked and further permeabilized with 20 mg ml^{-1} BSA and 0.4% Triton for 1 hour. Muscle preparations were agitated overnight at room temperature with appropriate antibodies: rabbit anti-TDP-43 (1:2,000; Proteintech, 10782-2-AP), rabbit anti-pTDP-43 (1:2,000; Proteintech, 22309-1-AP), chicken anti-NFH (1:500; Abcam, ab72996), rabbit anti-Rab27a (1:200; Proteintech, 17817-1-AP), mouse anti-Synapsin I (1:500; Millipore, AB1543), guinea pig anti-Synaptophysin (1:300; SYSY, 101004), CD63 (1:200; Santa Cruz Biotechnology, H-193, sc-15363), rabbit anti-CD9 (1:100; Abcam, ab92726), mouse anti-CD81 (1:100; Abcam, ab79559), rabbit anti-CHMP2a (1:500; Proteintech, 10477-1-AP) and chicken anti-GFP (1:500; Abcam, ab13970). This was followed by 4-hour incubation at room temperature with secondary antibodies: goat anti-chicken 405 (1:500; Abcam, ab175675), goat anti-chicken 488 (1:500; Abcam, ab150173), goat anti-mouse 488 (1:500; Abcam, ab150113), goat anti-rabbit 647 (1:500; Abcam, ab150083) and goat anti-guinea pig-488 (1:500; Abcam, ab150185). In case required, DAPI was diluted within PBS used for the secondary washes, incubated with the samples for 5 minutes and then washed. Finally, muscle bundles were cut and spread into thinner layers and mounted with VECTASHIELD (Vector Laboratories). Cover slides were sealed with nail polish until use.

Dissociation of muscle fibers prior to their labeling was done by incubating freshly isolated gastrocnemius muscle in DMEM (4.5 g l^{-1} glucose) containing 2.5% penicillin–streptomycin–nystatin (PSN, v/v; Biological Industries) and Collagenase I (2 mg ml^{-1}; Sigma-Aldrich, C-0130) for 3 hours at 37 °C and 5% CO_2. Afterwards, muscles were transferred into a BSA-coated (5% w/v in ultrapure water) 100-mm dish with 15 ml of DMEM (4.5 g l^{-1} glucose) containing 2.5% PSN and left in the CO_2 incubator for 30 minutes. Lastly, muscles were dissociated into single fibers by gradual trituration using a BSA-coated 1-ml tip (pre-cut to have a wider opening). Fibers were collected into a 1.7-ml Eppendorf tube using a fire-polished BSA-coated Pasteur pipette and briefly spun down, and medium was replaced with fresh 4% PFA. Dissociated muscle fibers were labeled similarly. To replace the various reagents during the staining procedure, fibers were gently spun down in each step for discarding maximal volume of the used solution.

miR-126-expressing viral particles

Genes of interest were cloned into a third-generation lentiviral pLL3.7 backbone with either cytomegalovirus (CMV) or hSynapsin promoters. HEK293T cells were transfected by employing the calcium phosphate method and a mixture consisting of the vector of interest and vesicular stomatitis virus glycoprotein, and group antigens–polymerase (reverse transcriptase) was used. The medium was replaced after 5–8 hours, and the supernatant was collected 48 hours later. Next, 50 mM HEPES was added before freezing to maintain a neutral pH for long-term storage at −80 °C. If necessary, the lentiviruses were concentrated using a PEG Virus Precipitation Kit (Abcam). Lastly, the lentiviruses were stored in Neurobasal medium (Gibco) at −80 °C. Lentiviruses were used to overexpress miR126-5p in muscle and MN primary cultures. Two hours after plating, the cells were infected with pLL-miR126-5p–GFP or with pLL–GFP (10^6 titer units). Custom-made single-stranded AAV vectors, serotype 9 variant PHP.eB expressing miR-126 or GFP, were designed and manufactured by the Viral Vector Facility of ETH Zurich. The titer of the viruses was verified by RT–qPCR in the facility and got virus concentration of approximately 3.2×10^{13} viral genomes per 1 ml.

AAV- PHP.eB miR-126 delivery to mice

The injection procedure was performed on presymptomatic approximately P60 mice. Mice were first anesthetized using a mixture of xylazin and ketamine. Then, double injection was performed: intramuscular injection to the right gastrocnemius and retro-orbital injection to the right eye. Each injection was of 25 μl of AAV.PHP.eB–GFP or AAV.PHP.eB miR126-5p–GFP (total of 50 μl per mouse, equal to 1.6×10^{12} viral genomes) using a 25-μl Hamilton syringe and a 30-gauge Hamilton needle. All animal experimentations were approved by the Tel Aviv University Animal Ethics Committee.

Gait analysis and phenotypic characterization of live animals

Evaluation of the motor abilities in $SOD1^{G93A}$ and healthy mice delivered with AAV.PHP.eB particles was performed using the CatWalk XT gait analysis platform (Noldus Information Technology). The test was done at the ages of P90 (early symptoms) and P130 (late symptoms), 30 days and 70 days after injections, respectively. Moreover, mice weight and survival were monitored throughout the entire experiment duration. Experiment endpoint was set at the point of which mice had reached endstage disease condition at neuronal score 5 or at P200, after which tissues were isolated for further analyses, such as immunofluorescence and PCR.

RNA extraction and cDNA synthesis

MN axonal RNA was extracted from the outer compartment of radial MFCs at 14 days in vitro (DIV). Axonal RNA was extracted by removing the PBS (from prior wash) from the outer compartment and adding 100 μl of QIAzol lysis reagent (Qiagen). The inner well was filled with higher volume of PBS to disable the inward flow of lysis reagent toward the inner (soma) compartment and prevent soma contamination. Axons were washed off the plate by pipetting the QIAzol around the outer well for 30 seconds. RNA from somata in the inner compartment was extracted with 100 μl of QIAzol reagent, and lysate was collected in a similar manner. cDNA for axon and soma was prepared with High-Capacity Reverse Transcription Kit (Thermo Fisher Scientific, 4368814).

For sciatic nerve RNA extraction, sciatic axoplasm was obtained from two adult mice sciatic nerves in a tube containing 100 μl of RNase/DNase-free ultrapure PBS, cut into small pieces and gently squeezed on ice. The axoplasm was then centrifuged at 17,000*g* for 15 minutes at 4 °C. RNA was extracted using the RNAeasy Micro Kit (Qiagen) according to the manufacturer's protocols, and RNA yield was quantified using a Qubit fluorometer (RNA Broad-Range Assay Kit; Thermo Fisher Scientific).

Exosomal RNA was extracted by dissolving the exosomal pellet in 700 μl of QIAzol.

RNA was extracted using the RNAeasy Micro Kit (Qiagen) according to the manufacturer's protocols, and RNA yield was quantified using a Qubit fluorometer (RNA Broad-Range Assay Kit; Thermo Fisher Scientific). For standard whole-cell RNA preparations from MN/muscle cultures, cultures were lysed in 700 μl of TRI reagent, and RNA was isolated with ordinary chloroform, isopropanol precipitation protocol.

Small RNA next-generation sequencing

For small RNA next-generation sequencing, libraries were prepared from 10–15 ng of total RNA using the QIAseq miRNA Library Kit and the QIAseq miRNA NGS 48 Index IL (Qiagen), by an experimenter who was blinded to the identity of samples. Samples were randomly allocated to library preparation and sequencing in batches. Precise linear quantification of miRNA is achieved by using unique molecular identifiers (UMIs) of random 12 nucleotides after 3′ and 5′ adapter ligation, within the reverse transcription primers[75]. cDNA libraries were amplified by PCR for 19 cycles, with a 3′ primer that includes a six-nucleotide unique index, followed by on-bead size selection and cleaning. Library concentration was determined with a Qubit fluorometer (dsDNA High-Sensitivity

Assay Kit; Thermo Fisher Scientific) and library size with TapeStation D1000 (Agilent). Libraries with different indices were multiplexed and sequenced on a NextSeq 500/550 version 2 flow cell or NovaSeq SP100 (Illumina), with 75-bp single read and 6-bp index read. FASTQ files were demultiplexed using the user-friendly transcriptome analysis pipeline (UTAP)[76]. Mouse miRNAs, as defined by miRBase[77], were mapped using the Qiagen RNA-seq Analysis Portal 1.0 and 2.5.1, GeneGlobe pipeline (https://geneglobe.qiagen.com/us/analyze). We defined 'true-positive' miRNAs and reduced the likelihood of considering 'false-positive' miRNAs by including only miRNAs with an average UMI count >100 across all samples and with at least a single UMI across all samples, similar to our previous works[78–80]. Data were further normalized and average read counts compared between groups using the DESeq2 package[81] under the assumption that miRNA counts followed negative binomial distribution. Significance was determined using the Wald test.

Axonal RNA-seq

RNA was extracted from primary MN axons grown in radial MFCs and purified as described above[13]. RNA yields were quantified using a Qubit fluorometer (RNA Broad-Range Assay Kit; Thermo Fisher Scientific). RNA integrity was assessed by TapeStation. cDNA libraries were prepared from 10 ng of axonal RNA by the genomic unit in the Weizmann Institute of Science using the MARS-seq pipeline[82]. MARS-seq libraries with different UMIs were multiplexed and sequenced on a NovaSeq SP100 flow cell (Illumina), with 75-bp single read and 15-bp UMI read. After demultiplexing, FASTQ files were mapped to mouse genome using the GenCode annotations (vM25, 2020) in the UTAP piepeline[76]. We defined 'true-positive' genes and reduced the likelihood of considering 'false-positive' genes by including only genes with an average UMI count >15 across all samples. Data were further normalized and average read counts compared between groups using the DESeq2 package[81] under the assumption that gene counts followed negative binomial distribution. Significance was determined using the Wald test.

RT–qPCR analysis

SYBR Green-based assays (PerfeCTa SYBR Green FastMix; Quantabio) and StepOne Real-Time PCR system (Thermo Fisher Scientific) were used in RT–qPCR to quantify differential expression of mRNAs in MNs, MN axons and primary skeletal muscles. GAPDH mRNA was used as a reference RNA when calculating ΔCT. RT–qPCR primers and their sequences are listed in Supplementary Table 5.

Actb mRNA was used as a reference RNA when calculating ΔCT in *Tardbp*/*Polb* relative expression in axons and somata cDNA preparations.

PCR amplification and Southern blot

Reverse transcription was performed with the High-Capacity Reverse Transcription cDNA Kit using random primers (Thermo Fisher Scientific). Standard PCR was used to amplify sciatic axoplasm cDNA for detecting *Tardbp*, *Polb* and *Actb* mRNA using KAPA ReadyMix. Primer sequences are listed in Supplementary Table 5.

TaqMan miRNA RT–qPCR

TaqMan RT–qPCR was done to evaluate the levels of mature miR-126-5p. U6 gene was used as a reference gene when calculating ΔCT, as we aim to quantify relative miR-126-5p levels in various tissues and cells.

For the TaqMan experiment, cDNA was extracted from the purified RNA using dedicated primers that will amplify miR126-5p signal using the High-Capacity cDNA Reverse Transcription Kit (Applied Biosystems, 4368813). Later, we ran the samples in qPCR using the TaqMan method to quantify the alteration in miR-126-5p levels using miR126-5p and U6 advanced TaqMan primers (Thermo Fisher Scientific, 4427975). qPCR TaqMan reactions were performed with TaqMan Fast Advanced Master Mix for qPCR (Thermo Fisher Scientific) in a StepOne Real-Time PCR system (Thermo Fisher Scientific).

TDP-43 isoforms quantification

Illumina FASTQ files were uploaded for bioinformatics analysis to CLC Genomics Workbench version 24 (https://digitalinsights.qiagen.com/products-overview/discovery-insights-portfolio/analysis-and-visualization/qiagen-clc-genomics-workbench/) and the 'RNA-seq analysis' tool with default options. In brief, reads were trimmed from 5′ adapter sequence of GTTCAGAGTTCTACAGTCCGACGATC. After this, trimmed reads were aligned to the GRCm39/mm39 mouse genome (downloaded from https://www.gencodegenes.org/mouse/) with the following parameters: mismatch cost of 2, insertion cost of 3, deletion cost of 3, length fraction of 0.8 and similarity fraction of 0.8. Aligned reads were annotated to mRNA tracks to define splicing isoforms per gene. Finally, isoforms were quantified by the CLC Genomics Workbench 'expectation–maximization' estimation algorithm.

Dual-luciferase reporter assay

HEK293A cells were seeded a day before transfection in three 60-mm wells ($2.5–3 \times 10^5$ per well; Thermo Fisher Scientific, 140675) per sample. Cells were co-transfected with mirVec plasmid expressing the pre-microRNA-126 and dual-luciferase (Firefly and Renilla Luciferase) plasmid (a kind gift from the Shomron laboratory, Tel Aviv University). Dual-luciferase plasmid was cloned downstream to Renilla Luciferase with 100-bp context sequence of the 3′ UTR of mmu-TDP-43 mRNA containing either the wild-type miR-126a-5p binding site or a mutant one where four nucleotides within this site have been mutated. Transfection was performed by Lipofectamine 2000 (Invitrogen, 11668-027) for 72 hours, after which cells were washed once with PBS (Sigma-Aldrich, D8537; 500 ml) and harvested according to the manufacturer's protocol.

Serum EV purification

Patient blood serum samples were collected from Caucasian patients with ALS aged 45–88 years (68.37 ± 14.49) and healthy controls aged 23–66 years (43.87 ± 16.81) from both sexes (Supplementary Table 5), with collaboration of Amir Dori from Sheba Hospital. From each sample, 1 ml was used to purify EVs in order to evaluate the levels of mature miR-126-5p. Using the exoRNeasy kit (Qiagen, 76064), we isolated EVs from the serum samples and purified total RNA. The levels were normalized to the same volume and process for all the samples and conditions.

Protein extraction

Gastrocnemius muscles were extracted from adult mice and homogenized in ice-cold PBS lysis buffer containing 0.1% Triton X-100, protease and phosphatase inhibitors (Roche). Sciatic axoplasm was obtained from both sciatic nerves from every mouse. Sciatic nerves were sectioned, and axoplasm was extracted into 100 µl of PBS with protease and phosphate inhibitors by gentle pressing the sections. Proteins from primary MNs and primary muscle cultures were extracted using PBS lysis buffer containing 0.1% Triton X-100, protease and phosphatase inhibitors.

Tissue/culture lysates were centrifuged at 10,000*g* for 15 minutes at 4 °C. Protein concentration was determined using Bradford (Bio-Rad) or BCA (Cyanogen) colorimetric assays.

Western blotting

Protein samples were mixed with SDS sample buffer and boiled at 95 °C for 10 minutes and then loaded to 10% acrylamide gels for SDS-PAGE. Proteins were transferred to nitrocellulose or PVDF membranes in buffer containing 20% MeOH. Membranes were blocked with 5% skim milk (BD Biosciences) or 5% BSA for 1 hour, followed by overnight incubation at 4 °C with primary antibodies: mouse anti-human-TDP-43 (1:2,000; Proteintech), rabbit anti-TDP-43 (1:2,000; Proteintech), rabbit anti-ERK1/2 (1:10,000; Sigma-Aldrich), mouse anti-α-tubulin (1:5,000; Abcam), rabbit anti-CD63 (1:100; Santa Cruz Biotechnology, H-193, sc-15363), rabbit anti-CD9 (1:100–1:1,000; Abcam, ab92726),

mouse anti-CD81 (1:100–1:2,000; Abcam, ab79559), rabbit anti-Ago2 (1:500; Abcam, ab32381), rabbit anti-ALIX (1:250; Abcam, ab76608), mouse anti-SOD1 (1:500; Santa Cruz Biotechnology, FL-154), rabbit anti-Rab27a (1:200; Proteintech, 17817-1-AP) and GM130 (1:200; BD Biosciences, 610823), followed by species-specific HRP-conjugated secondary antibodies: rabbit 111-035-003 and mouse 715-035-151, both 1:10,000 (The Jackson Laboratory). Membranes were then washed with TBS with 0.05% Tween 20 (TBS-T) and incubated for 2 hours at room temperature with secondary HRP antibody (1:10,000; The Jackson Laboratoy), washed with TBS-T and visualized in an iBright 1500 ECL imager (Life Technologies) after 5-minute incubation with ECL reagents. Quantification was performed using FIJI ImageJ software version 2.3.0/1.53q.

MFC preparation

MFCs were prepared as previously described[13,30,83]. In brief, PDMS (Dow Corning) was cast into custom-made epoxy replica molds, left to cure overnight at 60 °C, punched (6-mm/7-mm/9-mm punches according to the type of MFC), cleaned and positioned in 35-mm and 50-mm glass plates (WPI) or over 22 × 22-mm microscope cover glasses (Mariendfeld). Radial MFCs were positioned on pre-adhered round 13-mm cover glasses within 24-well plates.

MN culture and MN–myocyte co-culture

Ventral spinal cords from embryonic day 12.5 (E12.5) embryos were dissected in HBSS prior to dissociation. For Rab27a shRNA experiments, co-cultures were performed with ventral spinal cord explants isolated as previously described[29,30,83]. In brief, ventral spinal cords were acquired transversely, sectioning spinal cords into small pieces after dissecting the dorsal horns and plating in MFC proximal compartment in Neurobasal (Gibco), 2% B27 (Thermo Fisher Scientific), 1% GlutaMAX (Gibco), 1% penicillin–streptomycin and 25 ng ml^{-1} BDNF (Alomone Labs).

Dissociated MN cultures were obtained by further trypsinization and trituration of explants. Supernatant was collected and centrifuged through BSA (Sigma-Aldrich) cushion. The pellet was then resuspended and centrifuged through an OptiPrep (Sigma-Aldrich) gradient (containing 10.4% OptiPrep, 10 mM tricine and 4% w/v glucose). MN-enriched fraction was collected from the interphase, resuspended and plated in the proximal MFC compartment at a concentration of 200,000 MNs per regular MFC and 250,000 per radial MFC. MNs were maintained in complete neurobasal medium containing Neurobasal, 4% B27, 2% horse serum (Biological Industries), 1% GlutaMAX, 1% penicillin–streptomycin, 25 µM β-mercaptoethanol, 25 ng ml^{-1} BDNF, 1 ng ml^{-1} GDNF (Alomone Labs) and 0.5 ng ml^{-1} CNTF (Alomone Labs). Glial cell proliferation was restricted by the addition of 1 µM cytosine arabinoside (Sigma-Aldrich) to culture medium in 1–3 DIV. At 3 DIV, BDNF concentration in proximal compartment was reduced (1 ng ml^{-1}), whereas medium in distal compartment was enriched with GDNF and BDNF (25 ng ml^{-1}) to direct axonal growth.

Myocyte culture was performed as previously described[29]. In brief, gastrocnemius muscles from a P60 adult C57BL/6J mouse were extracted into DMEM with 2.5% PSN (Biological Industries) with 2 mg ml^{-1} Collagenase I (Sigma-Aldrich) for 3 hours and then dissociated and incubated with BIOAMF-2 (Biological Industries) in Matrigel (BD Corning)-coated plates for 3 days. Myoblasts were purified by performing pre-plating for three consecutive days and then plated at a density of 75,000 per MFC. Remaining myocytes were cryopreserved in 95% FBS, 5% DMSO and were used according to need by rapid thawing at 37 °C and resuspension in pre-warmed BIOAMF-2 medium (without antibiotics), followed by 300*g*, 4-minute-long centrifugation. Pellet was resuspended in BIOAMF-2 medium (without antibiotics), and muscles were plated in Matrigel-precoated 24-well plates for overnight recovery (150,000 myoblasts per well). In case the experiment performed required transfection of plasmids (that is, Rab27a shRNA, CD63–GFP, CD63-pHluorin, PLKO.1), myocytes were transfected 8 hours after their plating in the 24-well plates (further details in the transfection method section).

Prior to their co-culturing with primary MNs, primary myocytes in 24-well plates were washed once with pre-warmed PBS and then detached with 100 -µl-per-well Trypsin C solution (Biological Industries) for 15 minutes and then collected in fresh pre-warmed BIOAMF-2 medium and processed through 300*g*, 4-minute-long centrifugation. Myocyte pellets were resuspended in BIOAMF-2 medium and plated in the neuromuscular compartment of an MFC 1 hour after primary MNs were plated in the neuronal compartment. To aid NMJ formation, media in all compartments were then replaced to poor neurobasal (PNB) medium, which contained only 1% penicillin–streptomycin and 1% GlutaMAX.

Vectors and primary muscle transfection

As detailed above, transfection of genetic vectors into muscles was performed at the myocyte stage of differentiation and prior to their culturing in MFCs. Myocytes were transfected using 1 µg of DNA and 3 µl of TurboFect transfection reagent (Thermo Fisher Scientific) in 300 µl of Opti-MEM medium (Gibco). Transfection mix was prepared according to the manufacturer s instructions. Transfection mix was discarded after 12 hours, and myocytes were washed once with pre-warmed optimum medium and then left to recover for an additional 4 hours with BIOAMF-2 medium (no antibiotics). Muscles were then re-plated in MFCs as described previously.

CD63-peGFP C2 (plasmid no. 62964), pCMV-lyso-pHluorin (CD63-pHluorin; plasmid no. 70113) and pLKO-Tet-On-shRab27a (plasmid no. 120930) were acquired from Addgene repositories.

pLL3.7-Ago2-eGFP was constructed in the Tel Aviv University lentiviral facility. pLL3.7-TDP-43-eGFP was constructed by cloning TDP-43-eGFP into PLL3.7 backbone (acquired from Addgene).

For shRab27a experiments, doxycycline was applied exclusively at the neuromuscular compartment at 5 days into co-culture, in a concentration of 1 µg ml^{-1}.

Live imaging of CD63-pHluorin signals was performed using Tyrode's solution (2 mM $CaCl_2$, 2.5 mM KCl, 119 mM NaCl, 2 mM $MgCl_2$, 20 mM glucose and 25 mM HEPES (pH 7.4)) in the presence or absence of 50 mM NH_4Cl (instead of NaCl) to neutralize intracellular pH.

Tracking muscle-derived RNA in axons

Primary skeletal muscles were cultured and differentiated as mentioned above. Upon differentiation, SYTO RNASelect Green (5 µM; Invitrogen, S32703) was added to muscle growth media for 1 hour. Cultures were washed three consecutive times with PBS, and fresh collection media were added to cultures. Muscle conditioned media were collected for 3 hours and then centrifuged at 4,000*g* for 5 minutes and passed through a 0.45-µm filter. Medium was applied to the axons within the distal compartment of MFCs. Prior to conditioned media addition, neuronal RNA was labeled using SYTO64 (5 µM; Invitrogen, S11346) for 10 minutes and then washed away by consecutive PBS and medium washes.

GW4869 exosome/EV inhibitor

Muscle experiments were conducted using GW4869 inhibitor (Sigma-Aldrich, D1692) dissolved in DMSO creating a 5 mM stock solution. The inhibitor or the DMSO control was diluted to the culture media (BIOAMF-2) to a final concentration of 10 µM.

In vitro NMJ quantification

NMJ disruption was determined by high-magnification confocal imaging and quantification of the overlap of presynaptic and postsynaptic markers at the neuromuscular compartment in co-cultures. At the endpoint of the experiments (normally 10–14 days), co-cultures in MFCs were fixed with 4% PFA for 15 minutes at room temperature.

αBTX-ATTO Fluor-633 (1:200; Alomone Labs, B-100-FR) or TMR-αBTX (Sigma-Aldrich) was used to label the extracellular domain of postsynaptic nAchR prior to membrane permeabilization. The percentage of healthy NMJs was determined by dividing the number of intact co-localization events, with intact non-degenerated axons, by the total number of co-localization events identified in every MFC.

EV purification process

EVs were isolated from culture media using an ultracentrifuge protocol as previously described. In brief, the conditioned medium from differentiated primary muscle cultures (7 DIV) grown in 10-cm plates was collected in serum-free conditions for 16 hours. Conditioned medium was then centrifuged at 300*g* for 10 minutes at 4 °C, and supernatant was collected and transferred to a new tube centrifuged at 2,000*g* for 20 minutes at 4 °C. Supernatant was collected again and centrifuged at 10,000*g* for 30 minutes at 4 °C. Supernatant was then transferred into ultracentrifugation suitable tubes (Ultra-Clear centrifuge tubes; Beckman Coulter, 344059) and centrifuged at 100,000*g* for 70 minutes at 4 °C using the Optima-80 XPN ultracentrifuge (Beckman Coulter) with SW41 Ti rotor. Supernatant was discarded, and EV pellet was washed with ultrapure PBS 1× and centrifuged again at 100,000*g* for 60 minutes at 4 °C. The purified EVs were resuspended with 35 µl of 3.5× Laemmli sample buffer for western blot, 30 µl of PBS 1× for electron microscopy, 50 µl of PBS 1× for functional experiments or 700 µl of QIAzol for downstream RNA isolation.

In addition to the standard ultracentrifugation procedure, EVs for western blots and NTA in Supplementary Fig. 3a,b, Fig. 5d,e and Fig. 5m,n were isolated from primary muscle cultures grown in two 35-mm dishes per condition (total 4 ml) after 48 hours of medium collection in serum-free medium containing DMEM (4.5 g l^{-1} glucose), GlutaMAX (1%), B27 supplement (2%) and NEAA (1%) and in the presence or absence of the relevant treatment or control. EVs were purified using exoRNAeasy Midi exosome purification kit (Qiagen, 77144), following the manufacturer s protocol. For the NanoSight NTA, isolated EVs were further diluted 10× in PBS (0.1 µm filtered). Sample preparation for SDS-PAGE was done by lysing the isolated EVs in 10× RIPA buffer (Millipore) containing protease and phosphatase inhibitor mix. EV protein extracts were further concentrated using Amicon 0.5-ml centrifugal filters (10-kDa molecular weight cutoff). Whole-cell lysates were prepared by washing the culture once with 1× PBS and lysing the cultures with 1× RIPA buffer containing protease and phosphatase inhibitor mix. Protein concentrations were determined by BCA, and equal amounts of protein were loaded.

TEM imaging and negative staining

Samples were adsorbed on formvar/carbon-coated grids and stained with 2% aqueous uranyl acetate. Samples were examined using a JEM 1400Plus transmission electron microscope (Jeol). Images were captured using SIS Megaview III and the iTEM imaging platform (Olympus). Images were analyzed using FIJI software version 2.3.0/1.53q. Preparation and imaging of the samples in TEM were conducted by Vered Holdengreber at Tel Aviv University.

Fluorescence microscopy and image analysis

Confocal images were captured using a Nikon Ti microscope equipped with a Yokogawa CSU X-1 spinning disk and an Andor iXon897 EMCCD camera controlled by Andor IQ3 software version 3.0; an Andor BC-43 benchtop spinning disk confocal system controlled by Andor Fusion software version2.3a; or a 3i Marianas confocal system with a Zeiss Axio Observer 7 microscope, equipped with a Yokogawa CSU-W1 spinning disk and a Prime 95B Back-Illuminated Scientific CMOS camera controlled by SlideBook software version 6.0. Phase-contrast movies of muscle contraction were acquired using the same microscope. High-content imaging and analysis of phase neurite morphology was performed using Sartorius Incucyte S3, 2019A, including Neurotrack module (cat. no. 9600-0010). All live imaging experiments were performed with 5% CO_2 and 37 °C humidified using an in situ microscope setup.

smFISH

TDP-43 mRNA single-molecule inexpensive FISH (smiFISH) was performed as previously described[13,84]. In brief, primary MNs were isolated and cultured for 7 days on cover glasses. Labeling procedures were performed in an RNase-free environment and using RNAse-free reagents. Cultures were fixed with 4% PFA and permeabilized overnight with 70% ethanol. Before hybridization, 40 pmol of 27 oligo-mix probes were pre-hybridized to 50 pmol of the FLAP probe in 10 µl of 100 mM NaCl, 50 mM Tris-HCl and 10 mM $MgCl_2$ (pH 7.9). Pre-hybridization was performed on a thermocycler using the following program: 85 °C for 3 minutes, 65 °C for 3 minutes and 25 °C for 5 minutes. Samples were incubated with SSC (Sigma-Aldrich, S6639)-based 15% formamide (Thermo Fisher Scientific, 17899) buffer for 15 minutes. Samples were hybridized overnight at 37 °C with 27× FLAP-Y-Cy-3-tagged complementary oligonucleotide probes targeting regions in mouse *Tardbp* transcript variant 3 or with 23× FLAP-Y-Cy-3-tagged complementary probes targeting mouse *Actb* (Integrated DNA Technologies; Supplementary Table 5). The final hybridization mixture contained the probe duplexes (2 µl per 100 µl of final volume), 1× SSC, 0.34 mg ml^{-1} tRNA (Sigma-Aldrich, 1753), 15% formamide, 2 mM VRC (Sigma-Aldrich, R3380), 0.2 mg ml^{-1} RNAse-free BSA (Roche, 10711454001) and 10% dextran sulfate (Sigma-Aldrich, D8906). Samples were washed twice with warm 15% formamide and 1× SSC buffer (1 hour each), followed by 30 minutes with 1× SSC buffer and 30 minutes with 1× PBS supplemented with Phalloidin-FITC (1:250). Prior to mounting, samples were labeled with DAPI (0.2 µg ml^{-1}). Samples were mounted with VECTASHIELD antifade reagent.

Labeling of TDP-43 mRNA in NMJs in vivo was performed in a similar way with the following modifications. Freshly isolated EDL muscles were dissected into smaller fiber bundles and fixed in 4% PFA for 1 hour while rocking. After PFA washout, tissues were permeabilized for 1 hour with 1% Triton X-100 in diethylpyrocarbonate (DEPC) water while rocking. Samples were washed with DEPC-PBS and then pre-hybridized as mentioned above. smiFISH hybridization steps were performed similarly to cultured cell yet with continuous agitation. After post-hybridization washes as detailed above, tissues were fixed again with 4% PFA for 10 minutes, after which we performed standard whole-mount immunolabeled with chicken anti-NFH (1:500) overnight at room temperature while rocking. After primary antibody washout, samples were incubated with secondary Alexa Fluor-405 anti-chicken antibodies at room temperature for 4 hours while rocking. After secondary antibody washout, samples were mounted with VECTASHIELD antifade reagent.

TDP-43 puro-PLA

Combined TDP-43 and puro-PLA was performed as previously described[28] in order to evaluate the extent of TDP-43 protein synthesis in MN axons. In brief, primary MNs were grown in MFCs in the presence or absence of primary skeletal muscles in the neuromuscular compartment. Puromycin labeling was performed exclusively to the distal (axonal or neuromuscular compartment) for 30 minutes at a concentration of 10 µM, followed by two rapid cold PBS 1× washes and fixation in 4% PFA for 15 minutes. To validate the specificity of puro-PLA labeling, protein synthesis was exclusively inhibited in the distal/neuromuscular compartment by the addition of anisomycin (40 µM) for 30 minutes prior to and along with puromycin labeling. To reduce the background labeling in neuromuscular co-cultures and to expose the presynaptic PLA signals, primary muscles were transfected with empty backbone vector (PLKO.1) expressing the puromycin resistance gene puromycin acetyltransferase (PAC) prior to their co-culturing[13]. In co-cultures, postsynaptic AChRs were labeled before

permeabilization with αBTX-ATTO-633 (Alomone Labs, B-100-FR) or TMR-αBTX (Sigma-Aldrich). PLA was performed on the following primary antibodies: rabbit anti-TDP-43 (recognizing N terminal of TDP-43; 1:2,000; Proteintech, 10782-2-AP) and mouse anti-puromycin 12D10 clone (1:1,000; Millipore, MABE343). PLA was performed according to manufacturer guidelines (Sigma-Aldrich, Duolink Proximity Ligation Assay Kit, and Navinci, NaveniFlex PLA Kit). After completion of the PLA protocol, samples were fixed with 4% sucrose, 4% PFA for 10 minutes, and then standard immunofluorescence labeling was performed to visualize axonal markers.

Ex vivo TDP-43 puro-PLA

Ex vivo puromycilation was performed by extracting EDL muscles into pre-heated (37 °C), pre-oxygenized (95% O_2, 5% CO_2) and 0.22-µm filtered DMEM labeling medium (+glucose 4.5 g l^{-1}) containing 10% FBS, supplemented with puromycin (10 µM), anisomycin (40 µM) or none of those. Labeling media were infused into the EDL muscles at several locations using a 30-gauge insulin syringe (50–100 µl per injection site). Muscles were incubated in a 60-mm dish containing the labeling media for 40 minutes at 37 °C and 5% CO_2 and after which were rinsed for three times with rapid (2-minute) ice-cold PBS injections in a 60-mm dish with cold PBS prior to their fixation with cold 4% PFA in a similar injection fashion. Anisomycin-treated samples were further injected and incubated for 40 minutes with labeling media containing both anisomycin and puromycin. Muscle samples were kept for at least 2 hours in PFA fixation (but no longer than 16 hours) before proceeding with the protocol. EDL muscles were further cleared of connective tissues and dissected into smaller muscle fiber bundles (approximately 200 fibers per bundle) using a scalpel. BTX labeling was performed as described above using TMR-αBTX (Sigma-Aldrich) diluted in TBS buffer (20 mM Tris base and 150 mM NaCl (pH 7.6)) while rocking. After washing, samples were permeabilized with TBS containing 0.4% Triton X-100 for 30 minutes at room temperature while rocking, washed once and further permeabilized with ice-cold MeOH for 5 minutes. The ex vivo PLA reaction was performed using the NaveniFlex Tissue MR ATTO647N kit (Navici, NT.MR.100.Atto647N) following the manufacturer's instructions with slight volume modifications. Blocking and primary antibody incubations were performed using reagents supplied within the NaveniFlex kit. We used mouse anti-puromycin 12D10 clone (1:1,000; Millipore, MABE343), rabbit anti-TDP-43 (recognizing N terminal of TDP-43; 1:1,500; Proteintech, 10782-2-AP) or rabbit anti-β-actin (1:500; Abcam, ab8227) that were incubated with samples overnight at 4 °C while rocking. After washes according to protocol, samples were incubated with secondary NaveniFlex antibodies for 2 hours at 37 °C, rather than 1 hour as indicated by the manufacturer, for improving their penetration into the whole-mount muscle preparations. After completion of the PLA procedures, samples were postfixed with 4% PFA for 10 minutes, washed with TBS and labeled with chicken anti-NFH (1:500; Abcam, ab72996) and guinea pig anti-Synaptophysin (1:300; SYSY, 101004) in blocking solution (TBS, 5% goat serum, 1 mg ml^{-1} BSA and 0.1% Triton X-100) overnight at room temperature while rocking. After TBS-T washes, samples were incubated for 4 hours at room temperature while rocking with secondary antibodies: goat anti-chicken (1:500; Abcam, ab150173) and goat anti-guinea pig-488 (1:500; Abcam, ab150185). After TBS-T washes, samples were labeled with DAPI, washed and mounted using VECTASHIELD.

OPP labeling of axonal protein synthesis

The puromycin derivative OPP was used to label axonal and presynaptic protein synthesis in co-cultures and ex vivo in NMJs as previously described[13]. In brief, to reduce background labeling in muscles and to better visualize presynaptic protein synthesis, primary muscle cultures were transfected with a PAC-expressing vector prior to their co-culturing with primary MNs. At experimental timepoint, OPP (20 µM) was added exclusively to the neuromuscular compartment of MFCs for 30 minutes followed by two rapid cold PBS 1× washes and fixation in 4% PFA for 15 minutes. Postsynaptic AChRs were labeled before permeabilization with αBTX-ATTO-633 (Alomone Labs, B-100-FR) or TMR-αBTX (Sigma-Aldrich). OPP was labeled with Alexa Fluor-594 picolyl azide by click chemistry (Click-iT Plus OPP Kit; Molecular Probes, C10457) according to manufacturer instructions. After click reaction was washed, cultures were fixed once again with 4% sucrose, 4% PFA for 10 minutes before continuing with standard immunofluorescence labeling for visualizing axonal markers and additional proteins. Samples were mounted with ProLong Gold antifade reagent (Molecular Probes).

Ex vivo OPP labeling in EDL muscles was performed by bathing and infusing freshly isolated EDL or gastrocnemius muscles with 20 µM OPP in Ringer s solution or in DMEM medium (+glucose 4.5 g l^{-1} containing 10% FBS) (using a 30-gauge insulin syringe as described above in the ex vivo puro-PLA section) for 40 minutes at 37 °C, followed three rapid washes with cold PBS 1× and fixation with 4% PFA for 20 minutes. Postsynaptic AChRs were labeled as mentioned before permeabilization. Tissues were permeabilized in 100% MeOH at −20 °C for 5 minutes. Tissues were washed in PBS and then processed with the Click-iT protocol while rocking. After click reaction was washed, cultures were fixed once again with 4% sucrose, 4% PFA for 10 minutes before continuing with standard whole-mount immunofluorescence protocol. Samples were mounted with VECTASHIELD.

miR-126-5p inhibitor

miR-126-5p inhibitor (miR126i; Qiagen, miScript miRNA inhibitor) was transfected into the neuromuscular compartment at the fifth day of co-cultures at concentration of 100 nM. Transfection was performed using TurboFect transfection reagent (Thermo Fisher Scientific) at the following ratio: 0.75 µl of TurboFect per MFC (200 µl) with 1 µl of miR-126-5p inhibitor (20 µM stock) in BIOAMF-2 medium. Medium in transfected compartments was refreshed 3 days after transfection. NMJ function analysis was performed at the fourth day after transfection. Co-cultures underwent puromycin/OPP labeling and further fixation at the fifth day after transfection. Due to its discontinuation, the experiments in Fig. 7 done in combination with siRNAs for TDP-43 were performed with the new miRCURY LNA-miR-126-5p inhibitor (Qiagen, 339121) at a final concentration of 50 nM.

TDP-43 siRNA

To locally knock down TDP-43, we transfected axons and neuromuscular compartment in MFCs with two types of Silencer Select predesigned siRNAs for mmu-*Tardbp* or a negative control siRNA (s106687, s106688 and 4390843, respectively; Ambion; Supplementary Table 5). Lipofectamine 3000 was used to transfect a total of 80 nM siRNA mix or negative control into the distal compartment of MFCs either alone or in combination with 50 nM LNA-miR-126-5p inhibitor. Cultures were fixed and labeled 4 days after transfection to analyze axonal integrity and the TDP-43 distribution in axons.

miR-126a-5p FISH

miR-126a-5p FISH was performed on whole-mount EDL muscle tissues as previously described[85]. In brief, to visualize miR-126a-5p in mouse tissues, we adapted an LNA probe-based tyramide signal amplification protocol. EDL muscles were isolated, physically cleared of connective tissues and fixed in 4% PFA for 1 hour while rocking, followed by three PBS washes. Tissues were then permeabilized in 1% Triton X-100 in DEPC-PBS for 10 minutes while rocking. Samples were further acetylated for 5 minutes in acetylation buffer (60 nM HCl, 1.3% v/v TEA and 6% v/v acetic anhydride in DEPC water), followed by three PBS 1× washes. Samples were pre-hybridized in hybridization mix for 30 minutes at 60 °C while rocking (5× SSC, 50% formamide, 5% tRNA, 9.25 mM citric acid and 2% Denhardt's solution). Next, samples were hybridized with miR-126-5p miRCURY LNA detection probes (Qiagen, YD00612156-BCE) in hybridization solution for 1 hour at 60 °C while

rocking, followed by three 10-minute washes with 0.1% SSC at 65 °C and an additional wash with 2× SSC at room temperature for 5 minutes. Samples were exposed to 3% hydrogen peroxide for 10 minutes at room temperature, followed a single 5-minute wash with TN buffer. Samples were blocked for 30 minutes at room temperature in blocking buffer and then incubated for 1 hour with anti-DIG antibody (1:400) at room temperature while rocking, followed by three 5-minute washes with TNT buffer. Lastly, signal was amplified by incubation in amplification buffer containing Tyramide-647 for 10 minutes at room temperature, followed by three 5-minute washes with TNT buffer. Prior to continuing with standard whole-mount immunofluorescence protocol for labeling presynaptic axons, tissues were fixed once more with 4% sucrose, 4% PFA solution. Rabbit anti-NFH (1:500) and rabbit anti-Synapsin I (1:500) were incubated with samples overnight at room temperature while rocking, followed by three PBS washes and 4-hour incubation with secondary antibody Alexa Fluor-488-conjugated goat anti-rabbit (1:500). Samples were labeled with DAPI during secondary antibody washes and mounted in VECTASHIELD.

Statistics and reproducibility

Statistical parameters, tests used, sample sizes and number of repeats are noted in the figure legends. Assignment to experimental groups (in vivo and in vitro) was made random. Data collection was randomized. Data collection and analysis were performed blinded to the conditions of the experiments whenever possible, however not for all experiments. Exclusion of data points was performed based on standard GraphPad Prism outlier analysis (ROUT method, $Q = 1\%$). Images are representative of all experimental repeats. Statistical significance was determined using Student's *t*-test or Wald test when comparing between two groups and multiple comparisons ANOVA test when comparing more than two groups. In specific cases where samples did appear to not have a normal distribution, a normality test was performed, and the subsequent significance test was determined accordingly. Kruskal–Wallis test was used to assess significance in non-parametric datasets with more than two groups. In some instances, multiple *t*-test analysis was performed instead of two-way ANOVA, where groups on the same graph were not subject to comparison. Multiple comparisons were corrected using Holm–Sidak correction. Representative images of patient obturator nerve cross-section and muscle biopsy cross-section (showing intramuscular nerves) are from a single patient per genotype. Non-ALS and ALS samples, excluding SOD1 mutants, in both types of biopsies were previously validated by us and others as positive of phospho-TDP43 using the same antibodies and labeling and image acquisition techniques[13,15]. No statistical methods were used to predetermine sample sizes, but our sample sizes are similar to those reported in previous publications[35,86–89]. Threshold for determining statistical significance was $P < 0.05$. All statistical analyses were performed with GraphPad Prism 10.

Reporting summary

Further information on research design is available in the Nature Portfolio Reporting Summary linked to this article.

Data availability

The RNA and miRNA sequencing FASTQ files with raw sequencing data, text files with raw read counts and Excel files with processed read counts are available in the Gene Expression Omnibus (GEO) via accession number GSE286913. GRCm39/mm39 genome was accessed at https://www.gencodegenes.org/mouse/. All data generated in this study are provided in the Supplementary Information and Source Data files. Source data are provided with this paper.

Code availability

R codes that were developed within this study and used for RNA-seq analysis are available in the GEO via accession number GSE286913.

References

70. Brooks, B. R. El escorial world federation of neurology criteria for the diagnosis of amyotrophic lateral sclerosis. *J. Neurol. Sci.* **124**, 96–107 (1994).
71. Riva, N. et al. Motor nerve biopsy: clinical usefulness and histopathological criteria. *Ann. Neurol.* **69**, 197–201 (2011).
72. Boillée, S. et al. Onset and progression in inherited ALS determined by motor neurons and microglia. *Science* **312**, 1389–1392 (2006).
73. Gurney, M. E. et al. Motor neuron degeneration in mice that express a human Cu,Zn superoxide dismutase mutation. *Science* **264**, 1772–1775 (1994).
74. Fernandopulle, M. S. et al. Transcription factor–mediated differentiation of human iPSCs into neurons. *Curr. Protoc. Cell Biol.* **79**, e51 (2018).
75. Coenen-Stass, A. M. L. et al. Evaluation of methodologies for microRNA biomarker detection by next generation sequencing. *RNA Biol.* **15**, 1145–1145 (2018).
76. Kohen, R. et al. UTAP: user-friendly transcriptome analysis pipeline. *BMC Bioinformatics* **20**, 154 (2019).
77. Kozomara, A. & Griffiths-Jones, S. MiRBase: annotating high confidence microRNAs using deep sequencing data. *Nucleic Acids Res.* **42**, D68–D73 (2014).
78. Magen, I. et al. microRNA-based predictor for diagnosis of frontotemporal dementia. *Neuropathol. Appl. Neurobiol.* **49**, e12916 (2023).
79. Magen, I. et al. Circulating miR-181 is a prognostic biomarker for amyotrophic lateral sclerosis. *Nat. Neurosci.* **24**, 1534–1541 (2021).
80. Magen, I. et al. Muscle microRNAs in the cerebrospinal fluid predict clinical response to nusinersen therapy in type II and type III spinal muscular atrophy patients. *Eur. J. Neurol.* **29**, 2420–2430 (2022).
81. Love, M. I., Huber, W. & Anders, S. Moderated estimation of fold change and dispersion for RNA-seq data with DESeq2. *Genome Biol.* **15**, 550 (2014).
82. Keren-Shaul, H. et al. MARS-seq2.0: an experimental and analytical pipeline for indexed sorting combined with single-cell RNA sequencing. *Nat. Protoc.* **14**, 1841–1862 (2019).
83. Altman, T., Maimon, R., Ionescu, A., Pery, T. G. & Perlson, E. Axonal transport of organelles in motor neuron cultures using microfluidic chambers system. *J. Vis. Exp.* **2020**, 60993 (2020).
84. Tsanov, N. et al. smiFISH and FISH-quant – a flexible single RNA detection approach with super-resolution capability. *Nucleic Acids Res.* **44**, 1841–1862 (2016).
85. Silahtaroglu, A. N. et al. Detection of micrornas in frozen tissue sections by fluorescence in situ hybridization using locked nucleic acid probes and tyramide signal amplification. *Nat. Protoc.* **2**, 2520–2528 (2007).
86. Ionescu, A. et al. Targeting the Sigma-1 receptor via pridopidine ameliorates central features of ALS pathology in a $SOD1^{G93A}$ model. *Cell Death Dis.* **10**, 210 (2019).
87. Mead, R. J. et al. Optimised and rapid pre-clinical screening in the $SOD1^{G93A}$ transgenic mouse model of amyotrophic lateral sclerosis (ALS). *PLoS ONE* **6**, e23244 (2011).
88. Sahoo, P. K. et al. Axonal G3BP1 stress granule protein limits axonal mRNA translation and nerve regeneration. *Nat. Commun.* **9**, 3358 (2018).
89. Corradi, E. et al. Axonal precursor miRNAs hitchhike on endosomes and locally regulate the development of neural circuits. *EMBO J.* **39**, e102513 (2020).

Acknowledgements

The Perlson laboratory is supported by the Human Frontiers Science Program, the Ministry of Health, State of Israel—JPND program, three grants from the Israel Science Foundation and the

Muscular Dystrophy Association (grant numbers RGP0026/2020-102, 3-17160, 735/19, 3497/21, 794/24, 1063948, respectively) and by the Radala Foundation for ALS Research, the Sagol Center for Regenerative Medicine 2023–2024 award and the Ministry of Science and Technology, State of Israel (67982). Additionally, we would like to express our gratitude to L. Bikovski from the Myers Neuro-behavioral core facility at the Interdepartmental core facility, Faculty of Medicine, Tel Aviv University, for helping in the behavioral motor assays and to B. Barak, G. Levy and O. Ophir from the School of Psychological Sciences, Faculty of Social Sciences, Tel Aviv University, for helping with virus injection.
E.H. is the Mondry Family Professorial Chair and Head of the Andrea L. and Lawrence A. Wolfe Family Center for Research on Neuroimmunology and Neuromodulation. The Hornstein laboratory is funded by the Robert Packard Center for ALS Research at Johns Hopkins University; the Weizmann–Brazil Center for Research on Neurodegeneration at the Weizmann Institute of Science; the Israel Science Foundation (135/16, 3497/21, 424/22, 425/22 and 494/24); Target ALS; the United States–Israel Binational Science Foundation (2 021 181); Dr. Sydney Brenner and friends; Edward and Janie Moravitz; Yeda-Sela; Yeda-CEO; the Nella and Leon Benoziyo Center for Neurological Diseases; the Kekst Family Institute for Medical Genetics; the David and Fela Shapell Family Center for Genetic Disorders Research; the Vener New Scientist Fund; the Julius and Ray Charlestein Foundation; the Goldhirsh-Yellin Foundation; the Redhill Foundation; the Rothberg Charitable Trust; the Dr. Dvora and Haim Teitelbaum Endowment Fund; and the Anita James Rosen Foundation.

Author contributions

A. Ionescu, L. Ankol, D.G., T.A., Y.N., A.G.S., O.B.A. and N.S. performed cell culture, biochemical and/or staining experiments, imaging and analysis. I.M. and Y.C. performed RNA-seq and analyses. T.G.P. and R.C. performed image analyses. L. Ankol, A. Ionescu and A. Ibraheem executed RT–PCR analysis. A. Ionescu performed smiFISH, puro-PLA and OPP experiments. A. Ionescu., D.G., T.G.P. and L. Ankol isolated EVs and performed characterization. L. Ankol performed injections, in vivo experiment and behavioral motor assays. A.D., C.E.B.-K., Z.E.-U., D.A., E.T., N.R. and A.Q. provided human patient samples. Y.D. planned and executed the dual-luciferase assay. L. Alfahel and A. Israelson provided SOD1^{G37R} mice. F.R. and P.D. aided with FISH experiments. A. Ionescu, L. Ankol, A.D., E.H. and E.P. designed the study and wrote the manuscript.

Competing interests

The authors declare no competing interests.

Additional information

Extended data is available for this paper at https://doi.org/10.1038/s41593-025-02062-6.

Supplementary information The online version contains supplementary material available at https://doi.org/10.1038/s41593-025-02062-6.

Correspondence and requests for materials should be addressed to Eran Perlson.

Peer review information *Nature Neuroscience* thanks Thomas Lloyd, Giampietro Schiavo and Benjamin Wolozin for their contribution to the peer review of this work.

https://doi.org/10.1038/s41593-025-02062-6

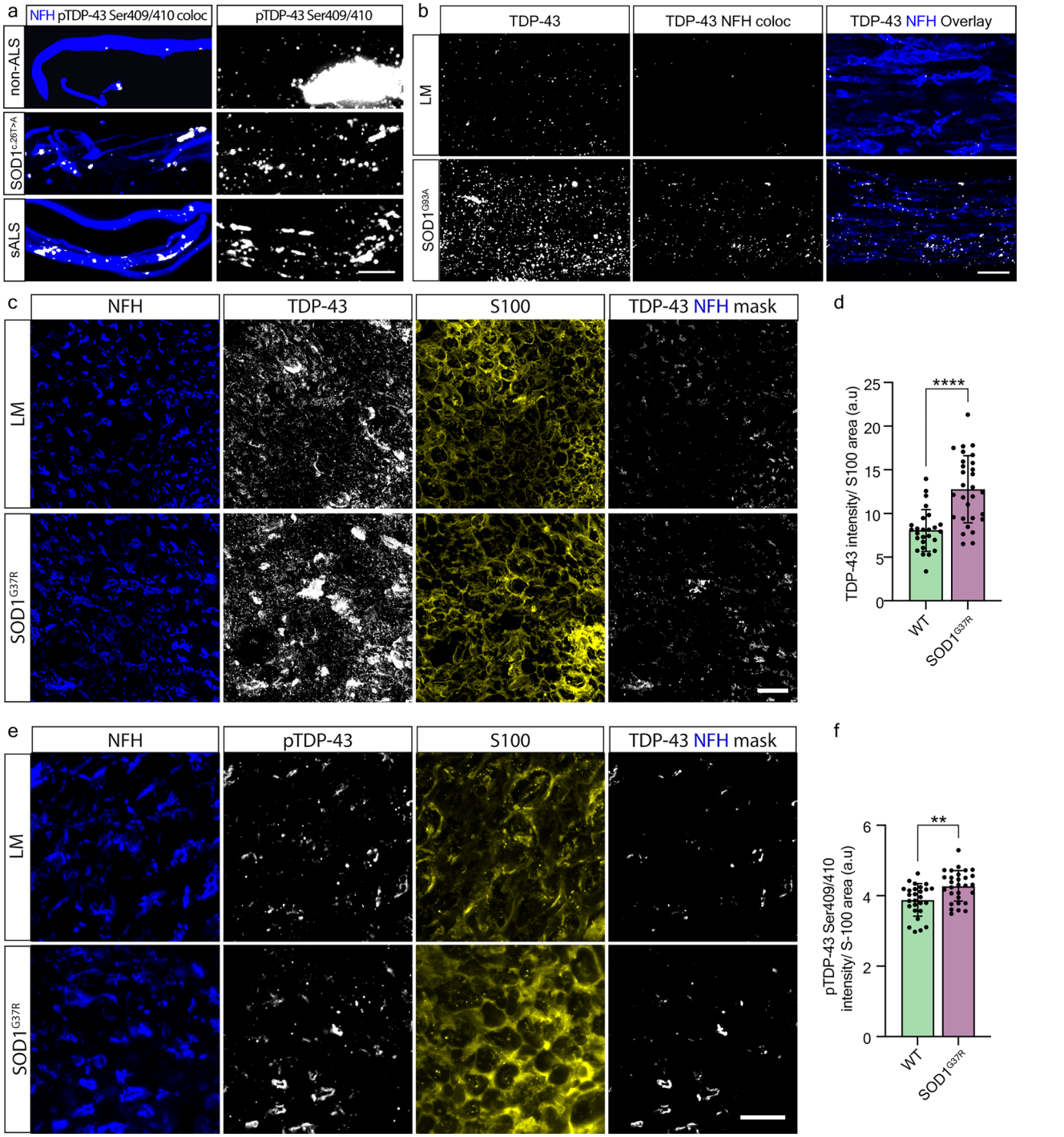

Extended Data Fig. 1 | TDP-43 peripheral pathology in SOD1 patients and SOD1 mouse models. a) Immunofluorescent staining for pTDP-43 in intramuscular nerves within muscle biopsies of non-ALS (spinal stenosis), *SOD1 (c.26 T > A)*, and sALS patients. Blue indicates NFH, Gray indicates pTDP-43 and colocalized pTDP-43 within NFH positive nerves (in the respective panel). Scale bar: 5 µm. **b**) Representative immunofluorescent images of TDP-43 in sciatic nerve longitudinal sections of $SOD1^{G93A}$ mice and their littermates (LM). Gray indicates TDP-43 and NFH-masked TDP-43 (in the respective panel), blue indicates NFH. Scale bar: 10 µm. **c**) Representative images of TDP-43 immunolabeling in sciatic nerve cross sections of p290 $SOD1^{G37R}$ mice and their littermates. Gray indicates TDP-43 and NFH-masked TDP-43 (in the respective panel), blue indicates NFH, yellow indicates S100β. Scale bar: 10 µm. **d**) Quantitative analysis of TDP-43 intensity within S100β region in sciatic nerve sections of p290 $SOD1^{G37R}$ mice and their littermates. Data is shown as the mean TDP-43 intensity in S100β mask ± SD. n = 26; 29 images from 3 mice in each condition. Two-tailed unpaired student's t-test. ****p = 2.11×10^{-6}. **e**) Representative images of pTDP-43 immunolabeling in sciatic nerve cross sections of p290 $SOD1^{G37R}$ mice and their littermates. Gray indicates pTDP-43 and NFH-masked pTDP-43 (in the respective panel), blue indicates NFH, yellow indicates S100β. Scale bar: 10 µm. **f**) Quantitative analysis of pTDP-43 intensity within S100β region in sciatic nerve sections of p290 $SOD1^{G37R}$ mice and their littermates. Data is shown as the mean pTDP-43 intensity in S100β mask ± SD. n = 27; 29 images from 3 mice in each condition. Two-tailed unpaired student's t-test. **p = 0.0018. For **a**, immunofluorescent labeling for pTDP-43 in SOD1 patient repeated once for 1 patient. Labeling on non-ALS and ALS patients was repeated for 6 patients and 6 healthy controls. For **b**, representative images of experiment repeated in 3 mice per genotype.

https://doi.org/10.1038/s41593-025-02062-6

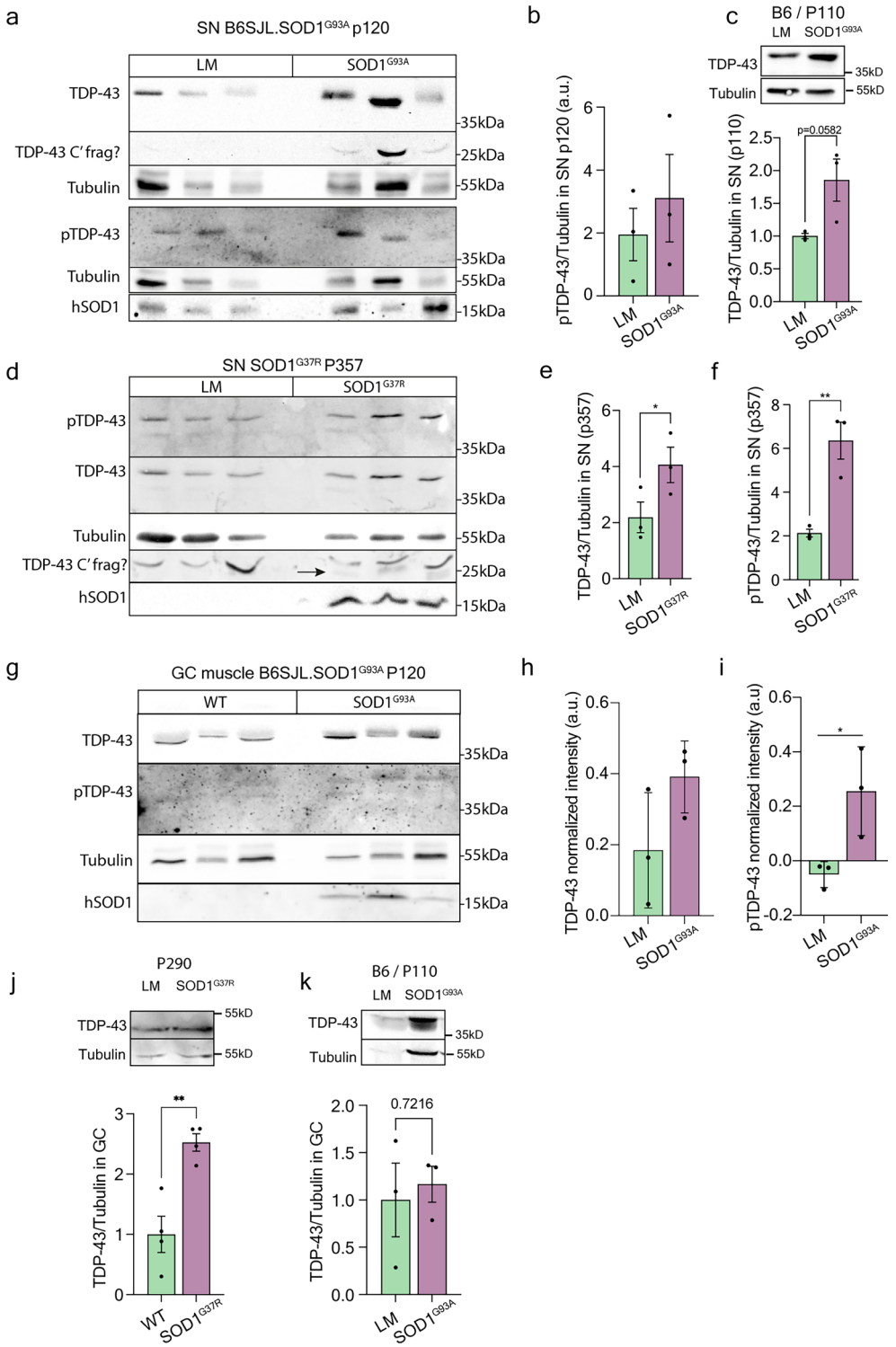

Extended Data Fig. 2 | See next page for caption.

https://doi.org/10.1038/s41593-025-02062-6

Extended Data Fig. 2 | TDP-43 Peripheral pathology in SOD1 mouse models. **a**) Western blots of sciatic nerve axoplasms from 3 p120 B6SJL.SOD1^{G93A} and 3 littermates for TDP-43 (43kD), pTDP-43 (43kD) and hSOD1 (17kD). Tubulin (55kD) was used as a loading control. A distinct 25kD additional band was observed in the TDP-43 blot of SOD1^{G93A} samples, suggested to be C-terminal fragments, as previously reported[10]. **b**) Quantitative analysis of the pTDP-43/tubulin intensities within blots from sciatic nerve axoplasms of p120 B6SJL.SOD1^{G93A} and littermates. n = 3 mice in each condition. Two-tailed unpaired student's t-test, p = 0.5146. **c**) Representative western blot image and quantitative analysis of the TDP-43/tubulin intensities within blots from sciatic nerve axoplasms of p110 B6.SOD1^{G93A} and littermates. n = 3 mice in each condition. TDP-43 (43kD), Tubulin (55kD). Two-tailed unpaired student's t-test. n = 0.0582. **d**) Western blots of sciatic nerve axoplasms from 3 p357 SOD1^{G37R} and 3 littermates for TDP-43 (43kD), pTDP-43 (43kD) and hSOD1 (17kD). Tubulin (55kD) was used as a loading control. A distinct 25kD additional band was observed in the TDP-43 blot of SOD1^{G37R} samples, suggested to be C-terminal fragments as previously reported. **e, f**) Quantitative analysis of TDP-43/tubulin (**e**) and pTDP-43/tubulin (**f**) in sciatic nerve axoplasms of p357 SOD1^{G37R} and littermates. n = 3 mice in each condition. Two-tailed unpaired student's t-test, **p = 0.0081, *p < 0.0118. **g**) Western blots of gastrocnemius muscle lysates from 3 p120 B6SJL.SOD1^{G93A} and 3 littermates for TDP-43 (43kD), pTDP-43 (43kD) and hSOD1 (17kD). Tubulin (55kD) was used as a loading control. **h, i**) Quantitative analysis of TDP-43/tubulin (**h**) and pTDP-43/tubulin (**i**) background subtracted thus the negative values in gastrocnemius muscles of B6SJL.SOD1^{G93A} and littermates. n = 3 mice in each condition. Two-tailed unpaired student's t-test, p = 0.1348(h), *p = 0.0355(i). **j, k**) Representative images and quantitative analyses of TDP-43/tubulin in gastrocnemius muscle lysates from p290 SOD1^{G37R} (**j**) and P110 B6.SOD1^{G93A} (**k**) mice versus their littermates. TDP-43 (43kD), Tubulin (55kD). n = 4 mice per condition (**j**); n = 3 mice per condition (**k**). Two-tailed, unpaired student's t-test. **p = 0.0038(j), p = 0.7216(k).

https://doi.org/10.1038/s41593-025-02062-6

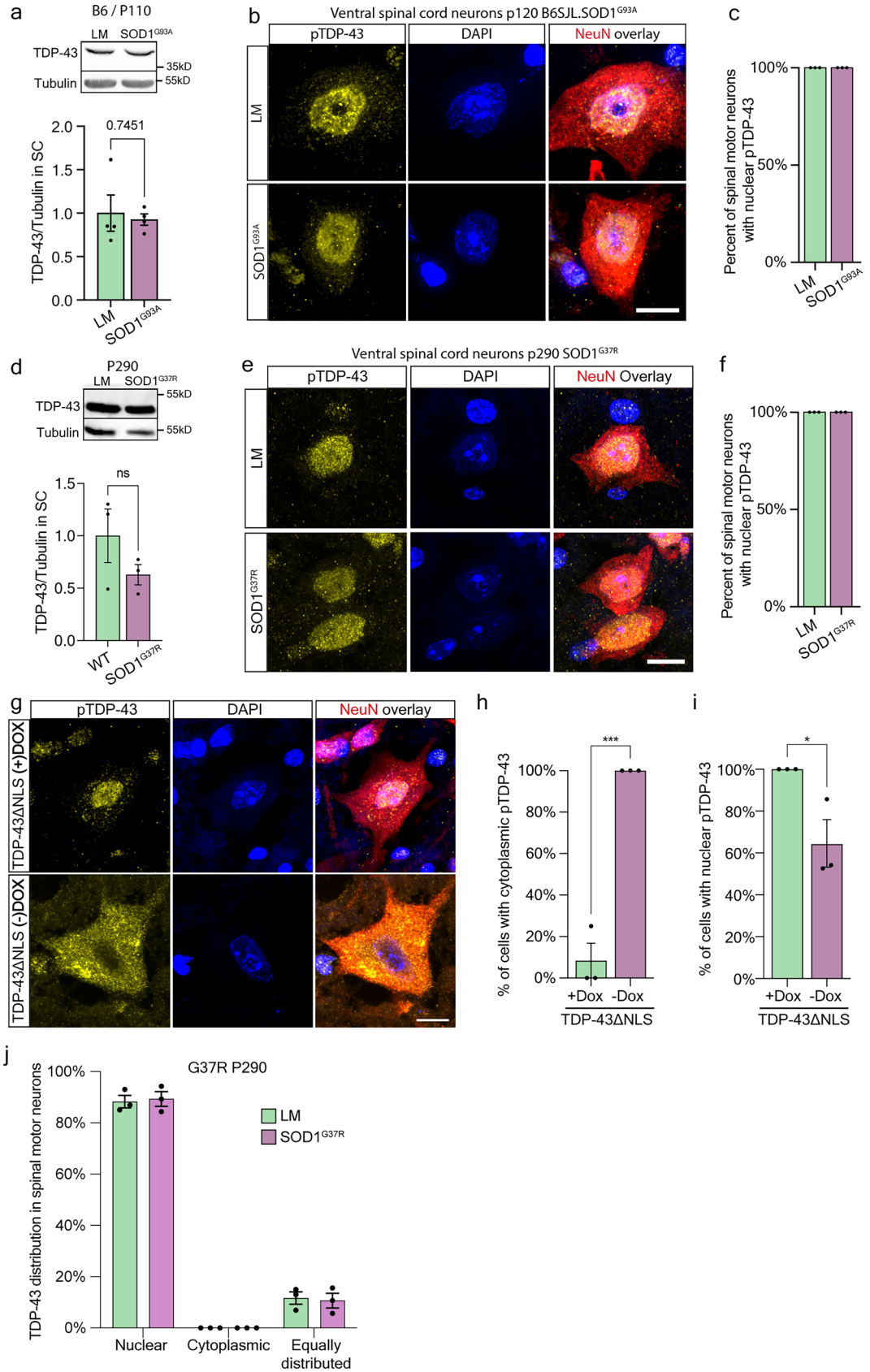

Extended Data Fig. 3 | See next page for caption.

https://doi.org/10.1038/s41593-025-02062-6

Extended Data Fig. 3 | TDP-43 pathology is non apparent in spinal cords of SOD1 mouse models. a) Representative images and quantitative analysis of TDP-43/tubulin in spinal cord lysates from p110 B6.SOD1^{G93A} mice and their littermates. TDP-43 (43kD), Tubulin (55kD). n = 4 mice per condition. Two-tailed, unpaired student's t-test. p = 0.7451 **b, c**) Representative images (**b**) and quantitative analysis (**c**) for the percent of ventral motor neurons with nuclear pTDP-43 in spinal cords of p120 B6SJL.SOD1^{G93A} mice and their littermates. Data are shown as the mean percent of ventral motor neurons with nuclear pTDP-43 ± SEM. n = 3 mice in each condition. Yellow indicates pTDP-43, blue indicates nuclei (DAPI), red indicates NeuN. Scale bars: 10 µm. **d**) Representative images and quantitative analysis of TDP-43/tubulin in spinal cord lysates from p290 SOD1^{G37R} mice and their littermates. TDP-43 (43kD), Tubulin (55kD). n = 3 mice per condition. Two-tailed, unpaired student's t-test. p = 0.2462 **e, f**) Representative images (**e**) and quantitative analysis (**f**) for the percent of ventral motor neurons with nuclear pTDP-43 in spinal cords of p290 SOD1^{G37R} mice and their littermates. Data are shown as the mean percent of ventral motor neurons with nuclear pTDP-43 ± SEM. n = 3 mice in each condition. Yellow indicates pTDP-43, blue indicates nuclei (DAPI), red indicates NeuN. Scale bars: 10 µm. **g**–**i**) Representative images (**g**) and quantitative analysis (**h-i**) for the percent of ventral motor neurons with cytoplasmic (**h**) or nuclear (**i**) pTDP-43 in spinal cords of induced (-Dox; 2 weeks) TDP43ΔNLS mice and non-induced controls (+Dox). Data are shown as the mean percent of ventral motor neurons with cytoplasmic/nuclear pTDP-43 ± SEM. n = 3 mice in each condition. Two-tailed student's t-test, ***p = 0.0004(h), *p = 0.0293(i). Yellow indicates pTDP-43, blue indicates nuclei (DAPI), red indicates NeuN. Scale bars: 10 µm. **j**) Quantitative distribution analysis for the percent of ventral motor neurons with either nuclear TDP-43, cytoplasmic TDP-43 or equally distributed TDP-43 in spinal cords of p290 SOD1^{G37R} mice and their littermates. Data are shown as the mean percent of TDP-43 positive neurons in the respective subcellular region ± SEM. Multiple unpaired t-test. p = 0.8013(mainly nuclear), p = 0.802(equally distributed) n = 3 mice from each condition.

https://doi.org/10.1038/s41593-025-02062-6

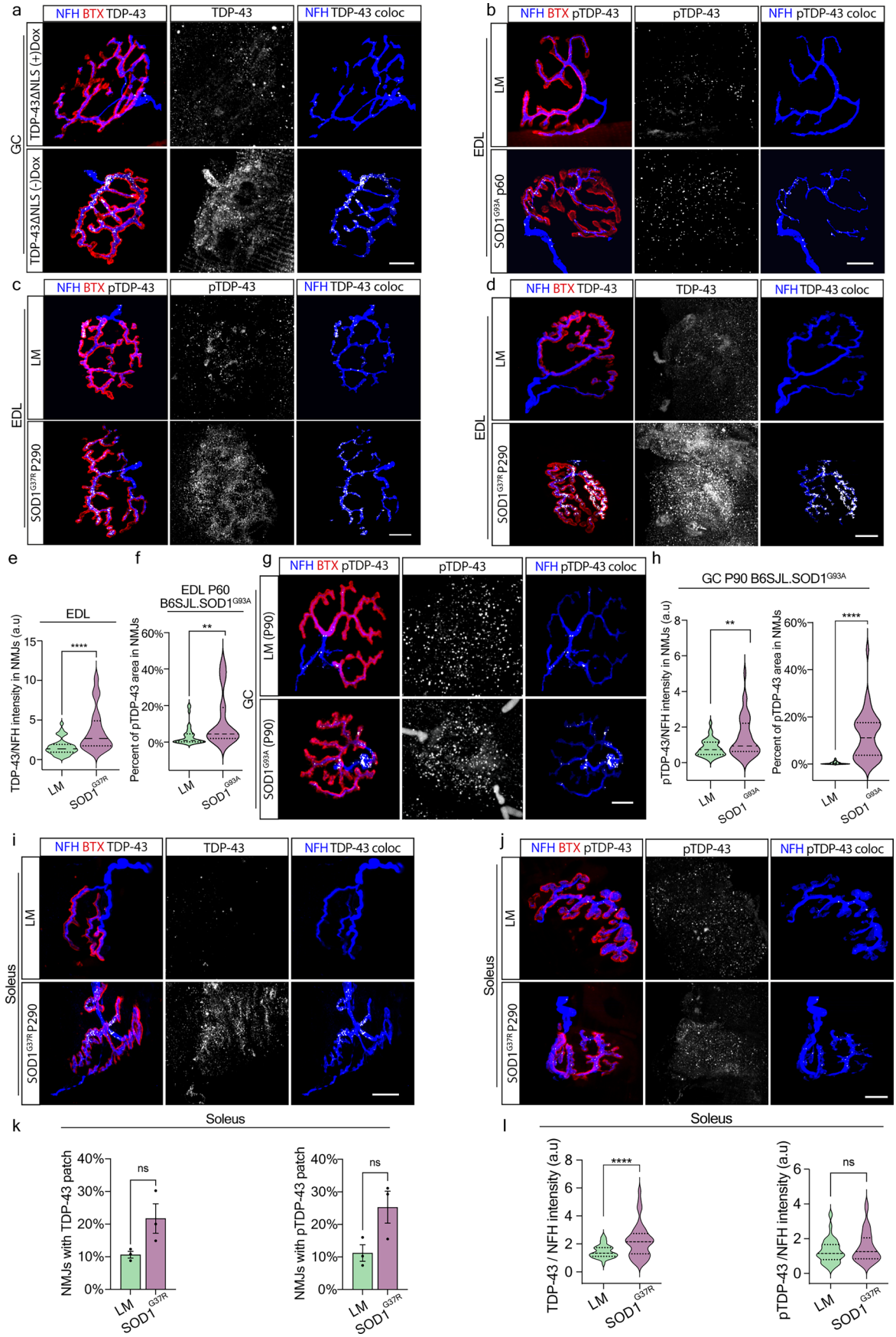

Extended Data Fig. 4 | See next page for caption.

https://doi.org/10.1038/s41593-025-02062-6

Extended Data Fig. 4 | Comparison of TDP-43 and pTDP-43 accumulation in NMJs of fast versus slow muscle fibers in SOD1 mouse models. **a**) Representative immunofluorescent images of TDP-43 localization in NMJs from gastrocnemius muscle of induced TDP43ΔNLS (-Dox; 2-weeks) and non-induced control (+Dox). Gray indicates TDP-43 and TDP-43:NFH 3D colocalization result (in the respective panel), blue indicates NFH, red indicates BTX. Scale bar: 10 µm. experiment repeated in 5 mice per genotype. **b**) Representative immunofluorescent images of pTDP-43 localization in NMJs from EDL muscle of p60 B6SJL.SOD1^{G93A} and littermate control mice. Gray indicates pTDP-43 and pTDP-43:NFH 3D colocalization result (in the respective panel), blue indicates NFH, red indicates BTX. Scale bar: 10 µm. experiment repeated in 3 mice per genotype. **c**) Representative immunofluorescent images of pTDP-43 localization in NMJs from EDL muscle of p290 SOD1^{G37R} and littermate control mice. Gray indicates pTDP-43 and pTDP-43:NFH 3D colocalization result (in the respective panel), blue indicates NFH, red indicates BTX. Scale bar: 10 µm. experiment repeated in 3 mice per genotype. **d, e**) Representative immunofluorescent images (**d**) and quantitative analysis (**e**) of TDP-43 in NMJs from EDL muscle of p290 SOD1^{G37R} and littermate control mice. Gray indicates TDP-43 and TDP-43:NFH 3D colocalization result (in the respective panel), blue indicates NFH, red indicates BTX. Scale bar: 10 µm. Data are shown in violin density plots with markings of first, median and third quartiles of mean TDP-43 intensity to NFH/Synaptophysin intensity in NMJs. Two-tail unpaired student's t-test. ****p = 2.57×10^{-5}. n = 38 NMJs from 3 mice per condition. **f**) Quantitative analysis of the percent of pTDP-43 colocalization area in presynapses at NMJs of P60 B6SJL.SOD1^{G93A}. Two-tail unpaired student's t-test. **p = 0.0071. n = 33;21 NMJs from 3 mice per condition. **g, h**) Representative immunofluorescent images (**g**) and quantitative analysis (**h**) of pTDP-43 in NMJs from EDL muscle of p90 B6SJL.SOD1^{G93A} and littermate control mice. Gray indicates pTDP-43 and pTDP-43:NFH 3D colocalization result (in the respective panel), blue indicates NFH, red indicates BTX. Scale bar: 10 µm. Data are shown in violin density plots with markings of first, median and third quartiles of mean pTDP-43 intensity to NFH intensity (left panel) or percent of pTDP-43 colocalization area in presynapses at NMJs. Two-tail unpaired student's t-test. **p = 0.0021(pTDP-43 intensity), ****p = 4.8×10^{-9} (pTDP-43 area). n = 39;36 NMJs from 3 mice per condition. **i, j**) Representative immunofluorescent images of TDP-43 (**i**) and pTDP-43 (**j**) localization in NMJs from soleus muscles of p290 SOD1^{G37R} and littermate control mice. Gray indicates TDP-43 and TDP-43:NFH 3D colocalization result (in the respective panel), blue indicates NFH, red indicates BTX. Scale bar: 10 µm. **k**) Quantitative analysis for the percent of NMJs with apparent TDP-43/pTDP-43 patch in soleus muscles from p290 SOD1^{G37R} and littermate controls. Data are shown as the mean percent of NMJs with TDP-43 (left panel) or pTDP-43 (right panel) patch ± SEM. n = 3 mice per group. Two-tailed, unpaired t-test. p = 0.0746(TDP-43), p = 0.0636(pTDP-43). **l**) Quantitative analysis of TDP-43 (left panel) and pTDP-43 (right panel) intensity in NMJs from soleus muscle of p290 SOD1^{G37R} and littermate control mice. Data are shown in violin density plots with markings of first, median and third quartiles of mean TDP-43 (left) or pTDP-43 (right) intensity to NFH/Synaptophysin intensity in NMJs. Two-tail unpaired student's t-test. n = 44;41 (TDP-43), n = 82,52 (pTDP-43) NMJs from 3 mice per condition. ****p = 5.295×10^{-5} (TDP-43), p = 0.0899(pTDP-43).

https://doi.org/10.1038/s41593-025-02062-6

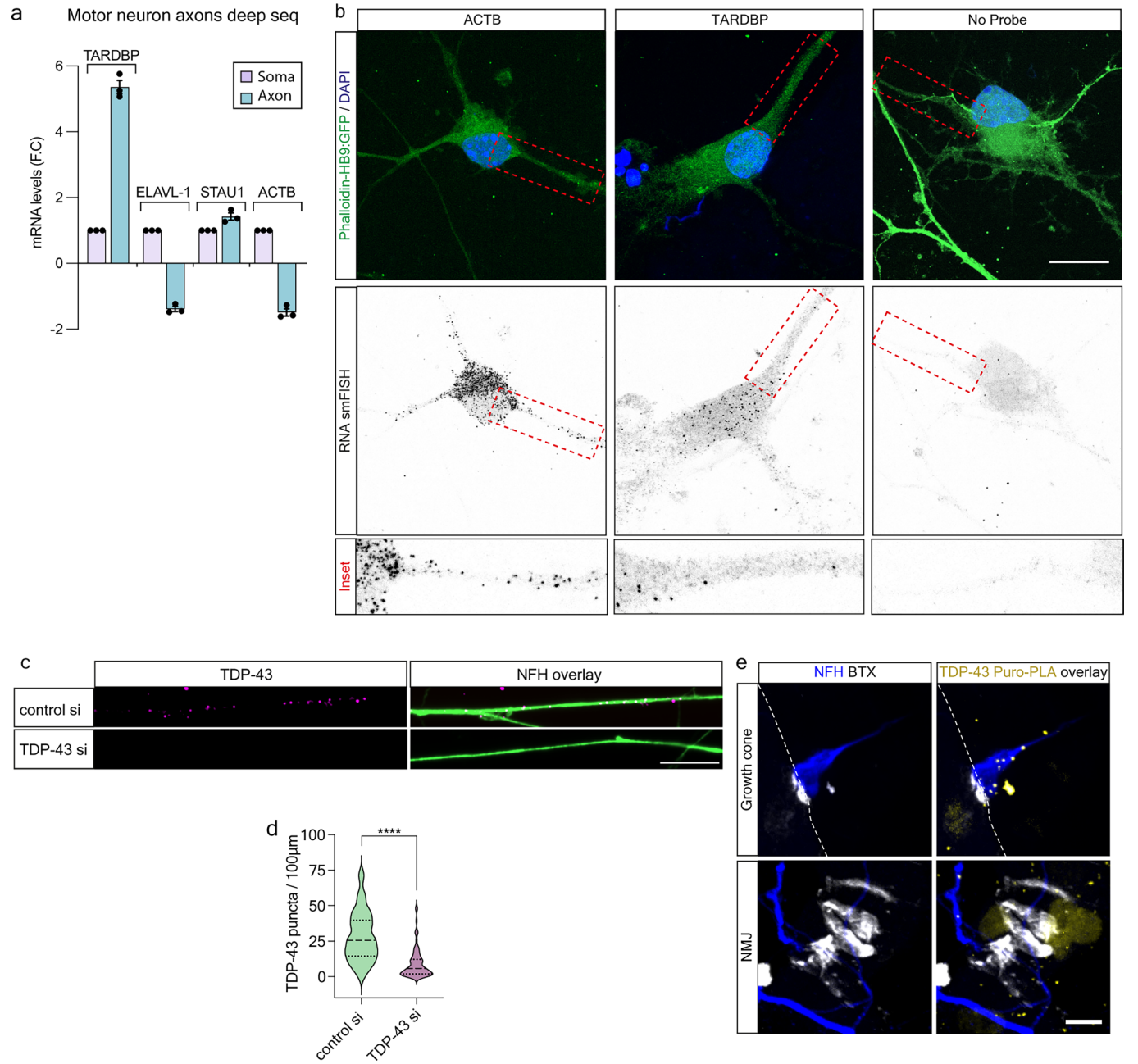

Extended Data Fig. 5 | TDP-43 mRNA localization and local translation in motor neuron axons. a) Relative mRNA transcript levels in axons versus cell-bodies (soma) of *Tardbp*, *Elavl1*, *Stau1*, and *Actb*. Data are shown as fold change (F.C) of normalized counts in axons over soma for each mRNA transcript. Raw data reanalysis of axonal and soma RNA-seq from primary motor neurons (Rotem et al., 2017). **b**) Representative images of smFISH for β-actin and TDP-43 mRNAs compared with no probe control in primary motor neuron cell bodies. Gray indicates RNA FISH, green indicates phalloidin/HB9:GFP, blue indicates nuclei (DAPI). Red dashed line marks proximal axon shown in magnified insets. Scale bar: 15 µm. Experiment performed in 3 neuronal cultures. **c-d**) Representative images (**c**) and quantitative analysis (**d**) of TDP-43 immunolabeling of distal axons in MFC 4 days after localized transfection with TDP-43 siRNA mix or with control siRNA. Magenta indicates TDP-43, green indicates NFH. Scale bar: 10 µm. Data are shown in violin density plots with markings of first, median and third quartiles of mean number of TDP-43 puncta in 100 µm axons. Two-tailed unpaired student's t-test. ****$p < 1 \times 10^{-14}$. n = 94;87 axons from 3 independently grown co-cultures. **e**) Representative immunofluorescent images of TDP-43 puro-PLA in a growth cone at a premature NMJ, and in a mature NMJ in healthy co-cultures. Blue indicates NFH, gray indicates BTX, yellow indicates TDP-43 puro-PLA, white dashed line indicates skeletal muscle margins (in NMJ panel, the entire region is over a skeletal muscle) Scale bar: 5 µm. Experiment repeated in 3 neuromuscular co-cultures.

https://doi.org/10.1038/s41593-025-02062-6

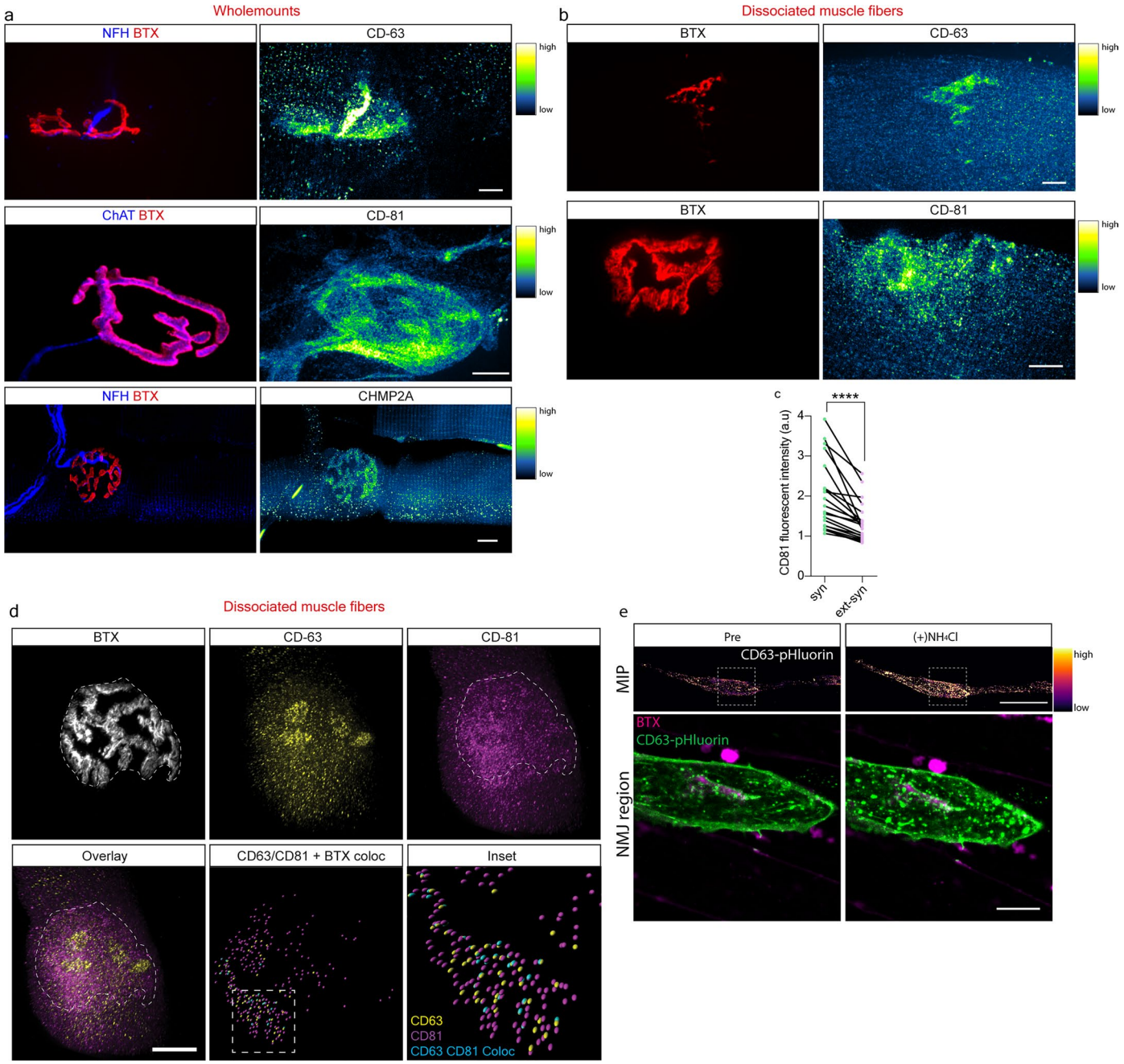

Extended Data Fig. 6 | Enrichment of extracellular vesicle machinery in post-synaptic apparatus of NMJs. a) Representative images for the localization of CD63 (upper panel), CD81 (mid panel) and CHMP2A (lower panel) in healthy GC muscle NMJs. Blue indicates NFH, red indicates BTX, Dynamic blue-green-yellow indicates CD63/CD81/CHMP2A according to raw fluorescent intensity (blue=low; yellow=high). Scale bar: 10 µm. Experiment repeated 3 times (CD63, CD81) and 6 times for CHMP2A. **b**) Representative images for the localization of CD63 (upper panel), CD81 (lower panel) in NMJs within dissociated muscle fibers following enzymatic digestion of surrounding cells and connective tissues. Red indicates BTX, Dynamic blue-green-yellow indicates CD63/CD81 according to raw fluorescent intensity (blue=low; yellow=high). Scale bar: 10 µm. Experiment repeated 3 times. **c**) Quantitative analysis of CD81 raw fluorescent signal in synaptic versus extrasynaptic regions within the same muscle fiber. Two-tail paired student's t-test. ****$p = 7.68 \times 10^{-5}$. n = 20 muscle fibers from 3 mice **d**) Representative images and 3D Imaris puncta colocalization analysis of extracellular vesicle machinery in postsynaptic apparatus of enzymatically denervated EDL muscle. White indicates BTX, yellow indicates CD-63, magenta indicates CD-81. Imaris puncta analysis was performed on BTX colocalization channels with CD-63 and CD-81. Scale bar: 10 µm. Experiment performed once. **e**) Representative max intensity projected (MIP) low magnification images (upper panel) and high magnification images of BTX-positive region (lower panel) of CD63-pHluorin signal in cultured primary muscle before (pre) and immediately after application of ammonium chloride (NH_4Cl). Dynamic magenta-orange-white indicates CD63-pHluorin intensity in low magnification images. Lower panel: magenta indicates BTX, green indicates CD63-pHluorin signal. Scale bars: 50 µm; 10 µm in upper and lower panels respectively. Experiment repeated in 2 neuromuscular co-cultures.

https://doi.org/10.1038/s41593-025-02062-6

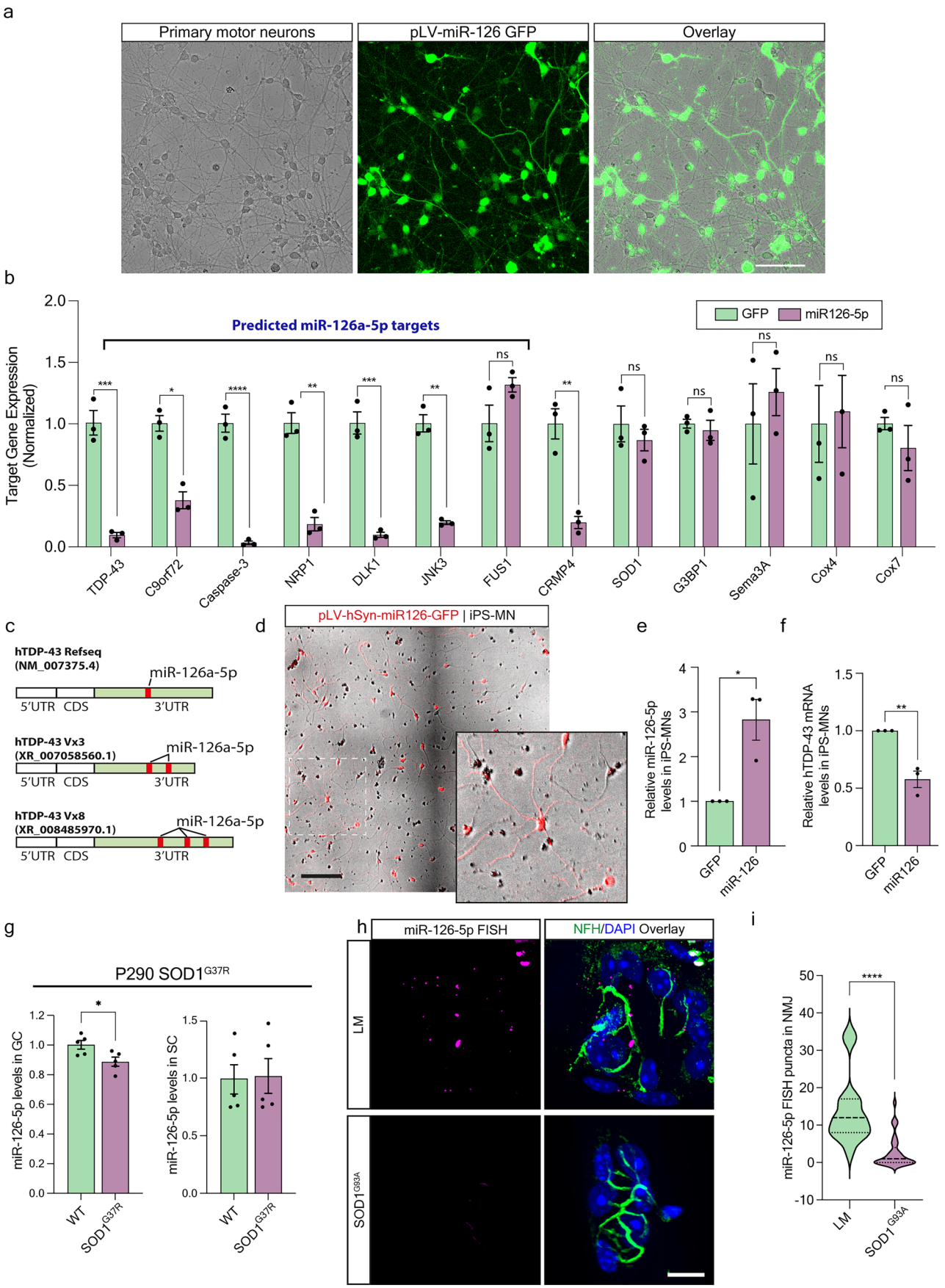

Extended Data Fig. 7 | See next page for caption.

https://doi.org/10.1038/s41593-025-02062-6

Extended Data Fig. 7 | miR-126a-5p regulates the mRNA of several predicted targets including the mouse and human mRNA of TDP-43, and is dysregulated in SOD1 NMJs. a) Representative images of a 6DIV primary motor neuron culture infected with lentiviral (pLV) miR-126 GFP. Green indicates GFP. Scale bar: 100 µm. Repeated in 3 neuronal cultures. **b**) Quantitative RT-PCR for multiple predicted and non-predicted mouse mRNA targets of miR-126a-5p in primary motor neurons expressing LV-GFP versus LV-miR126-GFP. Data are shown as the mean relative expression of each target in LV-miR126-GFP over LV-GFP ± SEM. Two-way ANOVA with Holm-Sidak correction for multiple comparisons. n = 3 neuronal cultures per condition. p = 0.0003(TDP-43), p = 0.0286(C9orf72), $p = 8.78 \times 10^{-5}$(Caspase-3), p = 0.012(NRP1), p = 0.0003(DLK1), p = 0.0016(JNK3), p = 0.7869(FUS1), p = 0.0017(CRMP4), p = 0.999(SOD1), p = 0.999(G3BP1), p = 0.9346(Sema3A), p = 0.999(COX4), p = 0.992(COX7). **c**) Graphical illustrations of the human TDP-43 mRNA and two more predicted isoforms. Green indicates 3'UTRs, red marks the putative miR-126-5p target sites. **d**) Representative low magnification image of healthy IPSC-derived motor neurons (IPSC-MN; KOLF) infected with pLV-hSyn-miR126. Red indicates GFP in infected neurons. Scale bar: 150 µm. image **e**) Quantitative Taqman RT-PCR for miR-126-5p in human IPSC-MN (KOLF) expressing either pLV-Syn-miR126-GFP or pLV-Syn-GFP. Data are shown as the mean relative miR-126-5p expression ± SEM in miR-126 infected IPSC-derived motor neurons versus GFP infected ones. Two-tailed unpaired student's t-test. n = 3 seperatly grown cultures. *p = 0.0162. **f**) Quantitative RT-PCR for human TDP-43 mRNA with primers targeting the coding sequence (CDS) in IPSC-derived motor neurons following 7 days of pLV-Syn-miR126 or pLV-Syn-GFP infection. Data are shown as the mean relative mRNA levels of human TDP-43 mRNA ± SEM. Two-tailed unpaired student's t-test. n = 3 separately grown cultures. **p < 0.0042. **g**) Quantitative TaqMan RT-PCR for miR-126-5p in p290 $SOD1^{G37R}$ GC muscles versus p290 $SOD1^{G37R}$ SC. Data are shown as the mean relative level of miR-126-5p ± SEM. U6 was used as endogenous loading control. Two-tailed unpaired t-test. n = 5 mice in each group. *p = 0.0263(GC), p = 0.888(SC). **h-i**) Representative images (**h**) and quantification (**i**) of miR-126a-5p FISH in NMJs of p60 B6SJL.$SOD1^{G93A}$ EDL muscles versus littermate controls. Blue indicates nuclei (DAPI), green indicates NFH, magenta indicates miR-126a-5p FISH. Scale bar: 10 µm. Data are shown in violin distribution plots of the miR-126a-5p puncta per NMJ with markings of first, median and third quartiles. Two-tailed unpaired student's t-test. n = 15; 33 NMJs from 3 mice in each condition. ****$p = 3.689 \times 10^{-7}$.

https://doi.org/10.1038/s41593-025-02062-6

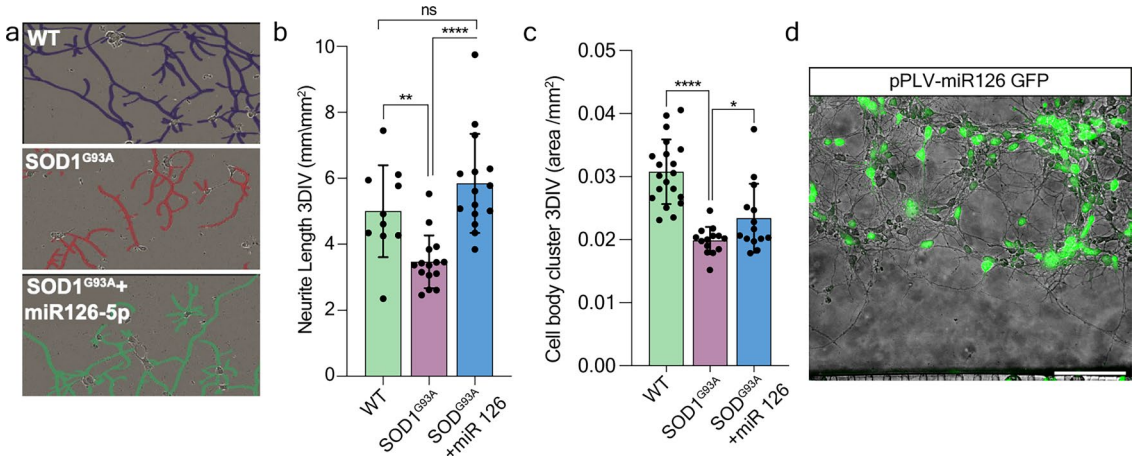

Extended Data Fig. 8 | miR-126-5p enhances neuronal growth of SOD1^{G93A} primary motor neurons. a–c) Representative phase images with axonal marking (**a**) and quantification of neurite length (**b**) and cell-body cluster area (**c**) in WT, SOD1^{G93A} or miR-126-GFP infected-SOD1^{G93A} primary motor neurons at 3DIV. Blue, red and green segmented lines indicate the neurite tracing. Scale bar: 100 µm. Data are shown as the mean neurite length/cell body cluster area (mm/mm^2) ± SEM (**c**), or cell body cluster area (area/mm^2) ± SEM (**d**). n = 10; 15; 15 wells (over 6,000 neurons analyzed in every condition). One-way ANOVA with Holm-Sidak correction, **p = 0.00942(**b**), ****p = 0.00002(**b**), p = 0.1065(**b**), ****p = 5.41×10^{-8}(**c**), *p = 0.0467. **d**) Representative image of pLV-miR-126 GFP infected primary motor neurons cultured in the proximal compartment of microfluidic chambers. Green indicates GFP. Scale bar: 100 µm.

https://doi.org/10.1038/s41593-025-02062-6

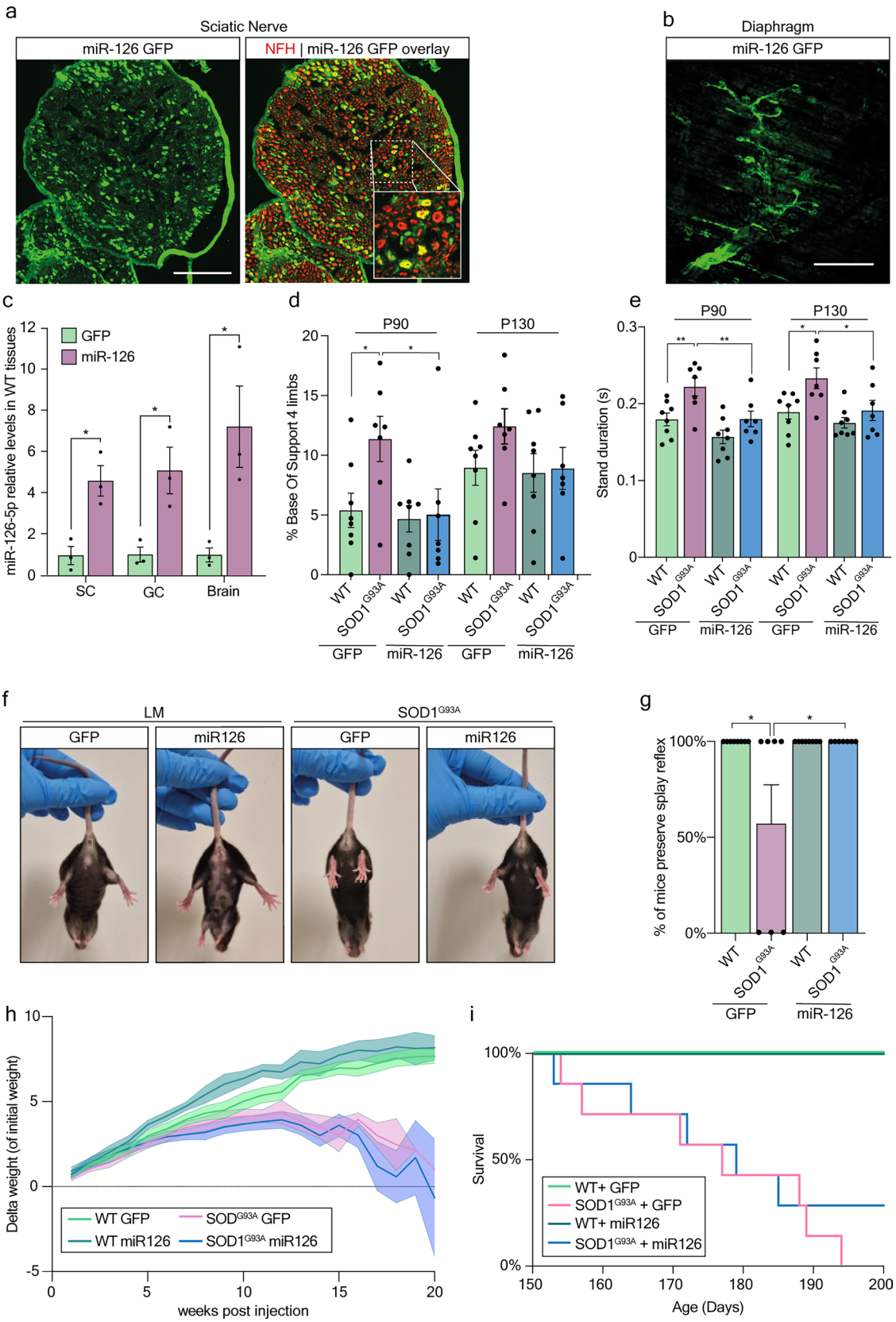

Extended Data Fig. 9 | See next page for caption.

https://doi.org/10.1038/s41593-025-02062-6

Extended Data Fig. 9 | miR-126a-5p overexpression in vivo. a-b) Representative images of sciatic nerve cross section (**a**) and phrenic nerve in the diaphragm (**b**) of control animals injected with AAV PhP.Eb miR-126 viral particles. Green indicates GFP, red indicates NFH. Scale bars: 200 µm. **c**) Quantitative Taqman RT-PCR analysis of miR-126a-5p expression in SC, GC and brains of GFP-infected versus miR126-infected healthy mice. Data are shown as the mean relative miR-126a-5p level ± SEM. n = 3 mice in each condition. Two-tailed unpaired student's t-test, *p = 0.0135(SC), 0.026(GC), 0.0363(Brain). **d-e**) Catwalk gait analysis of WT and $SOD1^{G93A}$ mice infected with either GFP or miR126, at symptomatic (p90) and late symptomatic (p130) stages. Data are shown as the mean stand duration (**d**; seconds) and % base of support on 4 limbs (**e**). n = 8 mice in each group. One-way ANOVA with Holm-Sidak correction. *p = 0.0277(d; p90; WT-GFP vs. SOD-GFP, and SOD1-GFP vs. SOD1-miR), p = 0.2587(d; p130; WT-GFP vs. SOD-GFP, and SOD1-GFP vs. SOD1-miR), **p = 0.0091(e; p90; WT-GFP vs. SOD-GFP, and SOD1-GFP vs. SOD1-miR), *p = 0.0143(e; p130; WT-GFP vs. SOD-GFP, and SOD1-GFP vs. SOD1-miR). **f, g**) Representative images (**f**) and quantification (**g**) of the hindlimb splay reflex in $SOD1^{G93A}$ mice and their littermates infected with either AAV PhP.Eb GFP, or with AAV PhP.Eb miR-126-GFP. Data are shown as the percent of mice who presented normal splay reflex ± SEM. n = 8; 8; 7; 7 mice in each group. Non-parametric Kruskal-Wallis test, *p < 0.02(WT-GFP vs. SOD1-GFP), *p = 0.0258(SOD1-GFP vs. SOD1-miR). **h, i**) In vivo longitudinal tracking of mouse weight (**h**) and survival (**i**) in all experimental groups. In (**h**), data are shown as the mean weight gain/loss at every timepoint compared with weight on injection day ± SEM. In (i), data are shown in a Kaplan-Maier survival curve starting at p150 (age of mice). n = (8,8;WT),(7,7;$SOD1^{G93A}$) mice in each group. For **a,b** – images are representative for 3 similarly injected mice.

https://doi.org/10.1038/s41593-025-02062-6

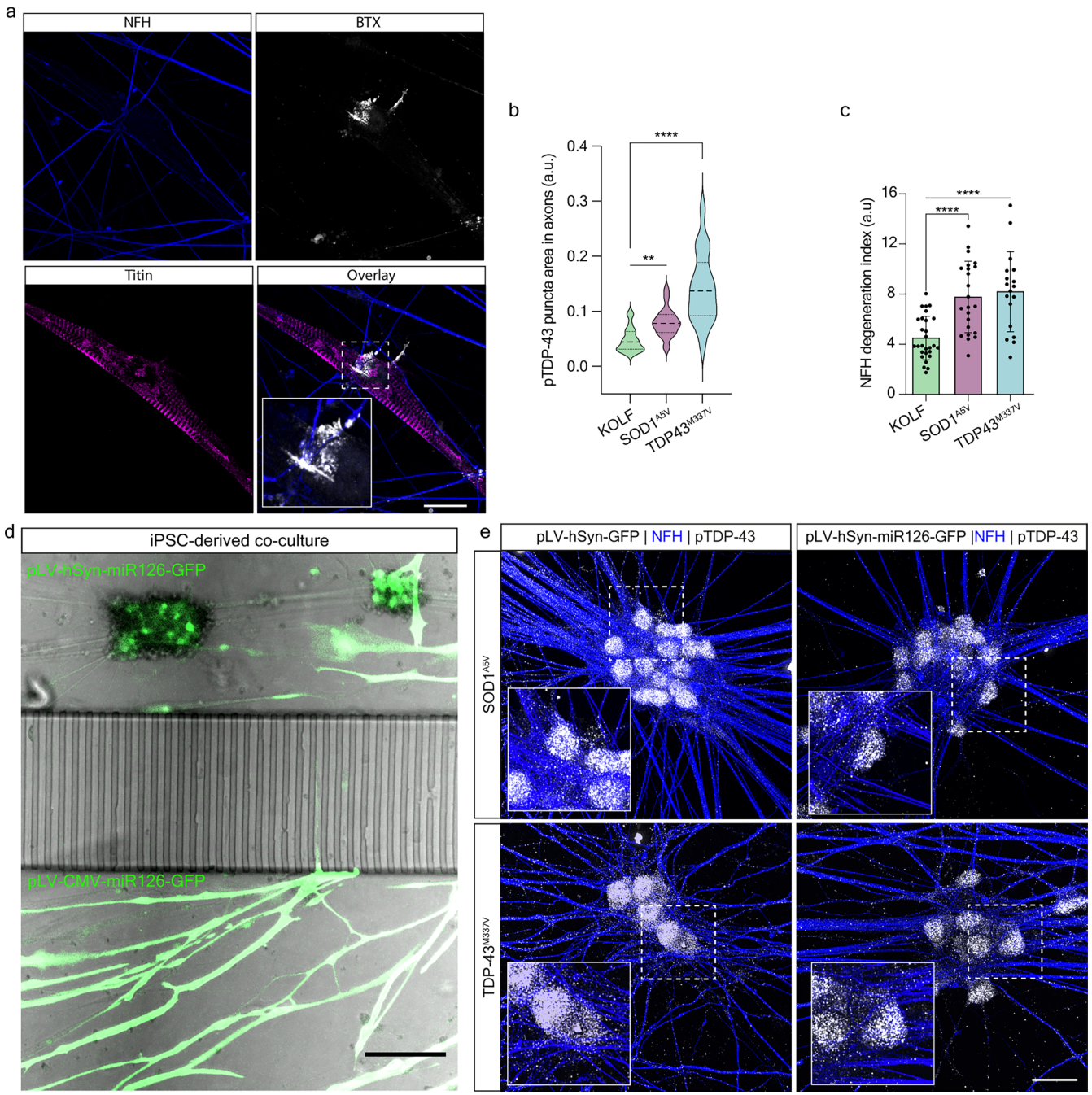

Extended Data Fig. 10 | IPSC-derived co-culture differentiation and NMJ formation. a) Representative images from the distal (NMJ) compartment IPSCC-derived co-culture of healthy (KOLF) motor neurons and skeletal muscles. Blue indicates NFH, gray indicates BTX, magenta indicates Titin. White dashed line indicates NMJ region shown in inset. Scale bar: 20 µm. **b-c**) Quantitative analysis of axonal pTDP-43 fraction (**b**) and axonal degeneration index (**c**) in iPSC-derived co-cultures of SOD1^{A5V}, TDP-43^{M337V}, and their isogenic control (KOLF). Data in (**b**) are shown in violin density plots of pTDP-43 puncta area out of NFH area of axons at the NMJ compartment with marking of first, median, and third quartiles. n = 21; 26, 18 imaging fields from 3 independently grown neuromuscular co-cultures. One-way ANOVA with Holm-Sidak correction. **p = 0.0064, ****p = 4.4×10^{-10}. Data in (**c**) are shown as the mean NFH degeneration index of axons in the NMJ compartment ± SD. n = 28; 23; 18 imaging fields from 3 neuromuscular co-cultures. One-way ANOVA with Holm-Sidak correction. ****p = 4.66×10^{-5}(SOD1^{A5V}), 1.96×10^{-5}(TDP43^{M337V}). **d**) Representative image for lentivirus-infected IPSC-MN and IPSC-muscles in co-culture within MFC. Green in IPSC-MN (upper compartment) indicates pLV-hSyn-miR126-GFP, Green in IPSC-muscles (lower compartment) indicates pLV-CMV-miR126-GFP. Scale bar: 150 µm. **e**) Representative immunofluorescent images for pTDP-43 nuclear localization in SOD1^{A5V} and TDP-43^{M337V} IPSC-MN in the proximal MFC compartment of co-cultures infected with either pLV-hSyn-GFP or pLV-hSyn-miR126-GFP. Blue indicates NFH, gray indicates pTDP-43. White dashed square marks the IPSC-MN magnified in the inset. Scale bar: 20 µm. For **a,d,e** experiments repeated in 3 neuromuscular co-cultures.

nature portfolio

Corresponding author(s): PERLSON Eran

Last updated by author(s): Jul 28, 2025

Reporting Summary

Nature Portfolio wishes to improve the reproducibility of the work that we publish. This form provides structure for consistency and transparency in reporting. For further information on Nature Portfolio policies, see our Editorial Policies and the Editorial Policy Checklist.

Statistics

For all statistical analyses, confirm that the following items are present in the figure legend, table legend, main text, or Methods section.

n/a	Confirmed
☐	☒ The exact sample size (*n*) for each experimental group/condition, given as a discrete number and unit of measurement
☐	☒ A statement on whether measurements were taken from distinct samples or whether the same sample was measured repeatedly
☐	☒ The statistical test(s) used AND whether they are one- or two-sided *Only common tests should be described solely by name; describe more complex techniques in the Methods section.*
☐	☒ A description of all covariates tested
☐	☒ A description of any assumptions or corrections, such as tests of normality and adjustment for multiple comparisons
☐	☒ A full description of the statistical parameters including central tendency (e.g. means) or other basic estimates (e.g. regression coefficient) AND variation (e.g. standard deviation) or associated estimates of uncertainty (e.g. confidence intervals)
☐	☒ For null hypothesis testing, the test statistic (e.g. *F*, *t*, *r*) with confidence intervals, effect sizes, degrees of freedom and *P* value noted *Give P values as exact values whenever suitable.*
☒	☐ For Bayesian analysis, information on the choice of priors and Markov chain Monte Carlo settings
☒	☐ For hierarchical and complex designs, identification of the appropriate level for tests and full reporting of outcomes
☒	☐ Estimates of effect sizes (e.g. Cohen's *d*, Pearson's *r*), indicating how they were calculated

Our web collection on statistics for biologists contains articles on many of the points above.

Software and code

Policy information about availability of computer code

Data collection	Data collection was done using software provided with the relevant equipment: Thermo-Fisher StepOne PCR machine running StepOne sofware (version 2.3), Andor iXon Revolution (Andor IQ3 software), Andor BC43 (Anor Fusion ver. 2.3 softare), 3i Marianas (3i SlideBook software version 6) Spinning Disk confocal systemems. JEM-1400Plus Transmission Electron Microscope - Images were captured using SIS Megaview III and iTEM, the TEM imaging platform (Olympus, Tokyo, Japan). Sartorius Incucyte s3, 2019A (Nerotrack software module; cat. no.9600□0010). NanoSight: Nanoparticle Tracking. western-blots and northern-blots images were acquired using iBright. RNA sequencing was performed on Illumina Novaseq SP100 flow cell sequencer.
Data analysis	Fiji/Image J software (version 2.3.0/1.53q) was used to analyze confocal raw files and western-blots, GraphPad Prism (version 10.1.0 (264)) was used for statistical analyses .StepOne qPCR 96-well module (Thermo-fisher) was used to determine differentially expressed genes, Andor Fusion (ver. 2.3), Andor iQ3 (ver. 3.0), 3i SlideBook softwares (ver. 6.0), Incucyte (ver.) were used for image viewing and analysis. Bitplain Imaris (Ver. 8.4.6; Oxford instruments) was used for 3-dimentional colocalization analyses. Annotated sequencing data were collected from Fastq files using GeneGlobe pipeline (Qiagen RNA-seq Analysis Platform 1 & 2.5.1; https://geneglobe.qiagen.com/us/analyze) for miRNA sequencing, and GeneCode (vM25, 2020; UTAP pipeline) for mRNA sequencing. Illumina fastq files were uploaded for bioinformatics analysis to CLC genomic workbench V.24 and the "RNA-seq analysis" tool with default options. Following this, trimmed reads were aligned to the GRCm39 - mm39 mouse genome (downloaded from: https://www.gencodegenes.org/mouse/). mRNA isoforms were quantified by CLC genomic workbench "expectation-maximization" estimation algorithm. DESeq2 package was used for normalization and comparison of read counts. R codes that were developed within this study and used for RNA-seq analysis were made available in the gene expression omnibus (GEO) via accession number GSE286913. For more information see Methods..

For manuscripts utilizing custom algorithms or software that are central to the research but not yet described in published literature, software must be made available to editors and reviewers. We strongly encourage code deposition in a community repository (e.g. GitHub). See the Nature Portfolio guidelines for submitting code & software for further information.

Data

Policy information about availability of data

All manuscripts must include a data availability statement. This statement should provide the following information, where applicable:

- Accession codes, unique identifiers, or web links for publicly available datasets
- A description of any restrictions on data availability
- For clinical datasets or third party data, please ensure that the statement adheres to our policy

The RNA and miRNA sequencing Fastq files with raw sequencing data, text files with raw read counts, excel files with processed read counts were made available in the gene expression omnibus (GEO) via accession number GSE286913.

Research involving human participants, their data, or biological material

Policy information about studies with human participants or human data. See also policy information about sex, gender (identity/presentation), and sexual orientation and race, ethnicity and racism.

Reporting on sex and gender	Human muscle, and nerve biopsies were collected from patients based on their clinical diagnosis as having ALS or non-ALS condition and based on their genetic background as carriers of mutant SOD1 gene. Human serum samples from ALS patients and healthy donors were collected based on patient clinical diagnosis as having ALS condition, or healthy patients with noneurological medical record. Serum samples include both male and female samples. We did not conduct a sex-based analysis of our results as we did not have specific hypotheses about putative differences.
Reporting on race, ethnicity, or other socially relevant groupings	We did not ask donors to report their race, ethnicity, or other socially relevant information.
Population characteristics	Patient biopsies were acquired from ALS and non-ALS Caucasian male patients aged 26–66 years (48.33±13.12). ALS patients were diagnosed with clinically definite or probable ALS according to El Escorial criteria. Non-ALS control muscles included a variation of findings, which were consistent with a diagnosis of normal muscle, severe, chronic ongoing denervation and reinnervation due to spinal stenosis. Patient blood serum samples were acquired from Caucasian ALS patients aged45-88 (68.37±14.49), and healthy controls aged 23-66 (43.87±16.81) from both sexes.
Recruitment	Muscle biopsy samples (sALS, non-ALS) and corresponding clinical data were collected for diagnostic purposes at the Sheba neuromuscular pathology lab and subsequently enrolled in this study (SMC 4485-17). Healthy subjects (serum donors) and ALS patients volunteers where evaluated at the Sheba Medical Center neuromuscular clinic, where clinical data, serum samples (6525-19, 6526-19) and muscle biopsies (Helsinki 4871-18) where collected and analyzed at the neuromuscular pathology lab. Muscle biopsy samples and corresponding clinical data were collected for diagnostic purposes at the Sheba neuromuscular pathology lab and subsequently enrolled in this study (SMC 4485-17). Healthy subjects and ALS patients volunteers where evaluated at the Sheba Medical Center neuromuscular clinic, where clinical data, serum samples (6525-19, 6526-19) and muscle biopsies (Helsinki 4871-18) where collected and analyzed at the neuromuscular pathology lab. Obturator nerve biopsies (sALS, SOD1-ALS, non-ALS) and corresponding clinical data were collected for diagnostic purposes followed by research application at the Institute of experimental neurology, San Raffaele hospital, Milan, Italy (RF-2019-12369320). Muscle biopsy (SOD1-ALS) and the corresponding clinical data was collected for diagnostic purposes at the Department of Neurology, Neuromuscular Diseases Research Laboratory, Hacettepe University, Turkey. All ALS patients were diagnosed with clinically definite or probable ALS according to El Escorial criteria.
Ethics oversight	Obturator nerve biopsies: The Local Ethics Committee of the San Raffaele Hospital on human experimentation approved the study protocol (RF-2019-12369320) Muscle biopsies: 1. Hacettepe university ethical committee approval number: GO20/177, 11/02/2020. 2. The Sheba Tel Hashomer medical center ethics committee for human experimentations approved the study protocol (IRB SMC 4871-18) Serum samples: The Sheba Tel Hashomer medical center ethics committee for human experimentations approved the study protocol (IRB SMC 6525-19 and 6526-19).

Note that full information on the approval of the study protocol must also be provided in the manuscript.

Field-specific reporting

Please select the one below that is the best fit for your research. If you are not sure, read the appropriate sections before making your selection.

☒ Life sciences ☐ Behavioural & social sciences ☐ Ecological, evolutionary & environmental sciences

Life sciences study design

All studies must disclose on these points even when the disclosure is negative.

Sample size	We chose to use sample size of at least three independent repeats which is sufficient to determine statistical significance. For in vivo descriptive experiments at least three mice from each group were measured. Sample sizes were determined based on ours and other previous publications with SOD1 mouse models. For in vivo AAV-miR126 injection experiment - sample sizes were determined based on previous publications: Ionescu, A. et al. Targeting the Sigma-1 Receptor via Pridopidine Ameliorates Central Features of ALS Pathology in a SOD1 G93A Model. Cell Death Dis 10, (2019). Maimon, R. et al. Mir126-5p downregulation facilitates axon degeneration and nmj disruption via a non–cell-autonomous mechanism in ALS. Journal of Neuroscience 38, (2018). Mead, R. J. et al. Optimised and Rapid Pre-clinical Screening in the SOD1G93A Transgenic Mouse Model of Amyotrophic Lateral Sclerosis (ALS). PLoS One 6, e23244 (2011). In general, the number of animals in each group was determined according to previous studies cited in our manuscript. For in vitro experiments at least 3 microfluidic chambers, each with at least 10 axons / NMJs from 3 independent biological repeats were used to overcome in-experiment variance between microfluidic chamber which tend to vary in the number of axons crossing from one compaerment to another, and in the number of skeletal muscles. High number of axons/NMJs was needed for immunoflourescent assays, to gain the full image of the axonal population, which is not homogeneous. For muscle contraction essays, higher number of microfluidic chambers were used (7-10), as there is variability in this assay compared to other methods in this manuscript and as each chamber was counted as a whole rather than counting single axons.
Data exclusions	In rare cases, single outliers from technical repeats with extremely abnormal values due to technical issues were excluded automatically by outlier-identification, performed via Graphpad Prism based on standard deviation. This was done only when sample size was n>10. Exclusion was done via ROUT method; Q=1%.
Replication	To ensure reproducibility, experiments were performed at least three independent times, other than when noted otherwise, using similar conditions and reagents. All attempts at replication were successful.
Randomization	In vitro studies: Co-culture exeriments, cells were divided randomly to wells/microfluidic chambers. For Rab27a shRNA experiments, muscles in all chambers were transfected with shRNA plasmids. Half of the co-cultures were treated with the doxycycline treatment to induce expression of the shRNA and the other half remained untreated. For miR-126-5p inhibitor experiments, half of the co-culture were transfected with miR-126-5p inhibitor and half were transfected with a mock control. For HB9 motor neurons, cells were divided randomly between wells/chambers. For IPSC derived motor neurons, cells were plated in similar numbers in wells/chambers based on known TDP-43 M337V\ SOD1 A5V or isogenic control cell genotype. For in vivo studies: Mice were predetermined by their genotype. For each experiment, to every randomly selected SOD1 mouse a littermate non-mutant control, age and sex matched, was assigned to serve as his biological control. For human sample studies: Samples from human participants were predetermined by their clinical diagnosis. The samples were labeled and slices from each patient were chosen randomly for the experimental immunoflourescent essay.
Blinding	Blinding was applied whenever possible, however not for all data due to insufficient manpower. The remaining experiments, were analyzed and perfomed by the same person who obtained the data.

Reporting for specific materials, systems and methods

We require information from authors about some types of materials, experimental systems and methods used in many studies. Here, indicate whether each material, system or method listed is relevant to your study. If you are not sure if a list item applies to your research, read the appropriate section before selecting a response.

Materials & experimental systems

n/a	Involved in the study
☐	☒ Antibodies
☐	☒ Eukaryotic cell lines
☒	☐ Palaeontology and archaeology
☐	☒ Animals and other organisms
☒	☐ Clinical data
☒	☐ Dual use research of concern
☒	☐ Plants

Methods

n/a	Involved in the study
☒	☐ ChIP-seq
☒	☐ Flow cytometry
☒	☐ MRI-based neuroimaging

Antibodies

Antibodies used

Primary antibodies:
1. Phospho (409/410)-TDP43, Proteintech Cat. 22309-1-AP. For WB/IF - 1:2000
Validation for WB and IF - https://www.ptglab.com/products/phospho-409-410--TDP43-Antibody-22309-1-AP.htm#testedapplications
2. TDP43, Proteintech. Cat. 10782-2-AP. For WB/IF - 1:2000. For pull down - 2µg per sample in 1ml.
Validation for WB, IP and IF - https://www.ptglab.com/products/TARDBP-Antibody-10782-2-AP.htm#tested-applications
3. Neurofilament 200 (rabbit), Sigma. Cat. N4142. For IF - 1:500-1:1000
Validation for IF - https://www.sigmaaldrich.com/IL/en/product/sigma/n4142
4. Neurofilament 200 (Chicken), Abcam. Cat. ab72996. For IF 1:500-1:1000
Validation for IF based on 24 references appearing in - https://www.abcam.com/neurofilament-heavy-polypeptide-antibodyab72996.html
5.Puromycin (clone 12D10), Millipore. Cat. MABE 343. For IF - 1:1000
Validation for IF - https://www.merckmillipore.com/INTL/en/product/Anti-Puromycin-Antibody-clone-12D10,MM_NF-MABE343?ReferrerURL=https%3A%2F%2Fwww.google.com%2F#anchor_Applications
6. ERK1/2 (065M4813V), Sigma. Cat. M5670. For WB - 1:10000
Validation for WB - 180 publications at https://www.sigmaaldrich.com/IL/en/product/sigma/m5670
7. alpha-Tubulin, Abcam. Cat. ab7291. For WB - 1:5000
Validation for WB - https://www.abcam.com/alpha-tubulin-antibody-dm1a-loading-control-ab7291.html
8. CD63 (H-193), Santa-Cruz. Cat. sc-15363. For WB - 1:200, for IF - 1:100. Both uses for IF and WB were validated in previously based on at least 34 reported articles in https://www.scbt.com/p/cd63-antibody-h-193#citations
9. CD-81 Abcam. Cat. ab79559. For WB - 1:2,000, For IF: 1:200. Both IF and WB uses were validated in over 104 prior works as indicated at: https://www.abcam.com/products/primary-antibodies/cd81-antibody-m38-ab79559.html
10. CD-9 Abcam Cat. ab92726. For WB - 1:100. WB used was validated in over 40 prior studies as indicated at: https://www.abcam.com/products/primary-antibodies/cd9-antibody-ab223052.html
11. Rab27a, Proteintech. 17817-1-AP, For WB - 1:200. For IF- 1:200. Antibody is KD/KO validated. Both WB and IF uses were validated in over 50 prior works as indicated at: https://www.ptglab.com/products/RAB27A-Antibody-17817-1-AP.htm#publications
12. Ago-2, Abcam. ab32381. For WB - 1:500. For IF -1:500. Both WB and IF uses were validated by over 340 prior works at indicated by: https://www.abcam.com/products/primary-antibodies/argonaute-2-antibody-ab32381.html
13. SOD1 (FL-154), Santa-Cruz. sc-11407. FOR WB - 1:500. WB use was previosly validated in over 99 prior works as indicated at: https://www.scbt.com/p/sod-1-antibody-fl-154#citations
14. CHMP2A, Proteintech. 10477-1-AP. For IF- 1:200. KO/KD validates. Over 40 prior works validate the use of this antibody: https://www.ptglab.com/products/CHMP2A-Antibody-10477-1-AP.htm#publications
15. GFP Abcam. ab38689. For IF - 1:1,000. KO validated. Referenced in over 3100 prior works as indicated at: https://www.abcam.com/products/primary-antibodies/gfp-antibody-ab13970.html
16. S100B, Sigma-Aldrich. S2532. For IF- 1:300. https://www.sigmaaldrich.com/IL/en/product/sigma/s2532?srsltid=AfmBOorSDHlttfWpOh1HBLVMUxZXKdaIDZYAj53MLQXLg3Iim4O5YTkC.
17. ALIX, Abcam. ab76608. wb 1:250. https://www.abcam.com/en-us/products/primary-antibodies/alix-antibody-ab76608?srsltid=AfmBOopAna05XiWfZsQ079yWXT97gM8iTKkk8tdAxN5QjnbSsoQtv5Fa.
18. GM130, BD biosciences. 610823. WB 1:200. https://www.bdbiosciences.com/en-in/products/reagents/microscopy-imagingreagents/
immunofluorescence-reagents/purified-mouse-anti-gm130.610823?tab=product_details.
19. Anti-Digoxigenin (DIG)-POD (poly), Fab fragments. Roche 11633716001 Used at 1:400 in miRNA-LNA FISH
Secondary antibodies:
1. Goat anti chicken 405, Abcam. Cat. ab175675. For IF - 1:500
2. Goat anti chicken 488, Abcam. Cat. ab150173. For IF - 1:1000
3. Goat anti mouse 488. Abcam. Cat. ab150113. For IF - 1:1000
4. Goat anti mouse 594. Invitrogen. Cat. A11032. For IF - 1:1000
5. Goat anti mouse 650. Abcam. Cat. ab96882. For IF - 1:1000
6. Goat anti rabbit 488. Invitrogen. Cat. A11034. For IF - 1:1000
7. Goat anti rabbit 594. Jackson Laboratories. Cat. 111-585-144. For IF - 1:1000
8. Goat anti rabbit 640. Abcam. Cat. ab150083. For IF - 1:1000.
9. Donkey anti mouse HRP. Jackson Laboratories. Cat. 715-035-151. For WB - 1:10000.
10. Donkey anti rabbit HRP. Jackson Laboratories. Cat. 715-035-152. For WB - 1:10000.

Validation

All antibodies were prevalidated by manufacturer and prior research, as stated in the supplied antibody data sheet and QA certificate.
1. Phospho (409/410)-TDP43, Proteintech Cat. 22309-1-AP. For WB/IF - 1:2000
Validation for WB and IF - https://www.ptglab.com/products/phospho-409-410--TDP43-Antibody-22309-1-

AP.htm#testedapplications
2. TDP43, Proteintech. Cat. 10782-2-AP. For WB/IF - 1:2000. For pull down - 2µg per sample in 1ml.
Validation for WB, IP and IF - https://www.ptglab.com/products/TARDBP-Antibody-10782-2-AP.htm#tested-applications
3. Neurofilament 200 (rabbit), Sigma. Cat. N4142. For IF - 1:500-1:1000
Validation for IF - https://www.sigmaaldrich.com/IL/en/product/sigma/n4142
4. Neurofilament 200 (Chicken), Abcam. Cat. ab72996. For IF 1:500-1:1000
Validation for IF based on 24 references appearing in - https://www.abcam.com/neurofilament-heavy-polypeptide-antibodyab72996.html
5.Puromycin (clone 12D10), Millipore. Cat. MABE 343. For IF - 1:1000
Validation for IF - https://www.merckmillipore.com/INTL/en/product/Anti-Puromycin-Antibody-clone-12D10,MM_NF-MABE343?ReferrerURL=https%3A%2F%2Fwww.google.com%2F#anchor_Applications
6. ERK1/2 (065M4813V), Sigma. Cat. M5670. For WB - 1:10000
Validation for WB - 180 publications at https://www.sigmaaldrich.com/IL/en/product/sigma/m5670
7. alpha-Tubulin, Abcam. Cat. ab7291. For WB - 1:5000
Validation for WB - https://www.abcam.com/alpha-tubulin-antibody-dm1a-loading-control-ab7291.html
8. CD63 (H-193), Santa-Cruz. Cat. sc-15363. For WB - 1:200, for IF - 1:100. Both uses for IF and WB were validated in previously based on at least 34 reported articles in https://www.scbt.com/p/cd63-antibody-h-193#citations
9. CD-81 Abcam. Cat. ab79559. For WB - 1:2,000, For IF: 1:200. Both IF and WB uses were validated in over 104 prior works as indicated at: https://www.abcam.com/products/primary-antibodies/cd81-antibody-m38-ab79559.html
10. CD-9 Abcam Cat. ab92726. For WB - 1:100. WB used was validated in over 40 prior studies as indicated at: https://www.abcam.com/products/primary-antibodies/cd9-antibody-ab223052.html
11. Rab27a, Proteintech. 17817-1-AP, For WB - 1:200. For IF- 1:200. Antibody is KD/KO validated. Both WB and IF uses were validated in over 50 prior works as indicated at: https://www.ptglab.com/products/RAB27A-Antibody-17817-1-AP.htm#publications
12. Ago-2, Abcam. ab32381. For WB - 1:500. For IF -1:500. Both WB and IF uses were validated by over 340 prior works at indicated by: https://www.abcam.com/products/primary-antibodies/argonaute-2-antibody-ab32381.html
13. SOD1 (FL-154), Santa-Cruz. sc-11407. FOR WB - 1:500. WB use was previosly validated in over 99 prior works as indicated at: https://www.scbt.com/p/sod-1-antibody-fl-154#citations
14. CHMP2A, Proteintech. 10477-1-AP. For IF- 1:200. KO/KD validates. Over 40 prior works validate the use of this antibody: https://www.ptglab.com/products/CHMP2A-Antibody-10477-1-AP.htm#publications
15. GFP Abcam. ab38689. For IF - 1:1,000. KO validated. Referenced in over 3100 prior works as indicated at: https://www.abcam.com/products/primary-antibodies/gfp-antibody-ab13970.html
16. S100B, Sigma-Aldrich. S2532. For IF- 1:300. https://www.sigmaaldrich.com/IL/en/product/sigma/s2532?srsltid=AfmBOorSDHlttfWpOh1HBLVMUxZXKdaIDZYAj53MLQXLg3Iim4O5YTkC.
17. ALIX, Abcam. ab76608. wb 1:250. https://www.abcam.com/en-us/products/primary-antibodies/alix-antibody-ab76608?srsltid=AfmBOopAna05XiWfZsQ079yWXT97gM8iTKkk8tdAxN5QjnbSsoQtv5Fa.
18. GM130, BD biosciences. 610823. WB 1:200. https://www.bdbiosciences.com/en-in/products/reagents/microscopy-imagingreagents/
immunofluorescence-reagents/purified-mouse-anti-gm130.610823?tab=product_details.
19. Anti-Digoxigenin (DIG)-POD (poly), Fab fragments. - Some validation are supplied by the manufacturer, yet these HRP-conjugated antibody fragments are well established and highly referenced for multiple uses.

Eukaryotic cell lines

Policy information about cell lines and Sex and Gender in Research

Cell line source(s)	HEK-293T cells were acquired from ATCC
Authentication	The cell line used was not autheniticaticated, other than determining Neomycin (G-418) resistance.
Mycoplasma contamination	Cell lines were routinly tested for mycoplasma, and found to be negative. We used mycoplasma detection kit (Biological Industries, Israel).
Commonly misidentified lines (See ICLAC register)	No commonly misidentified lines were used.

Animals and other research organisms

Policy information about studies involving animals; ARRIVE guidelines recommended for reporting animal research, and Sex and Gender in Research

Laboratory animals	1. HB9-GFP (Jax stock no. 005029). 2. ICR female mice 6-10-weeks old (Institute of Animal Science, Harlan) were used for maintenance of the HB9-GFP colony was maintained by breeding. 3. SOD1G93A (Stock No: 002726; Jackson Laboratories) colonies were maintained by breeding with C57BL/6J mice. Mice were euthanized at presymptomatic stages (p60), symptomatic stage (p90) and late symptomatic stage (p120-p130). PHP.eB injected mice were presymptomatic at the time of injection (p60) and were kept live until end stage as determined by the animla's incapability to rise from lying on its side for over 10 seconds, as indicated at https://www.ncbi.nlm.nih.gov/pmc/articles/PMC4692639/. 4. loxSOD1G37R mice (Stock No: 016149; Jackson Laboratory) harboring a floxed transgene comprising human SOD1 gene bearing G37R mutation. Colonies were maintained by breeding heterozygous loxSOD1G37R males with female with pure C57BL/6J background to eliminate confounding genetic influences.

5. SOD1G93A-ChAT::tdTomato and LM-ChAT::tdTomato mice were obtained by mating ChAT::ROSAtdTomato females (ChAT::cre and tdTomato::lox mice, (Jax stock no. 006410 and 007908, respectively) with SOD1G93A males. Mice were genotyped to distinguish WT from SOD1G93A as well as ChAT-ROSA tdTomato positive/neative genotypes.
6. B6.SOD1G93A (Stock No: 004435; Jackson Laboratories) colonies were maintained by breeding with female C57BL/6J mice. Mice were genotyped by PCR of DNA extracted from a tail biopsy.
For in-vivo studies, mice were between the ages of 60-180days, mixed sex.
Littermate mice that are age and sex matched to mutant animals were used as controls.
Genotype was pre-validated via PCR.

The animals were grown at Tel Aviv SPF facility, or at Ben-Gurion Barrier facility (SOD1G37R) under strict hygiene standards. Animal colonies are tested routinely for known pathogens according the list of Federation European Laboratory Animal Science Association (FELASA). In the facilities, Groups of up to five mice per cage were housed on a 12 h light/dark cycle, on autoclaved ASPEN wood chips bedding, at an ambient temperature of 22°C
±1°C, with humidity controlled at 50%, and were provided with UV-irradiated and micro-filtered Hydropac system for water.

Wild animals	No wild animals were used in this study.
Reporting on sex	Findings in this work apply to mice of both sexes. Sex of mice was taken into consideration in study desing upon injection of PHP.eBmiR-126 or GFP viral particles - each experimental group was assigned with mice of both sexes.
Field-collected samples	No field-collected animals were used in this study.
Ethics oversight	Animal experiments were approved and supervised by the Animal Ethics Committee of Tel-Aviv University All animal procedures were approved by the Institutional Animal Care and Use Committee (IACUC) of Ben-Gurion University of the Negev, in compliance with Israel's Animal Welfare Act (1994) and the NIH Guide for the Care and Use of Laboratory Animals (NRC, 2011). The animal facility is approved by the U.S. Office of Laboratory Animal Welfare (OLAW; assurance number A5060-01) and is fully accredited by the Association for Assessment and Accreditation of Laboratory Animal Care International (AAALAC).

Note that full information on the approval of the study protocol must also be provided in the manuscript.

Plants

Seed stocks	N/A
Novel plant genotypes	N/A
Authentication	N/A